THE UNIVERSITY
of EDINBURGH

This thesis has been submitted in fulfilment of the requirements for a postgraduate degree (e.g. PhD, MPhil, DClinPsychol) at the University of Edinburgh. Please note the following terms and conditions of use:

This work is protected by copyright and other intellectual property rights, which are retained by the thesis author, unless otherwise stated.
A copy can be downloaded for personal non-commercial research or study, without prior permission or charge.
This thesis cannot be reproduced or quoted extensively from without first obtaining permission in writing from the author.
The content must not be changed in any way or sold commercially in any format or medium without the formal permission of the author.
When referring to this work, full bibliographic details including the author, title, awarding institution and date of the thesis must be given.

EVOLUTIONARY AND THERAPEUTIC CONSEQUENCES OF PHENOTYPIC HETEROGENEITY IN MICROBIAL POPULATIONS

Nicholas C. Lowery

SUBMITTED TO THE UNIVERSITY OF EDINBURGH FOR THE DEGREE OF DOCTOR OF PHILOSOPHY

JUNE 2016

Declaration

I declare that the following statements (a-c) are true.

(a) that the thesis has been composed by the candidate, and

(b) either that the work is the candidate's own, or, if the candidate has been a member of a research group, that the candidate has made a substantial contribution to the work, such contribution being clearly indicated, and

(c) that the work has not been submitted for any other degree or professional qualification except as specified.

Nicholas Lowery (the candidate)

Table of Contents

Acknowledgements

I would like to thank my supervisor Dr. Sam Brown for patient guidance and the freedom to pursue the ideas I found interesting. I would also like to thank Dr. Chris French as my second supervisor, for constructive feedback in the early stages of many of these projects. I thank all the Brown lab members - Roman, Luke, Dan, Sylvie, Rich, Kristofer, Jennifer and Tim – for advice, input and discussions. I would also like to thank the Ashworth community for generally being outstandingly friendly and helpful, with specific thanks to Dr. Martin Waterfall in the flow facility. Finally, I thank the wider research community who made many of these projects possible, including Gabe Perron, Steve Diggle, Ariel Lindner, and all of the regular Brown lab collaborators.

I am grateful to the School of Biology for the scholarship that funded the majority of my PhD, and to the multiple funders of the Brown lab for their support of this work.

Finally, I would like to thank my family for support of my studies past and present, and special thanks to my wife Selena for her love, patience and for keeping me sane throughout.

Papers Arising

Lowery N, McNally L, Ratcliff WC, Brown SP. (*In preparation*). A cellular life history trade-off drives mixed bacterial biofilm investment strategies.

Lowery N, Brown SP. (*In preparation*). Persistence is age-independent in *E. coli*.

Abstract

The historical notion of a microbial population has been of a clonal population of identical swimming planktonic cells in a laboratory flask. As the field has advanced, we have grown to appreciate the immense diversity in microbial behaviors, from their propensity to grow in dense surface-attached communities as a biofilm, to the consequences of social dilemmas between cells, to their ability to form spores able to survive nearly any environmental insult. However, the historically biased view of the clonal microbial population still persists – even when a rare phenotype is investigated, the focus simply shifts to that narrower focal population - and this bias can lead to some of the broader questions relating to the consequences of phenotypic diversity within populations to be overlooked.

This work seeks to address this gap by investigating the evolutionary causes and consequences of phenotypic heterogeneity, with a focus on clinically relevant phenotypes. We first develop and experimentally validate a theoretical model describing the evolution of a microbial population faced with a trade-off between survival and fecundity phenotypes (e.g. biofilm and planktonic cells), which suggests that simultaneous investment in both types maximizes lineage fitness in heterogeneous environments. This model helps to inform the experimental studies in the following chapters. We find that biofilm-mediated phenotypic resistance to antibiotics is evolutionarily labile, and responsive to antibiotic dose and whether biofilm or planktonic cells are passaged. We also show that persistence in *E. coli* is age-independent, supporting the current hypothesis of stochastic metabolic fluctuations as the cause of this rare phenotype. Finally, we explore phenotypic variation across a library of natural isolates of *P. aeruginosa*, and find few organizing principles among key phenotypes related to virulence. Together these results suggest that phenotypic heterogeneity is a crucial component in the ecology and evolution of microbial populations, and directly affects pressing applied concerns such as the antibiotic resistance crisis.

Lay Summary

Historically, scientists have studied bacteria as populations of identical cells, swimming freely in rich nutrient broth. However, more recently it has been appreciated that bacterial cells even within the same species are far from identical, and cells within the same population can display multiple distinct behaviors that may influence growth and survival. Despite this impressive diversity, the historical bias of thinking of bacteria as identical persists, even when studying bacteria that are obviously different from the standard laboratory culture. This bias has caused important questions relating to why and how diversity evolved in the first place to be overlooked.

In this thesis, we attempt to answer the question of why some bacteria within the same population adopt very different modes of growth. In Chapter 2, we use mathematical models and experimental approaches to show that by diversifying between cell types that are specialized towards either survival or growth, bacteria maximize their overall growth over a wide range of conditions. In Chapter 3, we extend the results of Chapter 2 to show the relative degrees that bacteria invest in specialized survival and growth cells can evolve in response to antibiotic treatment, suggesting that relative investment between cell types may be important in considering how to treat infections. Chapter 4 addresses a specific type of cell that can survive antibiotic treatment, called persister cells. How persister cells are formed is not well understood; we hypothesized that the age of the cell might influence whether it becomes a persister, but our results indicated this was not the case. Finally, in Chapter 5 we ask whether there are patterns in the traits associated with bacterial survival and 'virulence', a measure of how much damage the bacteria may cause during infection, in a bacteria known for being able to grow in diverse habitats, *Pseudomonas aeruginosa*. However, we found little evidence for broad patterns between traits, reflecting the exceptional diversity that can be achieved even within a single species.

1 Introduction

1.1 The microbial world

Microbes inhabit virtually every niche on the planet, from hydrothermal vents on the ocean floor (Lutz and Kennish, 1993) to arctic glaciers (Skidmore *et al.*, 2000) and everywhere between. Microbes are also massively diverse, including the vast majority of the three kingdoms of life (bacteria, archaea and eukaryotes); it is simpler to say that life is microbial, with the exception of a few peculiar metazoans. Beyond their ubiquity and diversity, microbes serve key ecosystem functions on their own as producers, decomposers and recyclers. Furthermore, they are key symbionts to all multicellular organisms, including humans, shaping our development and health in a number of ways we are only beginning to unravel – as well as pathogens causing disease. Microbes are also highly adaptable, with short generation times leading to rapid evolutionary responses to environmental change (Elena and Lenski, 2003), and the ability to exchange genetic material horizontally via mobile genetic elements can accelerate adaptation to an even greater extent (Jain *et al.*, 2003).

1.1.1 Microbe-human interactions

Given their ubiquity and adaptability, microbes are a key interacting partner influencing human health and disease. Indeed, a healthy human is roughly equal parts human and bacteria (Sender *et al.*, 2016) by crude cell count - and mostly bacterial by number of genes. This vast resident population of microbes living on and within us (mostly in the gut) has been collectively named the 'human microbiome'. Microbiomes provide important site-specific mutualisms, such as assisting with the breakdown of food in the gut (which may have wide-ranging implications in other aspects of health), training the immune system, and keeping skin healthy (Pflughoeft and Versalovic, 2012; Flint *et al.*, 2012). Dysregulation in the microbiome can lead to various negative outcomes (Pflughoeft and Versalovic, 2012),

but we are only beginning to appreciate the impact microbiome function has on numerous aspects of human health.

1.1.2 Pathogens

On the other hand, numerous pathogenic microbial species and strains by definition induce harm to human hosts in order to reproduce and transmit themselves through the environment. Perhaps the most famous bacterial pathogen is *Yersinia pestis*, the causative agent of the 'black death' plague that killed tens of millions of medieval Europeans (Dennis and Staples, 2009). More modern well-known disease agents include *Vibrio cholerae*, responsible for various cholera outbreaks e.g. in the aftermath of earthquakes in Haiti (CDC, 2011), or hemorrhagic strains of *Eschericia coli*, causing frequent outbreaks of food-borne illnesses (Sperandio and Hovde, 2015). Pathogenic bacteria can infect and exploit diverse sites by means of numerous virulence mechanisms, which generally serve to provide nutrients to the bacteria by killing or damaging host cells (e.g. via toxin production in salmonella / VC), and aiding bacteria in the evasion of the host immune response (e.g. intracellular replication with *Mycobacterium leprae*, the causative agent of leprosy). The resident microbiome can also interact with pathogens, often functioning to protect against pathogen colonization (Buffie and Pamer, 2013; Buffie *et al.*, 2015), but these interactions have only just begun to be explored.

1.1.3 Environmental opportunistic pathogens

In contrast with the largely obligatory pathogens mentioned above, facultative or opportunistic pathogenic bacteria are also of concern. These are species that generally exist benignly in the environment or even as commensals with the host, but can cause disease when normally present barriers are compromised (hence the 'opportunist' title) - for example with bacterial pneumonia caused by *Streptococcus pneumoniae*, a normal resident of the upper airways in humans. Opportunists are of interest clinically in that infection is not simply tied to exposure to other infected individuals, thus making control of transmission problematic (which is of special

importance in the consideration of antibiotic resistance, discussed below), while also presenting challenges to the theoretical understanding of their evolution (Brown *et al.*, 2012) as they do not conform to the standard models of parasite evolution (Anderson and May, 1982; Alizon *et al.*, 2009).

1.1.4 Pseudomonas aeruginosa

Pseudomonas aeruginosa is an environmental generalist microbe, important opportunistic pathogen, and the main organism of concern in this work. It is ubiquitous in the environment, having been isolated everywhere from built environments, freshwater and marine aquatic sources, soil, plants and animals (see Chapter 5 and the Appendix), and in humans it is associated with infections of burn wounds, pneumonia, UTIs and surgical site infections, among others, (Driscoll *et al.*, 2007), and notably as the leading contributor to mortality in patients with cystic fibrosis (CF), where it can infect the lungs and persist for years (Davies, 2002; Gaspar *et al.*, 2013). Pathogenicity in *P. aeruginosa* is governed to a large extent by quorum sensing, a regulatory framework by which bacteria can infer information regarding both conspecifics (Cornforth and Foster, 2013; Diggle *et al.*, 2007b, 2007a) and physical characteristics of the environment (Cornforth *et al.*, 2014). Quorum sensing broadly regulates secreted products, which constitute the bulk of virulence factors such as proteases and pyocins produced by *P. aeruginosa* (Diggle *et al.*, 2007c; Jimenez *et al.*, 2012), but also influences other clinically relevant phenotypes such as biofilm formation and motility (Patriquin *et al.*, 2008; Wang *et al.*, 2014; de Kievit, 2009). Furthermore, *P. aeruginosa* is intrinsically predisposed to resistance to multiple antibiotics (Strateva and Yordanov, 2009), the specifics of which will be discussed further below.

P. aeruginosa is notable and potentially unique in the degree of genetic and phenotypic diversity it displays in both environmental and infection contexts. This is likely facilitated by its exceptionally rich regulatory networks (Stover *et al.*, 2000; Jimenez *et al.*, 2012; Balasubramanian *et al.*, 2013), allowing for precise tuning of physiological

states and expanding the capacity for plastic responses to diverse environmental conditions and perturbations.

A paradigm example of this capacity for phenotypic diversity is in the context of CF lung infections, where numerous studies have catalogued extensive heterogeneity in phenotypes related to morphology, physiology, virulence, and antibiotic resistance (Fonseca *et al.*, 2007; Huse *et al.*, 2010; Starkey *et al.*, 2009; Clark *et al.*, 2015; Workentine *et al.*, 2013; Jeukens *et al.*, 2014; Darch *et al.*, 2015). This diversification is at least in part likely driven by differences in numerous extrinsic factors associated with CF infections, such as the host immune system, disease progression, other co-localizing microbes (of the same and different species), bacteriophage, and chemotherapeutic treatments. While many of these factors are not unique to CF, their effects may be magnified given the extreme duration over which populations may persist in the CF lung, enhancing the degree of observed diversity within resident populations.

Furthermore, significant genetic variation within *P. aeruginosa* has also been noted in CF infections, for which the causes and consequences are only recently beginning to be unraveled. From a physical perspective, genotypic diversity in the CF lung is facilitated and maintained by spatial segregation of lineages within the lung into distinct niches with limited inter-population mixing (Markussen *et al.*, 2014; Jorth *et al.*, 2015), suggesting drift may play a significant role alongside adaptive evolution in the diversification process (Huse *et al.*, 2010), and facilitating the coexistence of distinct lineages through time (Williams *et al.*, 2015). However, it has also been noted that within-sample (i.e. within a single sputum exudate) variation is often greater than variation between samples or between patients (Winstanley *et al.*, 2016; Mowat *et al.*, 2011; Ashish *et al.*, 2013), indicating that within-local population processes remain the dominant driver of diversification. This is not surprising, given that numerous aspects of the CF lung environment can facilitate within-population genetic and phenotypic diversification, such as the nutritional environment (Wong *et al.*, 2012), growth primarily within biofilms (Boles *et al.*, 2004; Boles and Singh, 2008; Wessel *et al.*, 2014; Starkey *et al.*, 2009), exposure to antibiotics (Wright *et al.*, 2013),

social dynamics (Andersen *et al.*, 2015; van Gestel *et al.*, 2015), and persistence of mutator strains (Ciofu *et al.*, 2010).

There has been limited success in mapping genotypic markers of *P. aeruginosa* to phenotypic outcomes in the CF lung (Fonseca *et al.*, 2007; Jeukens *et al.*, 2014; Hilker *et al.*, 2015; Clark *et al.*, 2015; Darch *et al.*, 2015). The reasons for this lack of predictability remain unclear, but candidate processes include plastic phenotypic responses in the absence of genetic change, and mutations occurring in global regulators where specific phenotypic outcomes may be difficult to elucidate (Damkiær *et al.*, 2013). Mapping phenotypic outcomes onto genetic determinants remains an open question in infections of *P. aeruginosa* within the CF lung, and more generally is broadly important to disease ecology, as similar diversifying processes have been observed in *P. aeruginosa* infections in other disease sites (Buivydas *et al.*, 2013), hosts (Wright *et al.*, 2015), as well as in populations of other microbial pathogens (Goerke *et al.*, 2007; Lieberman *et al.*, 2014).

1.2 Pathogen control and drug failure

Control of pathogenic bacterial infections is mediated jointly by pharmaceutical treatment of infections, and by limiting pathogen transmission via epidemiological control and vaccination. Control of transmission is particularly effective against obligate pathogens, which generally have limited access to external reservoirs and therefore rely on rapid between-host transmission to spread throughout the population (Anderson and May, 1990). For example, limiting contact with rodent species (and their associated flea vectors) has largely mitigated outbreaks of the bubonic plague (Dennis and Staples, 2009). Opportunists, on the other hand, require more holistic approaches given the high rates of contact, and rely more heavily on antibiotic treatment (especially when vaccination is unavailable) for control (Brown *et al.*, 2012). However, the capacity for rapid adaptation in bacteria has led to the evolution of numerous mechanisms to resist antibiotic killing and vaccine control, and through heavy usage we have arrived at a crisis point in antimicrobial resistance

(Rossolini *et al.*, 2014), with strains emerging that are resistant to most or in some cases all of our current antibiotic arsenal.

1.2.1 Antimicrobial resistance

Antimicrobial resistance (AMR) is defined as an increase in the concentration of drug required to prevent any bacterial growth (the minimum inhibitory concentration, or MIC) (Brauner *et al.*, 2016), and can be mediated through one or a combination of several molecular mechanisms, including direct degradation of antibiotic molecules, modification of the cellular targets of antibiotics, blocking uptake of antibiotics into the cell, or using efflux pumps to reduce the intracellular antibiotic concentration (Blair *et al.*, 2014). Increases in AMR can result from regulatory shifts that increase expression of existing defensive mechanisms, and/or genetic changes leading to increased AMR functionality. Furthermore, genes mediating the above resistance mechanisms can be packaged into mobile genetic elements, which can facilitate rapid spread of resistance genes throughout microbial populations via horizontal gene transfer. This is particularly troublesome when multiple resistance alleles are packaged onto a single transmissible element, as uptake then confers multiple antibiotic resistances to an otherwise susceptible organism in a single step (Kruse and Srum, 1994).

1.2.2 Antimicrobial tolerance

Further compounding the problem of AMR are various phenotypic states which reduce the killing efficacy of antibiotics in otherwise genetically susceptible cells (Figure 1.1). With antibiotic tolerance, otherwise genetically susceptible cells can transiently survive antibiotic treatment due a decrease in the rate of killing relative to susceptible cells (though susceptibility remains over longer time scales) (Brauner *et al.*, 2016). In the simplest case, tolerance can result from the correlation between antibiotic killing rates and the growth rate of the population (Tuomanen *et al.*, 1986); therefore, various situations that reduce bacterial growth rates may increase antibiotic tolerance. Even transitory suppression of growth can increase antibiotic

tolerance, for example by extending the duration of the lag phase before growth begins, potentially altogether evading transient antibiotic exposure (Fridman *et al.*, 2014). In the following paragraphs, I discuss two specialized cases where heterogeneous phenotypes provide protection from antibiotics – persister cells and biofilms.

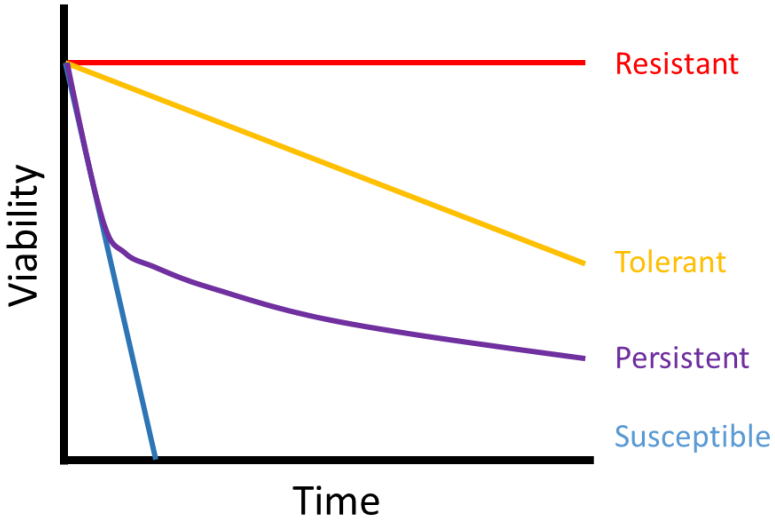

Figure 1.1: Resistance, tolerance and persistence reduce antibiotic efficacy. Schematic curves show viability through time for bacterial populations exposed to antibiotics, illustrating the signatures of various phenotypic classes that reduce antibiotic efficacy compared to susceptible cells. Resistance results in no killing, and can be mediated both genetically and phenotypically. Tolerance results in a decline in the rate of killing relative to susceptible cells, while persistence is indicated by a biphasic death curve.

1.2.3 Persistence

Persister cells are a distinct subpopulation identified by a biphasic death curve upon exposure to antibiotics (Figure 1.1), where the vast majority of the population dies off rapidly while a small subpopulation (at an average frequency of approximately 10^{-5}) 'persists' for an extended period of time (Keren *et al.*, 2004b, 2004a; Brauner *et al.*, 2016). Persister cells are generally thought to arise through transient metabolic arrest due to stochastic induction of toxin-antitoxin (TA) modules (Lewis, 2010; Wood *et al.*,

2013). Briefly, TA systems consist of a durable intracellular toxin and a labile antitoxin, which must be constantly produced in order to neutralize toxin activity, and their evolutionary origin is a subject of debate (Van Melderen and De Bast, 2009). It is hypothesized that stochastic dysregulations in cellular metabolism and/or signaling can transiently induce metabolic arrest by activating TA modules (Gerdes *et al.*, 2005; Maisonneuve *et al.*, 2013b; Lewis, 2010; Wood *et al.*, 2013; Nguyen *et al.*, 2011); however, apparent genetic redundancy in the persister phenotype (Hansen *et al.*, 2008) combined with the general difficulty in studying rare heterogeneous phenotypes have made elucidation of the details of persister formation elusive.

1.2.4 Biofilms and phenotypic resistance

Finally, biofilms, a major theme of this thesis, represent a key phenotypic class conferring tolerance and resistance to antibiotics. Biofilms are conventionally defined as dense clusters of surface attached cells encased in a polymer matrix (extracellular polymeric substance, EPS) composed of a combination of polysaccharides, protein and extracellular DNA (Hall-Stoodley *et al.*, 2004); the matrix may also harbor active factors such as degradative enzymes or signaling molecules (Flemming and Wingender, 2010). In this thesis, we adopt a broader definition of biofilms as any multicellular group of attached bacteria – including pellicles (mats of cells at the air liquid interface), suspended aggregates of cells (Schleheck *et al.*, 2009; Haaber *et al.*, 2012), and microcolonies (smaller clusters of surface-attached cells) (Monds and O'Toole, 2009). Biofilms are generally accepted to be a ubiquitous feature of bacterial growth, and thought to develop via a loose biphasic life cycle where the adhered biofilm functions as the 'soma' and motile planktonic cells as the dispersive propagules (Monds and O'Toole, 2009; O'Toole *et al.*, 2000).

Biofilm cells grow slowly relative to their planktonic counterparts, likely due to limitations on nutrient diffusion and spatial constraints (Stewart, 2003). Slowed growth, limited resources and the physical barrier provided by the matrix combine to provide biofilm cells with exceptional 'phenotypic resistance' not only to antibiotics, but to a wide array of external threats, including chemical insult,

desiccation, predation, bacteriophages, and host immune cells and factors (Strateva and Yordanov, 2009; Wiuff *et al.*, 2005; Vega and Gore, 2014; Corona and Martinez, 2013; Van Acker *et al.*, 2014; Matz *et al.*, 2008). EPS also functions as a physical glue, adhering the biofilm cells to the surface and making physical removal of biofilm cells difficult as well. This general recalcitrance leads to biofilms causing problems not only when attempting to be treated in an infection site within a host, but also when transmitted on e.g. medical devices (Francolini and Donelli, 2010; Marks *et al.*, 2014; Kramer *et al.*, 2006), as well as in numerous industrial applications in which surface fouling is undesirable (e.g. shipping and food safety).

This general recalcitrance has led to much work devoted to understanding the cues and signals regulating biofilm formation and dispersal, often with the aim of developing novel methodologies to prevent colonization or facilitate their removal. In *P. aeruginosa*, biofilm formation is a multifactorial process, with colonization being sensitive to QS signals (de Kievit, 2009; Karatan and Watnick, 2009) and physical factors such as flagella and pili (Wang *et al.*, 2014; Belas, 2014; O'Toole and Kolter, 1998), while dispersal can be induced by environmental cues such as starvation, nutrient induction, changes in iron or oxygen availability, or the presence of competitors (Huynh *et al.*, 2012; Taylor and Buckling, 2010; Sauer *et al.*, 2004; McDougald *et al.*, 2011). Considerable study has also been devoted to understanding the process of endogenous dispersal (as part of the developmental program discussed above), which relies on c-di-GMP, a global regulator of the biofilm phenotype (Ueda and Wood, 2009; Valle *et al.*, 2013; Lori *et al.*, 2015; Starkey *et al.*, 2009): endogenously produced NO as well as quorum sensing signals interact to alter levels of c-di-GMP (Barraud *et al.*, 2006; Ueda and Wood, 2009), which goes on to regulate expression of surfactants, phages and other degradative factors which facilitate dispersal from the biofilm (Harmsen *et al.*, 2010; Kaplan, 2010; McDougald *et al.*, 2011).

While there is intense interest in plastic regulatory responses governing biofilm formation, many evolutionary aspects of biofilm formation remain poorly understood, though this appears to be changing with several important recent

studies. For example, dispersal phenotypes from the biofilm have been linked to social evolution dynamics, with 'cheater' lineages that exploit biofilm investment (by not producing EPS matrix – though we note there is some contention as to whether matrix production is indeed a cheatable phenotype, and this may depend on the species and even specific component under investigation (Xavier and Foster, 2007; Irie *et al.*, 2016)) being proposed as primary dispersal agents in a primitive form of division of labor (Hochberg *et al.*, 2008; Hammerschmidt *et al.*, 2014), and in line with the biphasic life cycle model previously proposed. The relative degree and mode of dispersal may also be an important factor for biofilm transmission. For instance, dispersal via multicellular aggregates may confer fitness benefits upon subsequent colonization (Kragh *et al.*, 2016; Melaugh *et al.*, 2016); dispersal via this mechanism may also help to alleviate Allee effects associated with subsequent colonization (Smith *et al.*, 2014) or maintain cooperativity within the group (Kümmerli *et al.*, 2009a). Growth within and dispersal from biofilms also facilitates diversification in cellular morphotypes and physiology (Stewart and Franklin, 2008; Rainey and Travisano, 1998; Kassen *et al.*, 2004), and this diversification can be leveraged to optimize dispersal and colonization cycles imposed via experimental evolution (Poltak and Cooper, 2010; Hammerschmidt *et al.*, 2014). Given the capacity for biofilms to potentiate AMR, further exploration of the evolutionary causes and consequences of biofilm formation likely hold important insights towards their effective management in the clinic.

1.3 Synopsis

The work presented here is aimed to sit at the intersection between antimicrobial resistance, phenotypic heterogeneity, and evolutionary ecology. As reviewed above, heterogeneous phenotypes (e.g. biofilms, persisters, etc.) contribute to failure of antibiotic treatment, and may lead to evolution of genetic resistance; furthermore, the ecological and evolutionary causes and consequences of these diverse phenotypes remain largely unexplored (Figure 1.2). We hypothesize that better understanding of

the evolutionary dynamics of phenotypic heterogeneity conferring tolerance or resistance to antibiotics will yield insights into defining effective treatment strategies in the face of the antibiotic resistance crisis. Four projects seeking to move towards this goal are summarized below.

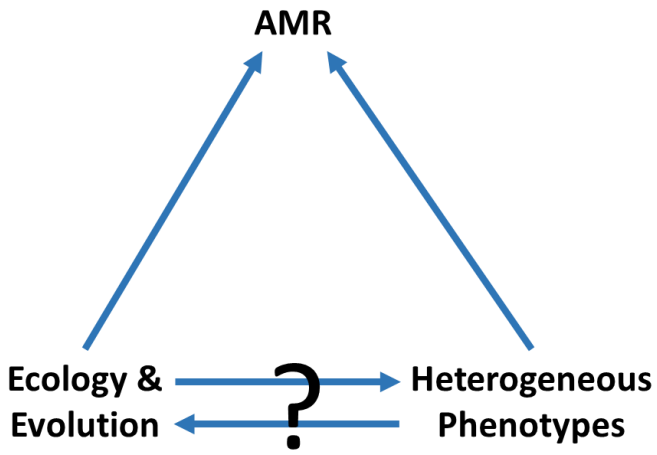

Figure 1.2: Intersection of AMR, evolution and heterogeneous phenotypes. The influence of heterogeneous phenotypes and evolution on antibiotic resistance are well established, but the interactions between evolution and heterogeneous phenotypes on AMR evolution remain poorly understood.

In Chapter 2, we use a combination of theoretical and experimental approaches to construct and validate a population dynamical model of a bacterial lineage that may allocate cellular resources between two specialized phenotypes: robust biofilm cells, and fecund planktonic cells. Our model predicts that conditions restrictive to growth favor trade-offs between the two fractions, with resource allocation devoted to whichever phenotype is favored for transmission. Under more permissive conditions, however, we find that populations can leverage reproduction in the planktonic phase to drive expansion in the biofilm, resulting in mixed investment strategies even when planktonic cells provide no transmission routes to future growth patches. Using experimental evolution, we show that phenotypic heterogeneity is tunable, but always maintained in *P. aeruginosa* when transmission

is restricted to solely planktonic or solely biofilm cells. Furthermore, our model predicts a hump shape between biofilm and planktonic cell densities due the planktonic 'growth engine', which was consistent with the relationship observed across a library of over 200 natural isolates of *P. aeruginosa*. We also found indications that biofilm may function as a cost-effective hedge against environmental catastrophe. This work indicates that the reverse conceptualization of the biofilm life cycle – i.e., where the 'soma' is composed not of the biofilm but of rapidly dividing planktonic cells, and biofilm aggregates function as dispersal propagules – is not only viable, but favored under a broad range of environmental conditions.

Chapter 3 expands the reasoning in Chapter 2 to the clinical problem of antibiotic resistance. Specifically, we ask whether biofilm-mediated phenotypic resistance is an evolvable trait, and whether phenotypic resistance helps or hinders evolution of conventional genetic resistance mechanisms. To answer these questions, we experimentally evolved populations of the opportunistic pathogen *P. aeruginosa* exposed to antibiotics, with treatments manipulating the type and dose of antibiotic, as well as which cellular fraction (biofilm or plankton) was passaged, and monitored the relative cell densities in the biofilm and planktonic fractions through time. Preliminary experimental results suggest that phenotypic resistance is evolutionarily labile (i.e. not simply a plastic response to environmental conditions), and responsive to the complex costs associated with the interaction between antibiotic and transmission environments. However, further study, particularly acquisition of genetic information, will be necessary to confirm these observations. Nevertheless, the preliminary results suggest that phenotypic resistance is an important component contributing to antibiotic treatment failure, and can evolve in a similar manner as conventional resistance mechanisms.

In Chapter 4, focus is shifted towards persistence. We hypothesize that persister formation at the individual cell level is not fully stochastic, but instead driven by demographic determinants; specifically, we hypothesized that cellular age drives persister formation, as phenotypes associated with cellular aging in bacteria agree

well with those attributed to persistence. We tested this hypothesis by segregating cells based on age using fluorescence-activated cell sorting (FACS) and a strain of *E. coli* with a fluorescent label whose brightness correlates with the age of the cell. However, no differences in persister fraction were detected between the age-fractionated subpopulations. Still, we posit that seeking other non-genetic determinants (for instance biochemical parameters such as metabolic activity or membrane potential) will be important in determining both the proximate and ultimate causes of persister formation, and will become more accessible as single-cell assay technologies improve.

Finally, in Chapter 5 we seek to investigate the extent and patterns of natural variation across a range of bacterial phenotypes liked to virulence and resistance by screening a diverse library of 230 natural and clinical isolates of *P. aeruginosa*. While probing isolate libraries regarding a phenotype of interest is relative common, understanding how virulence and resistance determinants co-vary outside of the laboratory is relatively unknown, and the ubiquity of *P. aeruginosa* in both natural and clinical settings provides an unparalleled source of natural diversity to probe. We find that phenotypes are highly variable across isolates, but the environmental source of the isolates does leave a significant trace on several phenotypes including antibiotic resistance, biofilm composition and siderophore preference. Gross patterns suggest phenotypes may segregate into 'survival' (high biofilm, low growth/virulence) and 'virulent' (high growth/virulence, low biofilm), but this only explained a small portion of overall variance in phenotypes. However, using environmental source as a proxy for evolutionary history is problematic, and work is currently underway to sequence the genomes of all 230 isolates, and build a robust phylogeny to better inform our comparative analyses among *P. aeruginosa* phenotypes.

2 A cellular life history tradeoff drives mixed bacterial biofilm investment strategies

Nicholas Lowery, Luke McNally, Will Ratcliff & Sam P. Brown

2.1 Abstract

Bacterial cells, just like multicellular organisms, face tradeoffs between longevity and fecundity. 'Planktonic' cells are fast growing and fragile, while 'biofilm' cells (also spores or persisters) are slower growing and more resistant. Here we ask, why do bacterial lineages invest simultaneously in both fast and slow growing types? We develop a population dynamical model of lineage expansion across a patchy environment, and find that mixed investment is favored across a range of environmental conditions, even when transmission is entirely via biofilm cells - this is because of a division of labor, where exponentially dividing planktonic cells can act as an engine for the production of future biofilm cells, which grow more slowly. We use experimental evolution to test our predictions, and show that phenotypic heterogeneity is persistent even under selection for purely planktonic or purely biofilm transmission. Our model further predicts a humped relationship between biofilm and planktonic cell densities due to the 'growth engine' effect of planktonic expansion, and we find support for this relationship using a comparative analysis of over 200 isolates of the opportunistic bacterial pathogen *P. aeruginosa*.

2.2 Introduction

After billions of years of evolution, few opportunities remain for organisms to gain increases in survival or reproduction that are not subject to trade-offs in other traits. Indeed, understanding how adaptation occurs when key fitness parameters trade off lies at the core of life history theory (Stearns, 1992). While most life history theory has been developed with large multicellular organisms in mind, microbes also exhibit classical trade-offs in fecundity and longevity, with faster growing lineages tending to be more fragile (De Paepe and Taddei, 2006; Heineman and Brown, 2012).

Understanding how microbes manage such trade-offs remains a major goal in microbiology, both from mechanistic (Gudelj *et al.*, 2010) and ecological (Green *et al.*, 2008) perspectives.

Multiple mechanisms of enhancing durability and longevity are available to microbes, but typically come at the cost of reduced metabolic proficiency. Spore formation is perhaps the clearest example of a high survival, low fecundity phenotype; by encasing the genome and some essential metabolic machinery in a thick and extremely resistant cell wall, dormant spores can survive for extraordinarily long durations (Cano and Borucki, 1995; Vreeland *et al.*, 2000). Alternatively, cells may form metabolically dormant persister cells capable of surviving diverse environmental insults (Lewis, 2010; Wood *et al.*, 2013). Finally, many microbial species form biofilms where dense cell packing leads to limits on space and nutrient availability, thereby reducing growth rates and gaining broad resistance to stressors such as desiccation, predation, or chemical insult (Van Acker *et al.*, 2014).

Clonally reproducing microbes present an interesting and experimentally tractable system to examine mixed-behavioral strategies. Across many species of microbe, single genotypes can produce coexisting subpopulations of rapidly dividing planktonic cells and slow-growing or dormant stress-tolerant cells, but focus is often given to a specific phenotype of interest rather than the balance between alternate phenotypes. In this study, we examine how the trade-off between survival and growth of individual cells drives the evolution of mixed biofilm / planktonic investments on a lineage scale under diverse environmental conditions. Specifically, we build population dynamical models of bacteria in patchy environments, where cells can switch between biofilm and planktonic states within ephemeral patches (via biofilm colonization and dispersal), and can also transmit among patches either as biofilm or planktonic cells. We then ask, under what conditions is investment into biofilm favored, given that biofilms grow more slowly? If only one phenotype (i.e. biofilm or plankton) is favored for transmission to a new patch, does it ever pay to diversify into the cell type that is, from a transmission perspective, a 'dead end'? Our

model predicts that phenotypic diversification can pay across a range of environmental conditions, as rapidly growing planktonic cells can function as a 'growth engine' providing higher levels of future planktonic and biofilm cells for transmission. We then test our model predictions using stochastic simulations, experimental evolution and comparative analyses of biofilm allocation in the environmental microbe *Pseudomonas aeruginosa*.

2.3 Methods

2.3.1 Biofilm allocation experiment

A diverse library of 235 natural and clinical isolates of *P. aeruginosa* was kindly provided by Dr. G Perron (Bard College), see the Appendix for strain information. Each strain was grown to mid-exponential phase in 1 mL 'growth medium' (M9 salts supplemented with 10 mM Glucose, 1% Cas-amino acids, 1mM $MgSO_4$, 100uM $CaCl_2$ and 1X Hutner's trace elements (Hutner *et al.*, 1950)) in a 48-well plate, and these starter cultures were used to inoculate 150 uL of fresh growth medium in a tissue culture-treated 96-well plate at an OD(600) of 0.05. Plates were incubated statically in a humidified chamber at 37 °C for 6 hours; this time was chosen to minimize plastic phenotypic changes that commonly occur as *P. aeruginosa* enter stationary phase. After growth, the OD(600) of the planktonic phase was measured, then removed and the attached biofilms washed with sterile water via pipetting. 150 mL of sterile 0.85% NaCl was then added to each well, along with 5-10 sterile 1 mm glass beads. The plate was then sealed with acetate tape and vortexed at 2000 rpm for 15 minutes to resuspend the attached biofilm; the resuspended biofilm was then transferred to a new 96-well plate and the OD(600) measured.

2.3.2 Passaging experiment

A mid-exponential phase culture of *P. aeruginosa* PA01 was used to inoculate 200 uL LB and one 4 mm sterile glass bead in each of 24 wells in a 96 well plate at an OD of 0.05. Plates were sealed with Aeraseal tape and grown statically at 24 °C in a humidified chamber. Every 12 hours (again, growth conditions were chosen to

prevent entry into stationary phase), biofilm allocation was measured by removing and measuring the OD(600) of the planktonic phase, then washing, resuspending and measuring the density of the attached biofilm as above in 200 uL fresh LB. 12 lines had only the planktonic cells passaged, while the other 12 had only biofilm cells passaged; in each case, cells were diluted to an inoculum OD of 0.05, and 20 passages were performed.

2.3.3 Statistics and mathematical analysis

All non-analytical modelling and statistics were performed in R (Soetaert *et al.*, 2010; R Core Team, 2015), unless otherwise noted. Agent based simulations were performed using iDynoMiCs (Lardon *et al.*, 2011), and analytical analyses were performed using Mathematica (Wolfram, 2015).

2.4 Results

2.4.1 Biofilm Growth Dynamics

While it is well known that planktonic cells accumulate exponentially in nutrient-rich environments, it is less clear whether close-packed biofilm cells would suffer any penalty to growth under similar conditions (note that here we are considering biofilm growth in the absence of any coupling with the planktonic compartment, i.e. no cells dispersing from the biofilm or colonizing from the bulk). We hypothesize that when the surface on which the biofilm grows is sparsely colonized, lineages can grow exponentially. However, once confluence across the surface is reached, further growth is restricted to linear expansion in the z-direction (i.e. towards the bulk), due to cell division being largely restricted to a fixed depth within the outermost layer in biofilms due to space and diffusion limitations (Werner *et al.*, 2004; Fux *et al.*, 2005). We explore this conjecture using the individual-based simulation platform iDynoMiCS (Lardon *et al.*, 2011) (Figure 2.1).

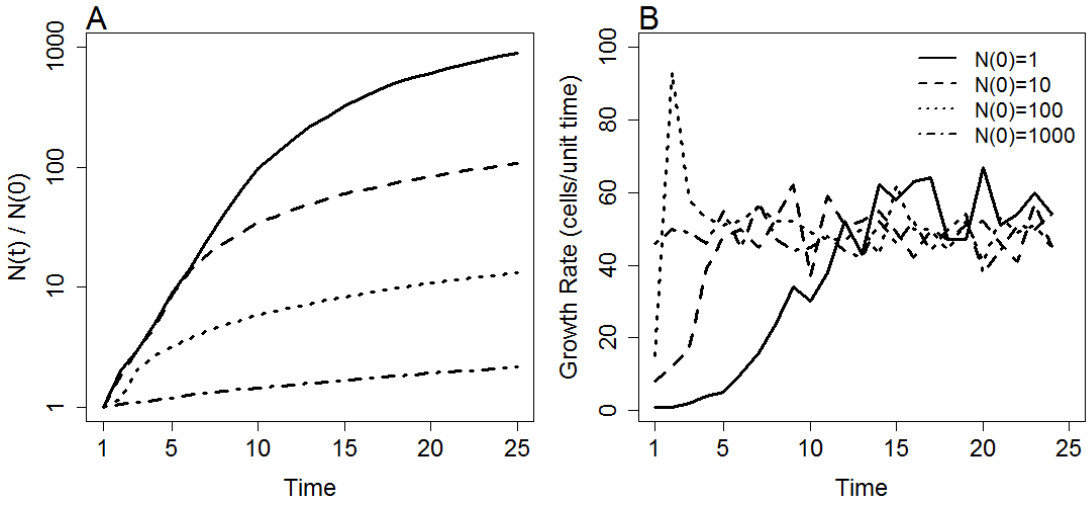

Figure 2.1: Biofilms grow linearly. Agent-based simulations of a 2D biofilm growing on a surface. **A**, accumulated cells and **B**, lineage growth rate through time. Varying inocula (see legend) were allowed to grow for a fixed time period under nutrient-rich conditions. Smaller inocula (i.e. sparse colonization) lead to prolonged periods of exponential growth that decay to linear growth once confluent colonization occurs (under these conditions, after roughly 100 cells have accumulated, at a rate of 50 cells/time step). Simulations were implemented using the agent-based simulation platform iDynoMiCS (Lardon *et al.*, 2011).

The simulations support our conjecture that biofilm lineage growth plateaus at some maximal rate constant, likely influenced by the nutrient diffusion rates and cell packing efficiency specific to each instance considered. Small inocula (i.e. low surface coverage; Figure 2.1, solid line) showed an extended period of exponential growth that eventually decayed to linear accumulation, and as the inoculum size increases, the duration of exponential growth decreases until it disappears completely for large initial populations (Figure 2.1, dot-dash lines). Figure 2.1 highlights that while biofilm cells do not face the extreme growth penalty of resistant spores or persister cells, they face a significant and compounding growth deficit in comparison with the exponential growth of planktonic populations.

2.4.2 Coupled Biofilm-Plankton Dynamics

We next model a growing bacterial microcosm within which cells grow in one of two compartments, the planktonic (P) phase within the bulk fluid, and the biofilm (B)

phase attached to a surface and in contact with the bulk. The compartments are coupled, such that biofilm cells can disperse to the planktonic phase, and planktonic cells can colonize the biofilm. Cells in each compartment also divide, with planktonic cells growing exponentially, and biofilm cells growing linearly (Figure 2.1).

Because the biofilm is limited to linear expansion, we reasoned that the effects of growth within and dispersal from the biofilm would be negligible when coupled to exponential growth in the planktonic phase. This simplification was shown to be reasonable by comparing numerical simulations of the full and simplified models (Supplemental Figure 2.1), yielding the model system outlined in Figure 2.2A, and Equations 1.1, 1.2, 2.1 and 2.2 for within-patch growth.

We also note that setting the growth of the biofilm to zero in the simplified model framework renders biofilm cells functionally equivalent to spores or persister cells as described above, i.e. a subpopulation of non-dividing cells supported by the growth of vegetative cells, which presumably must provide some other benefit (e.g. environmental resistance) to the overall population to counteract this loss in fitness, or else be lost from the population.

Our simplified model framework results in the following coupled differential equations:

1.1) $$\frac{dP}{dt} = (r - c)P$$

1.2) $$\frac{dB}{dt} = cP$$

Solving equations 1.1 and 1.2 as a function of time yields our within-patch population model,

2.1) $$P(t) = P_0 e^{(r-c)t}$$

2.2) $$B(t) = \frac{c}{r - c}(P(t) - P_0)$$

where r is the exponential growth rate, c is the rate of colonization of the biofilm (with $0 \leq c < r$), and P_0 is the planktonic inoculum. Note that in general c need not be

bounded by r, and arbitrarily high values for c would result in a decline in P as switching to the biofilm phase outpaces planktonic growth, giving a trade-off between the two fractions; we discuss this case in the context in which it arises below.

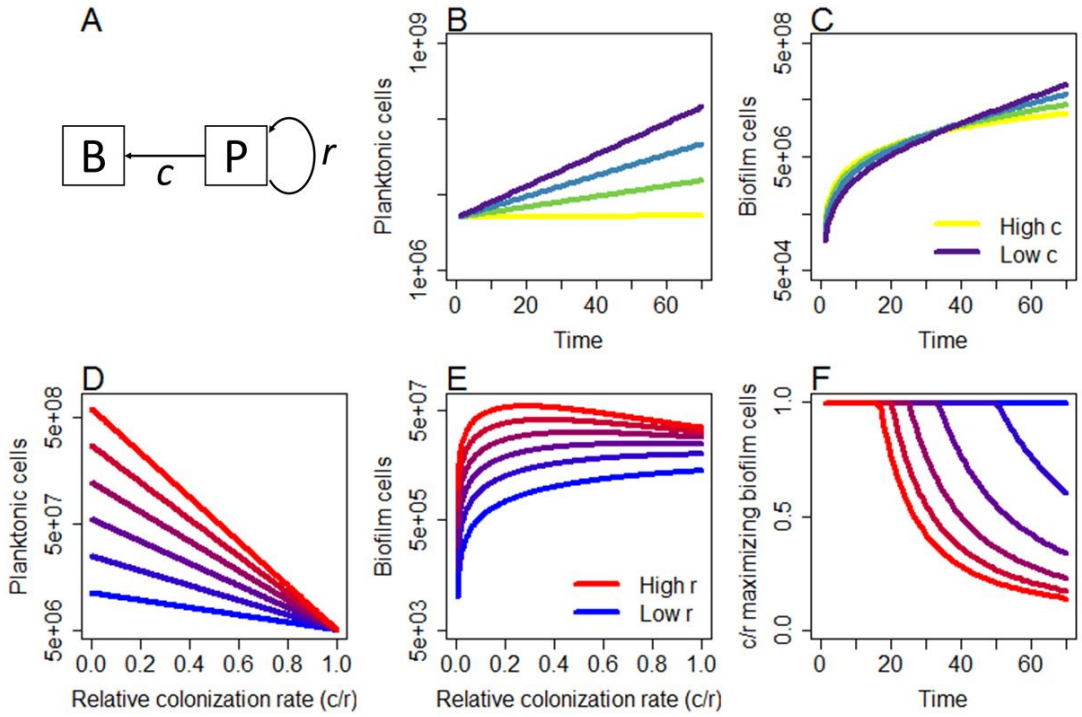

Figure 2.2: Trade-offs in duration and rate of growth lead to maximal biofilm at intermediate rates of colonization. **A**, Schematic model process. **B** and **C**, time series of planktonic and biofilm cells, respectively, for low to high colonization rates c (yellow-purple color scale). c is normalized to 40 – 99% of r, with $r = 0.08$. Note that decreasing c allows for greater rates of exponential expansion in the biofilm (yellow curve represents approximately linear growth in the biofilm). **D**, planktonic, and **E**, biofilm cells as a function of colonization rate relative to growth rate for $t = 40$, $0.02 \leq r \leq 0.12$ (blue-red color scale), $P_0 = 5{,}000{,}000$. **F**, Relative colonization rate at which biofilm is maximized. Note in panel E the limit of $c = 0$ is omitted, as this prevents any formation of biofilm cells.

As expected, planktonic cells decline monotonically with increasing colonization rate c, as more cells are siphoned from the planktonic to the biofilm compartment (Figure 2.2, B and D). The biofilm, however, shows more interesting dynamics with changing rates of colonization (Figure 2.2, C and E). At $c = 0$, no biofilm cells accumulate, while

at $c = r$, all new planktonic cells colonize the biofilm, resulting in a static planktonic population and linear accumulation of biofilm cells (P_0 cells per time step; Figure 2.2, yellow lines). However, when the planktonic fraction is allowed to expand exponentially (with $c < r$), the biofilm also accumulates cells exponentially at a constant fraction $\frac{c}{r-c}$ of the planktonic population, leading to a temporal trade-off in total biofilm with increasing c (Figure 2.2C), where high colonization rates provide more biofilm cells at short time scales, while lower colonization rates maximize biofilm over longer periods of growth.

The conditions governing a maximum in biofilm at $c < r$ are explored in Figure 2.2E and F and in Equation 2.3. In Figure 2.2E, biofilm initially increases with c, but at higher growth rates we see a hump shape appear, with further allocation to the biofilm reducing the number of biofilm cells, similar to the temporal trade-off in Figure 2.2C. We can solve for an analytical condition for this humped relationship by examining the slope of B as a function of c as c approaches r (Equation 2.3, see supplemental data for derivation).

2.3) $$\lim_{c \to r} \left(\frac{dB}{dc} \right) = -\frac{1}{2} P_0 t(rt - 2)$$

If the slope is negative, this would imply an interior maximum in B at some $c < r$ (as biofilm cells necessarily increase as c increases from zero). We find that this limit is negative for $rt > 2$, i.e. the presence of a humped relationship in B requires patch quality to exceed some minimal threshold value, and thereby explaining the parallel trade-offs in biofilm accumulation with changing r and t (Figure 2.2F).

2.4.3 Evolutionary Model

Given that any allocation of resources to the biofilm comes as a direct cost to total cell number, what conditions would favor maintenance of a biofilm? We can examine the evolutionary consequences of allocation in the within-patch population model by constructing a life cycle in which a population colonizes successive patches through space and/or time. We define a fitness function (Equations 3.1 and 3.2) by assigning transmission probabilities k_p and k_b that a given cell from the respective planktonic or

biofilm compartments will go on to found a new patch (analogous to the reproductive number 'R0' framework common to parasite virulence, e.g. Frank 1996).

3.1) $W = k_p P(t) + k_b B(t)$,

or, explicitly, per-founding cell

3.2) $W(c, r, t) = k_p e^{(r-c)t} + k_b (e^{(r-c)t} - 1) \frac{c}{r-c}$

Equation 3.2 allows us to interrogate the fitness consequences of colonization rate across a wide array of ecological parameters. k_p and k_b capture the reproductive value of each cell type, and can be interpreted equivalently as a per-cell transmission probability or as the fraction of the population able to transmit successfully; they dictate how well a given cell can survive the inter-patch transition, and are influenced by the nature of the environment. Growth time t describes the disturbance regime, i.e. how long a population can stay in a single patch, and r measures the nutrient quality of individual patches, or how rapidly planktonic cells can divide within the patch. We define c^* as the optimal colonization rate (the rate maximizing fitness W under a given ecological condition), and display the behavior of c^* as a function of transmission parameters k_p and k_b in Figure 2.3.

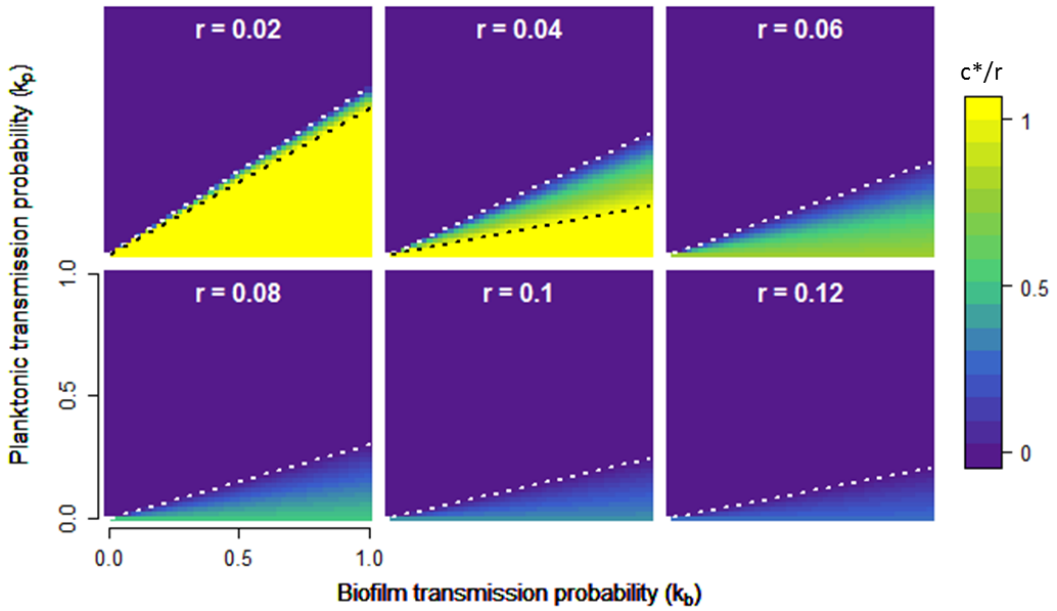

Figure 2.3: Optimal colonization rate c^* as a function of reproductive value for planktonic and biofilm cells. Contour plots showing the relative colonization rate (c^*/r, yellow-purple color scale) optimizing fitness (Equation 3.2). Each panel displays c^*/r as a function of k_p and k_b. Across panels, the growth rate r increases from r = 0.02 to 0.12, with t = 40 in all cases; similar plots varying t are displayed in Supplemental Figure 2.2. White dotted line indicates the threshold at which $c^* > 0$, and black dotted line indicates the threshold at which $c^* < 1$.

There are three general strategies populations may adopt in maximizing fitness: devoting all resources to the biofilm fraction ($c^* = r$), splitting resources between the two fractions ($0 < c^* < r$), or devoting all resources to the plankton ($c^* = 0$). We investigate the conditions governing the two transitions defining these regimes by examining the behavior of Equation 3.2 in more detail.

2.4.3.1 Biofilm only / coexistence threshold

To examine the case where biofilm is maximally favored, we follow a similar logic to that employed in the analysis of the within-patch model in Equation 2.3 by examining the slope of W as c approaches r (see supplemental data for derivation):

3.3) $\lim_{c \to r}\left(\frac{dW}{dc}\right) = -\frac{1}{2}t\left(2k_p + k_b(rt-2)\right)$

In the limiting case of $k_p = 0$, we recover an equivalent scenario to that in equation 2.3, where biofilm (and thereby fitness) increases as c moves away from the minimum at zero, and is maximized at $c^* = r$ for $rt < 2$ (i.e. $\frac{dW}{dc}$ is always positive and approaches the limit from below). Generally, fitness is maximized at $c^* = r$ when $\frac{k_p}{k_b} < \frac{rt-2}{2}$, and at $c^* < r$ when $\frac{k_p}{k_b} > \frac{rt-2}{2}$, setting the condition separating the strict trade-off and coexistence fitness regimes (black dashed lines, Figure 2.3).

2.4.3.2 Coexistence / plankton only threshold

Sole investment into the planktonic phase will be favored when fitness is maximized at $c^* = 0$; for our model, this condition is met when 1) $W(c=0) > \lim_{c \to r}(W)$, i.e. fitness declines with increasing c, and 2) $\left.\frac{dW}{dc}\right|_{c=0} < 0$, i.e. the decline in fitness is monotonic. Evaluating Equation 3.2 under condition 1 yields

3.4) $k_p e^{rt} > k_p + k_b rt,$

while condition 2 gives

$\frac{k_b}{r}(e^{rt} - 1) - k_p t e^{rt} < 0,$

which simplifies to

3.5) $k_p e^{rt} > \frac{k_b}{rt}(e^{rt} - 1).$

Both conditions are linear in k_p and k_b; solving for k_p as a function of k_b in equations 3.4 and 3.5 and comparing the slopes reveals that Equation 3.5 presents the higher threshold for all values of r and t examined in this work (data not shown). Therefore, we conclude cellular investment is routed wholly into the planktonic phase for $\frac{k_p}{k_b} > \frac{e^{rt}-1}{rte^{rt}}$, while cells begin to be allocated into the biofilm when $\frac{k_p}{k_b} < \frac{e^{rt}-1}{rte^{rt}}$ (white dashed lines, Figure 2.3).

2.4.3.3 Trade-offs in allocation

Strict trade-offs are defined by the regions where $c^* = r$ and $c^* = 0$. This region covers nearly all of the transmission space at low growth rates (Figure 2.3), where divergent selection towards one extreme or another is expected, and relaxes as conditions become more permissive to growth. In the limit of zero within-patch growth, the allocation decision becomes a 'zero-sum' game:

3.6) $$\left.\frac{dW}{dc}\right|_{r=0} = te^{-ct}(k_b - k_p)$$

If $k_b > k_p$, c will increase to the limit of $c^* = r$, while $k_p > k_b$ will cause c^* to decline to zero, giving a strict trade-off defined by whichever fraction is preferentially transmitted between patches.

This simple zero-sum logic is intuitive, but fails significantly under more permissive growth conditions (i.e. increasing r and/or t; Figure 2.3 and Figure S2.2), where we see an intermediate level of colonization is favored over a relatively large portion of the parameter space. Despite large transmission advantages to biofilm cells, the intermediate colonization regime extends to the boundary of $k_p = 0$ (black dashed line undefined for $r > 0.04$, Figure 2.3), such that even when planktonic cells have zero probability of founding a new patch, the vast majority of the population is still allocated to that fraction.

Why would such a small fraction of replicating cells be allocated to the biofilm when that is the only source of reproductive value to the population? To address this, we return to the within-patch population dynamics of the model, in Figure 2.4.

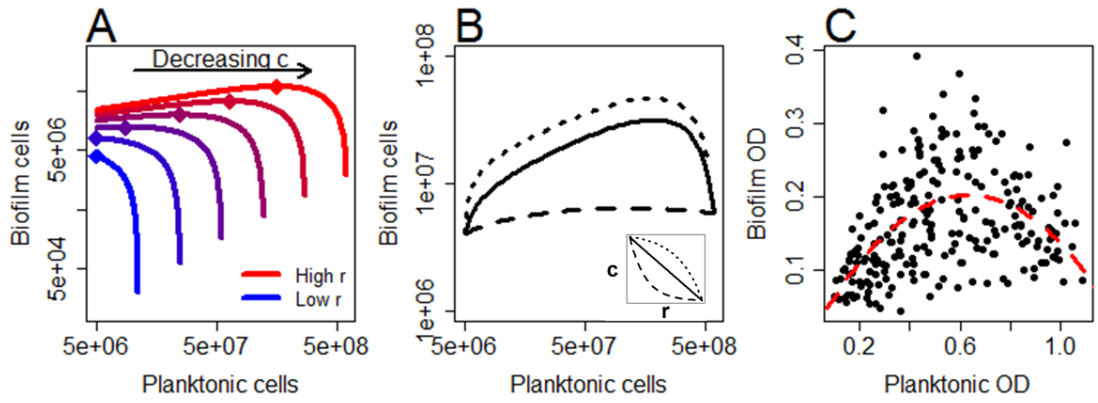

Figure 2.4: Biofilm is maximized at reduced colonization rates with increasing growth rates. **A**, Solutions to the within-patch model (Equations 2.1, 2.2) are plotted for $t = 40$, $0.02 \leq r \leq 0.12$ (blue-red color scale), $P_0 = 5{,}000{,}000$ (same as in Figure 2DEF). Biofilm cells are plotted against planktonic cells to show regions of positive slope, with colonization rate decreasing from r at the left end of each curve and approaching zero at the right end (the point where $c = 0$ is omitted), and the maximum in biofilm marked along each curve. **B**, Solutions to the within-patch model are plotted as in A, but with r and c combinations biased to reflect expectations for analogous experiments in panel C (see main text). Inset depicts putative relationships between r and c, and are matched to the main panel via line type. **C**, Population allocation for a library of *P. aeruginosa* natural isolates, with each point representing a single strain. Dashed curve in C depicts the regression of biofilm OD onto a quadratic in planktonic OD (see main text).

As was noted in Figure 2.2C and 2.2F, reducing the colonization rate away from the maximum allows for exponential growth in both fractions of the population, yielding more biofilm cells at lower rates of colonization given sufficiently long periods or fast rates of growth. This results in a transition from a trade-off to a hump shape in the allocation space as the opportunity for within-patch growth is increased (Figure 2.4A). At low r (blue lines), the expected outcome of a trade-off between biofilm and planktonic cells across c is recovered as discussed above: increasing the number of cells in either compartment comes at a direct cost to the other. As r increases (red lines), two separate regimes emerge. Moving from left to right along the trajectories, a positive relationship is maintained between biofilm and planktonic cells as c decreases, up to some intermediate value of c maximizing biofilm (diamonds in

Figure 2.4A; also see Figure 2.2F). As colonization decreases beyond this point, biofilm declines sharply as colonization tends to zero.

The colonization rates maximizing biofilm (points in Figure 2.4A) represent the points at which the effective colonization rate (i.e. in cells per unit time, not as a proportion of the planktonic population, as in all cases up to this point) is maximized for a given set of growth conditions. In other words, the planktonic fraction may be viewed as a 'growth engine' for the biofilm: when within-patch conditions are sufficiently favorable to planktonic division (Equation 2.3), reducing the colonization rate c increases the net flux of cells into the biofilm by expanding the pool of dividing planktonic cells, P. This growth engine effect is sufficient to drive colonization rates down to a fraction of the growth rate, even when planktonic cells provide no reproductive benefit to the population (Figure 2.3, Figure 2.2F).

We sought to validate our model findings in Figure 2.4A by measuring population allocation between the biofilm and planktonic phases across a library of natural isolates from the model biofilm-forming bacterium *Pseudomonas aeruginosa*. Under our model, we generally expect strains with low growth rates to tend towards higher rates of colonization, those with intermediate growth rates to favor intermediate rates of colonization, and the fastest growing strains to have the lowest rates of colonization; this negative relationship between r and c leads to a hump shape when biofilm cells are plotted against planktonic cells, indicating total biofilm is maximized at high (but not extreme) growth rates and low colonization rates (Figure 2.4B). We found that allocation within our *P. aeruginosa* isolate library tended to follow this pattern as well (Figure 2.4C), with a regression of biofilm cells onto a negative quadratic in planktonic cells being highly significant ($B = 0.62*P - 0.49*P^2$, with standard errors of 0.07 ($p = 2.13*10^{-15}$) and 0.06 ($p = 2.65*10^{-13}$) for the linear and quadratic predictors, respectively).

2.4.4 Biofilm as a bet hedge against environmental instability

In our evolutionary model (Figure 2.3), we assume that lineages can adapt their allocation decision making (c^*) in the context of constant transmission weightings k_p and k_b. However, the relative success of biofilm vs. planktonic cell propagules is likely to vary extensively in time as a function of unpredictable biotic and abiotic stresses (i.e. changing k_p relative to k_b). The nature of the relationship between the biofilm and planktonic populations as the colonization rate changes (Figure 2.4A) indicates that the biofilm compartment has the potential to function as a relatively cost-effective bet hedge against changes in the environment within and/or between patches. At all growth rates, populations can exchange a small reduction in the size of the planktonic population for a massive increase in the biofilm population by raising the rate of colonization from a minimal value: returning to Equations 1.1 and 1.2, taking the ratio of the biofilm to planktonic growth rate yields the fraction $\frac{c}{r-c}$, which approaches infinity as c approaches r.

It is therefore relatively cheap for populations to maintain a small but reasonably robust biofilm presence, while still devoting the vast majority of cellular resources to the immediately productive planktonic phase. This result suggests selection would be unlikely to purge biofilm altogether, and simple passaging experiments show that even when only the planktonic fraction is transmitted, biofilm is still maintained after 20 transfers (Figure 2.5). Ancova of fraction biofilm after the initial period of divergence (i.e. starting from passage 7) found a reduction of 0.47 (from the intercept of 0.59 in the biofilm-passaged lines) when the planktonic fraction is transferred (SE=0.02, $p < 2*10^{-16}$), and a small but significant decline in fraction biofilm with continued passaging when biofilm was transferred (-0.007 per passage, SE=0.001, $p = 5.8*10^{-13}$) but not when the plankton were transferred (estimate for interaction between planktonic transfer and passage of 0.009 (SE=0.001, $p = 1.9*10^{-11}$), negating the effect in the biofilm-selected lines). This gradual decline in fraction biofilm in biofilm-passaged lines is due to the planktonic fraction expanding relative to the biofilm fraction over the course of the experiment (see Figure S3.1; ancova of OD over passage, selection regime and fraction measured; increase of 0.01 OD units / passage

in planktonic OD relative to biofilm OD when biofilm cells are passaged, SE = 0.0005, $p < 2*10^{-16}$), consistent with the findings of our evolutionary model.

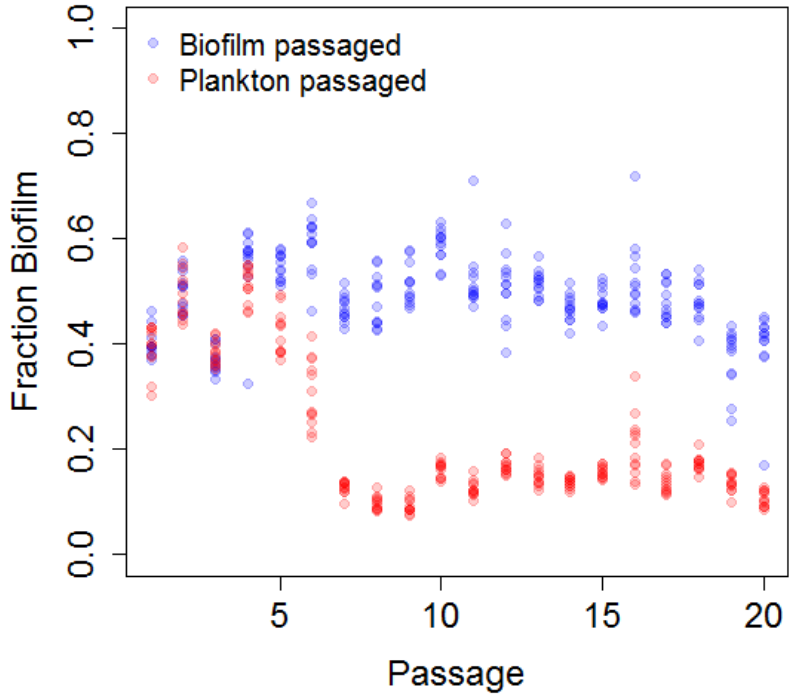

Figure 2.5: Selection for planktonic transmission fails to purge biofilm from experimental populations. *P. aeruginosa* (PAO1) was grown in 96-well plates containing a glass bead at room temperature, and every 12 hours populations were fractionated, measured, and passaged to a new well. Fraction biofilm is defined as the ratio of the biofilm OD to the sum of the ODs of the two fractions. Points represent 12 independently evolving lineages per treatment.

The low cost of maintaining biofilm makes it well suited as a potential bet-hedging strategy, trading instantaneous mean fitness to increase the long-term geometric mean fitness in unpredictable environments by reducing the variance in fitness through time. To test this prediction, we used our model framework to construct a simulated passaging regime in which growth and transmission parameters were subject to differing levels of variance. We assigned inoculum populations of

planktonic cells a fixed colonization rate c (applied relative to r), which were then subjected to alternating periods of growth and transmission. Parameters r, t, k_p and k_b were drawn from normal distributions with fixed means μ, and differing variances σ^2 between treatments. The values for r, t and c were used to solve Equations 2.1 and 2.2; proportions k_p and k_b of these new cells were then passaged to the next growth phase, as in Equation 3.1. R0 (Frank, 1996) was used as our fitness metric for these simulations, calculated as the ratio of founding cells in a given passage relative to the number of founding cells in the previous passage. Simulation results are displayed in Figure 2.6.

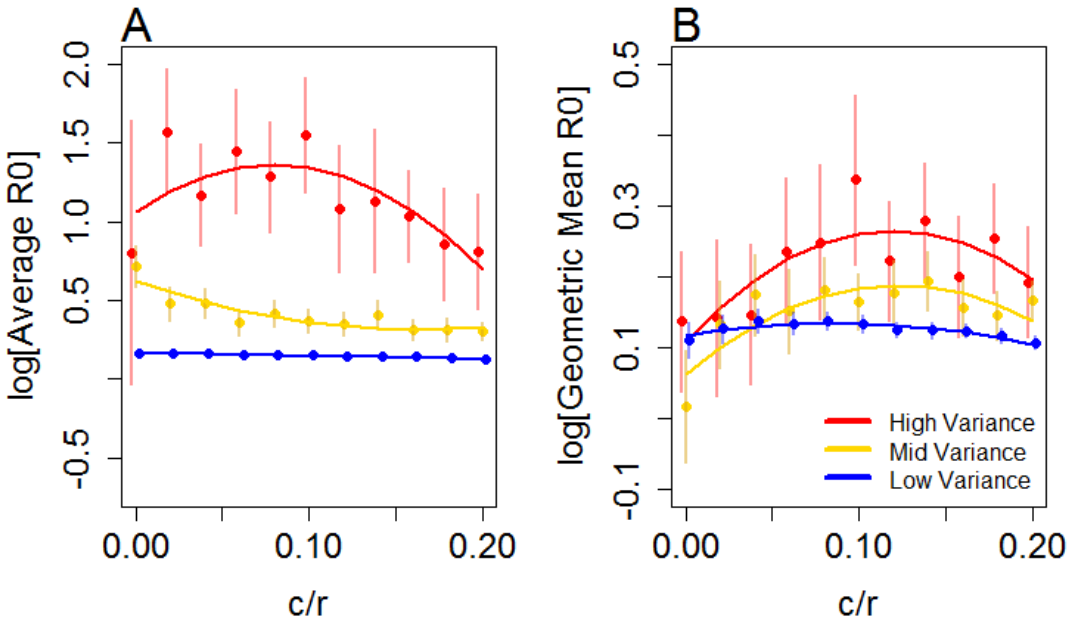

Figure 2.6: Increased colonization maximizes geometric mean fitness under unpredictable conditions. Log-scale plots of **A**, Average R0 across passages, and **B**, geometric mean of R0, are plotted as a function of relative colonization rate for lineages subject to passaging simulations with different levels of environmental instability. 100 replicate inocula of 5000 planktonic cells with the same fixed colonization rates $c \in [0,0.2]$ were subjected to 10 passages. For all cases, $\mu_r = 0.06$, $\mu_t = 40$, $\mu_{kp} = 0.1$ and $\mu_{kb} = 0.6$. Under fixed conditions these parameters would favor $c^* = 0.49$. Variance treatments modified σ^2 of the distributions from which r, t, k_p and k_b were drawn, with $\sigma^2_{low} = \mu/100$, $\sigma^2_{mid} = \mu/9$ and $\sigma^2_{high} = \mu/2.75$. Parameters were

restricted to logical values, with $0 \leq k_b , k_p \leq 1$; $r > 0$; and $t \geq 1$; this thresholding did not change the overall mean of any parameter by more than ±3%. R0 was calculated as the ratio of founding cells at a given passage relative to the founding cells of the previous passage. Points and error bars (offset to reduce overlap) represent averages with 95% confidence intervals, and solid lines display best-fit quadratic regressions (Table S2.1).

For low and medium degrees of unpredictability, the average R0 declines monotonically in c, while with high unpredictability there is a pronounced hump in mean R0 (Figure 2.6A, Table S2.2), in agreement with our hypothesis that biofilm may function as a bet hedge. This is also reflected in the geometric mean of R0 across the passaging simulation, where all treatments show a significant hump shape (Figure 2.6B, Table S2.2), indicating the increased risk of extinction if sufficient biofilm investment is not maintained, even for relatively low levels of unpredictability.

Interestingly, our simulations found that the colonization rate maximizing geometric mean fitness (c/r at roughly 0.1) is lower than the corresponding c^* in the static condition, and that average and geometric mean fitness is maximized under the greatest degree of unpredictability (red lines, Figure 2.6). Together, these findings suggest an asymmetry in the costs and benefits associated with assuming risk under unpredictable conditions. A moderate reduction in colonization rate can increase fitness by more fully leveraging the planktonic growth engine, the benefits of which outweigh the small increase in assumed risk (as suggested by the gradual decline in biofilm allocation even under biofilm selection in Figure 2.5). However, reducing the colonization rate too drastically eventually results in extinction risks that overcome the net benefit (as in Figure 2.6), suggesting an optimum minimal level of biofilm investment that maximizes growth but may still survive extreme environmental perturbations.

2.5 Discussion

In this work, we constructed a simple deterministic model of allocation between the coupled biofilm and planktonic compartments within a growing bacterial

population. Within the biofilm, cell division limited by geometry and nutrient diffusion rendered its effects inconsequential to the dynamics of the population as a whole, relative to the exponentially expanding pool of planktonic cells. Under inhospitable conditions, in which the population experienced restricted growth and/or frequent disruption, trade-offs between the biofilm and the planktonic compartment forced lineages to specialize in whichever fraction was favored to transmit between patches. When conditions become more permissive, the lineage is able to leverage exponential planktonic growth to maintain robust populations in both compartments, and at a fraction of the cellular cost of initial biofilm allocation (i.e. at reduced colonization rates c); in general, such cost saving measures are likely to be favored in any cooperative trait during periods of growth (Cornforth *et al.*, 2012). Because maintenance of a biofilm comes at little cost under conditions favoring planktonic growth, biofilm is able to function as a robust and cost-effective bet hedge against changing environments. Conversely, the planktonic fraction is a useful amplifier of biofilm cells even when biofilm is the transmissible propagule – this growth/transmission division of labor is more obvious for strictly non-growing phenotypes (e.g. spores), but the same logic holds for slow growth in biofilms as well.

We focus primarily on biofilm-planktonic cell populations as a model of survival-fecundity alternate states, and therefore use the language of colonization (of biofilms by planktonic cells) and dispersal (from the biofilm) to represent the switching processes between the two phenotypes. However, the model logic applies to other classes of resistant cells as well, such as persisters and spores. Indeed, there are instances where biofilm formation functions as a prerequisite or amplifying step in the formation of other types of resistant cells: persister cells are often enriched in biofilms (Singh *et al.*, 2009; Lewis, 2010; Nadell *et al.*, 2009; Haaber *et al.*, 2012; Høiby *et al.*, 2010a), and biofilm formation is a prerequisite step in fruiting body formation (the preferential site of sporulation) in *Bacillus subtilis* (Branda *et al.*, 2001; Aguilar *et al.*, 2010); it would be interesting to investigate how investment would be optimized with multiple phenotypes available in both simultaneous and sequential contexts.

Given the costs inherent to cellular investment into a growth-limited state, one may expect lineages to evolve the ability to efficiently switch between biofilm and planktonic phenotypes, thereby optimizing fitness by reducing lag times and minimizing unnecessary mortality in the event of environmental disturbance, and indeed such systems appear to be abundant in nature (Schuster *et al.*, 2013; Cornforth *et al.*, 2014; Barraud *et al.*, 2009; Huynh *et al.*, 2012; Dow *et al.*, 2003; Sauer *et al.*, 2004). However, we note that phenotypic switching in this case would not supplant the need to maintain some level of biofilm as a bet hedge (Figure 2.5, Figure 2.6), but rather to enhance the efficiency of such maintenance; in environments where catastrophic disturbances occur even at very low frequency, lineages that maintain biofilm regardless will still have better chances of survival. One would therefore predict biofilm to be completely lost in only the most constant environments (Figure 2.5).

Phenotypic regulation to further optimize allocation between biofilm and planktonic lifestyles would also help expedite the evolution of rudimentary life cycles at the population level, alternating between a growing 'soma' and dispersive 'propagules' with distinct demographies associated with each phase. Under the formalism presented here, either the biofilm or planktonic compartments alone, or some combination thereof, may serve as either stage of the life cycle.

The historical archetype has generally held that the biofilm functions as the soma, with motile planktonic cells as dispersive propagules (O'Toole *et al.*, 2000; Sauer *et al.*, 2002; Monds and O'Toole, 2009); more recently Hammerschmidt et al. (2014) found that alternating selection on dispersive and biofilm phenotypes in *Pseudomonas fluorescens* leads to the evolution of a lifestyle in which cooperative biofilm cells producing shared adhesive molecules form a pellicle that functions as the growing soma, and planktonic non-adhesive cheats are co-opted as dispersive propagules, thereby dividing labor between the two cellular fractions and increasing the overall fitness of the lineage.

Our results indicate that the opposite cycle (biofilm cells as propagules, planktonic cells as soma) could also be viable, as the population can still reap the benefits of

dividing labor between specialized cellular fractions. Indeed, where individual patches are permissive to growth, but transmission between patches is exceedingly harsh (e.g. wind- or animal-dispersal), dispersal via biofilm aggregates and growth within a planktonic 'soma' would offer the greatest advantage, as the 'soma' would accumulate biomass rapidly, and dispersal propagules would enjoy increased survival at little reproductive cost given the hostile transmission conditions. For example, biofilm formation and other survival phenotypes are likely important to successful transmission via fomites, upon which bacteria can remain viable for months (Kramer *et al.*, 2006). Dispersal in physically linked groups (i.e. budding dispersal, (Kümmerli *et al.*, 2009a)) may also help maintain cooperative traits during dispersal, thereby potentially accelerating colonization when a new patch is reached. The biofilm 'streamers' observed by Drescher et al. (2013) may be another example of this mode of transmission, where flow rates are such that the biofilm forms physical bridges to allow colonization of vacant surfaces in a topographically complex environment, as full detachment would prevent recolonization of adjacent surfaces due to extreme shear forces.

Taken together, our results highlight the evolutionary significance of within-population phenotypic heterogeneity and its consequences for survival and fecundity in mixed transmission environments. By optimizing the switching rate between robust and fecund specialists (here, the colonization rate from the planktonic to biofilm fractions, though we note that other mechanisms could lead to equivalent outcomes, such as the steady-state frequencies of genotypes arising from within-population diversification, as in (Poltak and Cooper, 2010)), lineages were able to maximize fitness and transmission across a wide range of environments, as well as enhance survival in the face of catastrophic changes within the environment. The rate of phenotypic switching is therefore an essential parameter upon which selection may act when multiple phenotypes can persist within lineages, and given the breadth of environmental parameters investigated here, we posit that the conditions dictating the trade-off and coexistence regimes ($\frac{e^{rt}-1}{rte^{rt}} < \frac{k_p}{k_b} < \frac{rt-2}{2}$) may hold quite generally.

2.6 Supplemental Material

2.6.1 Supplemental Data

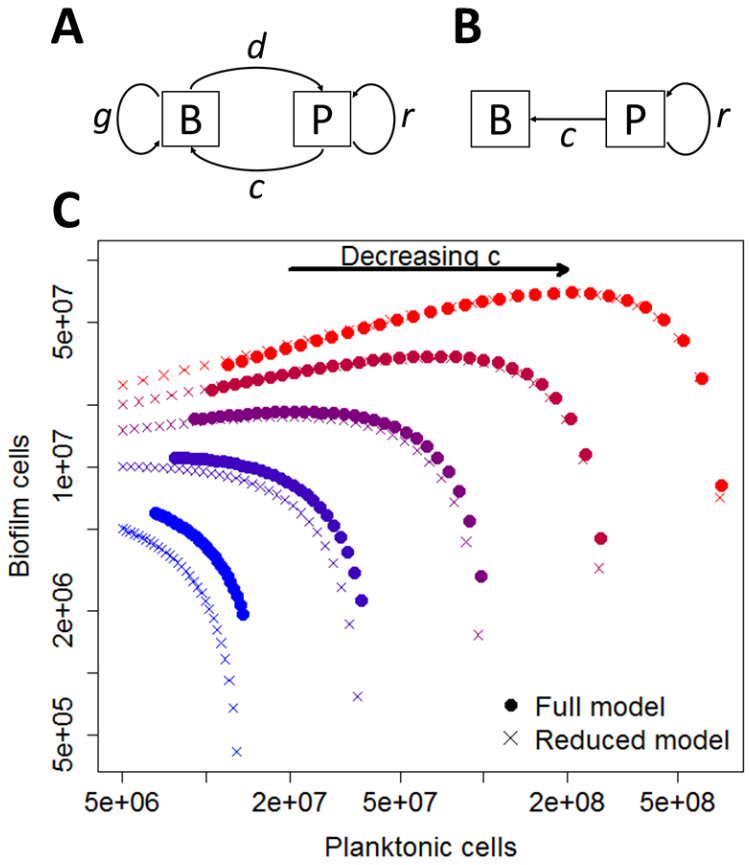

Supplemental Figure 2.1: Comparison of full and simplified models. **A** and **B**, schematics of the full and reduced models, respectively. **C**, Numerical simulations comparing the full and reduced models. Simulations evolved for 50 time steps, with $B_0 = 0$, $P_0 = 5{,}000{,}000$, $0.02 \leq r \leq 0.1$ (blue-red color scale). For the full model, $d = 0.01$ and $g = 40{,}000$ (as a linear rate); the reduced model sets $d = g = 0$. Overall dynamics are quite similar; in general, the reduced model tends to underestimate cells in the planktonic fraction at high colonization rates (and more so at high growth rates), and to a lesser extent underestimate cells in the biofilm at low colonization rates (more so at lower growth rates).

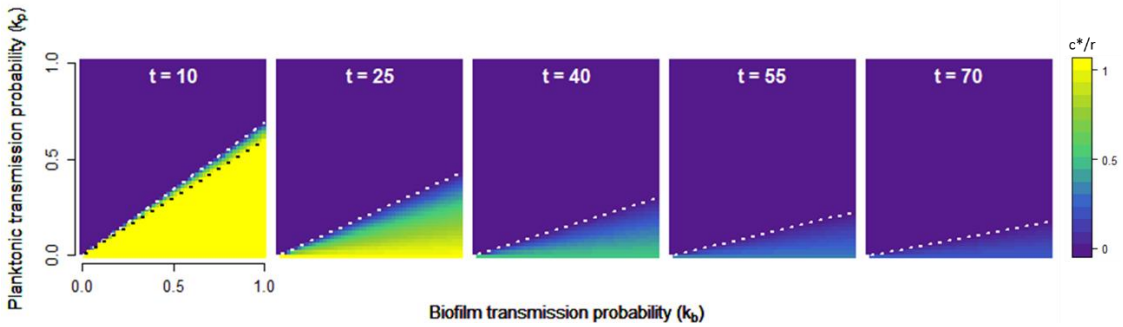

Supplemental Figure S2.2: Optimal colonization rate c^* as a function of reproductive value for planktonic and biofilm cells. c^*/r is plotted under the same conditions as in Figure 2.3, but panels vary growth period as opposed to growth rate (here $r = 0.08$), increasing from left ($t = 10$) to right ($t = 70$).

Table S2.1: Regression models for bet-hedging simulations (see Figure 2.6). Parameter estimates for models displayed in Figure 2.6. Linear and quadratic regressions were fit and compared for each variance treatment, and the best model chosen on the basis of lower AIC (Akaike, 1981); this was the quadratic regression in all cases except the average R0 under low variance, where the linear model was the best fit to the data.

		Model	Estimate	SE	P-value
log[Average R0]	*low*	*Intercept*	0.17	0.01	< 2E-16
		c	-0.19	0.04	2.05E-06
	mid	*Intercept*	0.63	0.03	< 2E-16
		c	-3.84	0.80	1.82E-06
		c^2	11.95	3.86	0.002
	high	*Intercept*	1.06	0.17	4.52E-10
		c	7.35	3.94	0.06
		c^2	-46.0	19.0	0.015
log[Geometric Mean R0]	*low*	*Intercept*	0.12	0.01	< 2E-16
		c	0.39	0.13	3.20E-03
		c^2	-2.26	0.63	3.80E-04
	mid	*Intercept*	0.06	0.02	0.001
		c	2.04	0.46	8.60E-06
		c^2	-8.31	2.19	1.60E-04
	high	*Intercept*	0.11	0.04	3.69E-03
		c	2.60	0.87	2.91E-03
		c^2	-10.83	4.20	9.95E-03

2.6.2 Supplemental Derivations

2.6.2.1 Derivation for Equation 2.3

Combining equations 2.1 and 2.2 yields

$$B(c,r,t) = \frac{c}{r-c}P_0(e^{(r-c)t}-1)$$

Taking the derivative with respect to c, applying the quotient rule yields

$$\frac{dB}{dc} = \frac{P_0(r-c)\frac{d}{dc}\left[c\left(e^{(r-c)t}-1\right)\right] - \frac{d}{dc}[r-c]ce^{(r-c)t}-1)}{(r-c)^2}$$

Further evaluation gives

$$\frac{dB}{dc} = P_0(\frac{(r-c)\left(-tce^{(r-c)t}+e^{(r-c)t}-1\right)+c(e^{(r-c)t}-1)}{(r-c)^2}$$

which simplifies to

$$\frac{dB}{dc} = \frac{P_0((tc^2-rtc+r)e^{(r-c)t}-r)}{(c-r)^2}$$

Taking the limit as c approaches r yields equation 2.3

$$\lim_{c\to r}\left(\frac{dB}{dc}\right) = -\frac{1}{2}P_0t(rt-2)$$

2.6.2.2 Derivation of Equation 3.3

Our fitness function is defined as

$$W(c,r,t) = k_pe^{(r-c)t} + k_b(e^{(r-c)t}-1)\frac{c}{r-c}$$

in equation 3.2. Differentiating the first and second terms with respect to c gives

$$\frac{dW}{dc} = -k_pte^{(r-c)t} + k_b\frac{(r-c)\frac{d}{dc}\left[c\left(e^{(r-c)t}-1\right)\right] - \frac{d}{dc}[r-c]c(e^{(r-c)t}-1)}{(r-c)^2}$$

via the product and quotient rules; further simplification yields

$$\frac{dW}{dc} = -k_pte^{(r-c)t} + k_b\frac{(r-c)\left(-tce^{(r-c)t}+e^{(r-c)t}-1\right)+c(e^{(r-c)t}-1)}{(r-c)^2}$$

which simplifies to

$$\frac{dW}{dc} = -\frac{\left(\left(k_b-k_p\right)tc^2+\left(k_b-2k_p\right)rtc+k_pr^2t-k_br\right)e^{(r-c)t}-k_br}{(c-r)^2}$$

Evaluating the derivative as c approaches r yields equation 3.3,

$$\lim_{c\to r}\left(\frac{dW}{dc}\right) = -\frac{1}{2}t\left(2k_p+k_b(rt-2)\right)$$

3 Genetic evolution of phenotypic antibiotic resistance

Nicholas Lowery & Sam P. Brown

3.1 Abstract

Biofilm formation is a virtually ubiquitous growth phenotype available to microbes in both natural and clinical settings. Biofilms are relatively recalcitrant, and thought to contribute to the failure of antibiotic treatments in clearing microbial infections by providing resistance towards the antibiotic in otherwise genetically susceptible cells, which we define as 'biofilm resistance'. By experimentally evolving the opportunistic pathogen *Pseudomonas aeruginosa* under antibiotic exposure and monitoring the relative investment of cellular resources to the biofilm, we found preliminary evidence suggesting that biofilm resistance is evolutionarily labile, and can be strongly induced in a cost-dependent manner, as dictated by the antibiotic profile and transmission bias towards or against biofilm cells. Some evidence also tentatively indicates that biofilm resistance may facilitate evolution of genetic resistance mutants; however, this and other observations require validation via further sequencing and phenotypic analysis.

3.2 Introduction

We currently face a crisis in antibiotic resistance, with resistant bacterial infections increasing in frequency and few leads on new drugs to combat them. Classic resistance is achieved through genetic modifications that directly impact drug efficacy, such as alteration of drug targets, direct degradation of antibiotics, or prevention of drug entry into the cell (Blair *et al.*, 2014). However, bacteria can also resist antibiotic killing by inducing physiological changes in the absence of genetic mutation, providing 'phenotypic resistance' (Wiuff *et al.*, 2005; Corona and Martinez, 2013) to antibiotics. Phenotypic resistance can occur via diverse mechanisms, for

instance by formation of persister cells (Lewis, 2010), or forming multicellular biofilms (Høiby *et al.*, 2010b; Van Acker *et al.*, 2014; Gupta *et al.*, 2013), and allows for otherwise genetically susceptible cells to persist under drug treatment, resulting in recurrent infections (Fauvart *et al.*, 2011; Zhang *et al.*, 2012), increased mutation pools from which genetic resistance can evolve (Cohen *et al.*, 2013), and decreasing effective drug doses potentially accelerating genetic resistance evolution (Høiby *et al.*, 2010b; Greulich *et al.*, 2012).

In this work, we are primarily concerned with phenotypic resistance mediated by biofilm formation, hereafter referred to as 'biofilm resistance' (Figure 3.1). Because biofilm formation provides resistance to multiple threats and can have profound effects on the overall growth of a population (see Chapter 2), it is often plastically regulated and responsive to multiple environmental cues. For example, biofilm formation in *P. aeruginosa*, a widespread biofilm model organism, rapidly responds to quorum sensing signals (de Kievit, 2009), changes in the nutrient environment (Huynh *et al.*, 2012; Sauer *et al.*, 2004; McDougald *et al.*, 2011), and cues from conspecifics (Bragonzi *et al.*, 2012; Oliveira *et al.*, 2015); notably, biofilm formation may also be induced in direct response to antibiotic damage (Cornforth and Foster, 2013; Oliveira *et al.*, 2015). However, our previous work has also shown considerable genetic variation in the biofilm phenotype (Chapters 2 and 5), highlighting how such plastic responses can be genetically modified in response to selection; the relative contributions of plastic and evolved responses in biofilm and other tolerance phenotypes remain poorly understood.

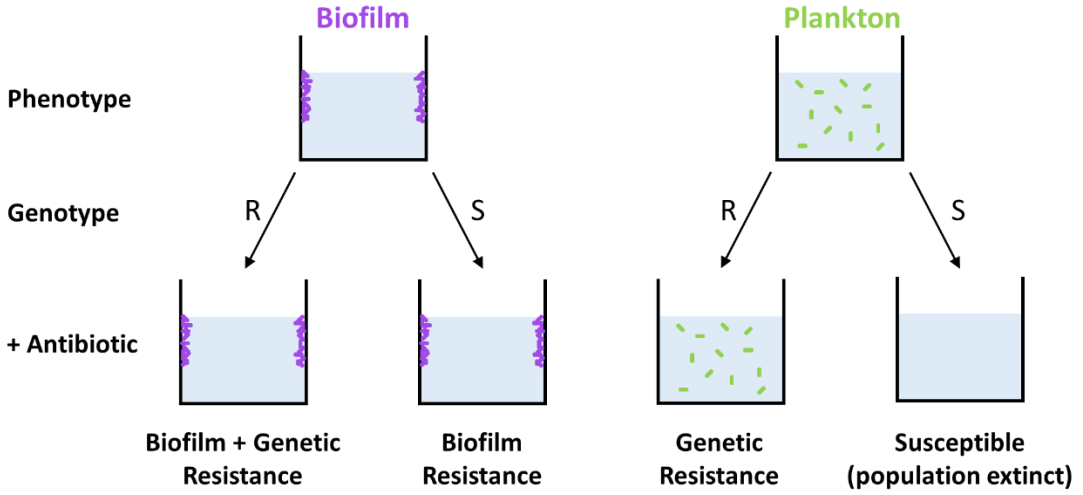

Figure 3.1: Schematic depiction of biofilm vs. genetic resistance. Bacterial cells can exist in either the biofilm or the planktonic phenotypes. Within these phenotypes, the population can be genetically susceptible (S) or resistant (R) to antibiotics. Upon antibiotic exposure, susceptible planktonic cells die off, while resistant planktonic cells survive. Conversely, biofilm cells survive due to resistance inherent to the biofilm phenotype, regardless of genotype; in this case, genetic and phenotypic resistance cannot be differentiated without further information, e.g. presence vs. absence of genetic resistance mutations.

The tension between plastic and evolutionary responses are of critical importance to the evolution of resistance. Theory suggests plasticity will limit evolutionary responses to smaller environmental changes by allowing individuals to respond appropriately in the absence of genetic mutation, while evolution will be accelerated when plasticity facilitates initial establishment and persistence in environments otherwise too extreme for colonization (West-Eberhard, 2003; Leggett *et al.*, 2014). In the context of antibiotic resistance, this implies that biofilm resistance mechanisms may either slow or accelerate evolution of genetic resistance mutants in a dose-dependent manner. Furthermore, it suggests that biofilm resistance will be an important bridge to genetic resistance when direct resistance loci are rare or inaccessible (a generally desirable characteristic for antimicrobial therapeutics).

Evolution of genetic resistance mutants will likely create selective feedbacks onto biofilm resistance traits. Given that biofilms and other tolerance phenotypes are generally slow growing (Yang *et al.*, 2008; Tuomanen *et al.*, 1986; Brauner *et al.*, 2016),

previous theory suggests relaxing selection on phenotypically resistant cells will lead to rapid decline in the allocation of resources to that phenotype (Chapter 2), i.e. biofilm will likely decline upon evolution of faster-growing genetic resistance mutants. However, even in the presence of genetically antibiotic resistance mutants, selection to maintain biofilm may persist due to damage accrued via competition with conspecifics (Cornforth and Foster, 2013; Oliveira *et al.*, 2015) or the host immune system. It therefore remains unclear regarding the effects of genetic resistance mutants on biofilm investment.

We sought to experimentally investigate the dynamics of the interaction between biofilm and genetic resistance by monitoring the relative level of biofilm investment in evolving populations of the opportunistic pathogen *Pseudomonas aeruginosa* under varying types and doses of antibiotic. Furthermore, we simultaneously imposed transmission requirements such that only biofilm or planktonic cells were transferred between passages, exaggerating the selective pressures acting for or against biofilm resistance. A model schematic of the putative underlying process of population allocation and expectations for the experiment are summarized in Figure 3.2. Based on our previous work in Chapter 2, we hypothesize that biofilm resistance will be evolutionarily labile (Figure 3.2C), and that the degree and direction of the evolutionary response will be sensitive to the environment (the antibiotic profile and B vs. P transmission). Furthermore, we predict that biofilm resistance will facilitate evolution of genetic resistance, by providing a safe haven to a population of growing cells from which direct genetic resistance mutants may evolve.

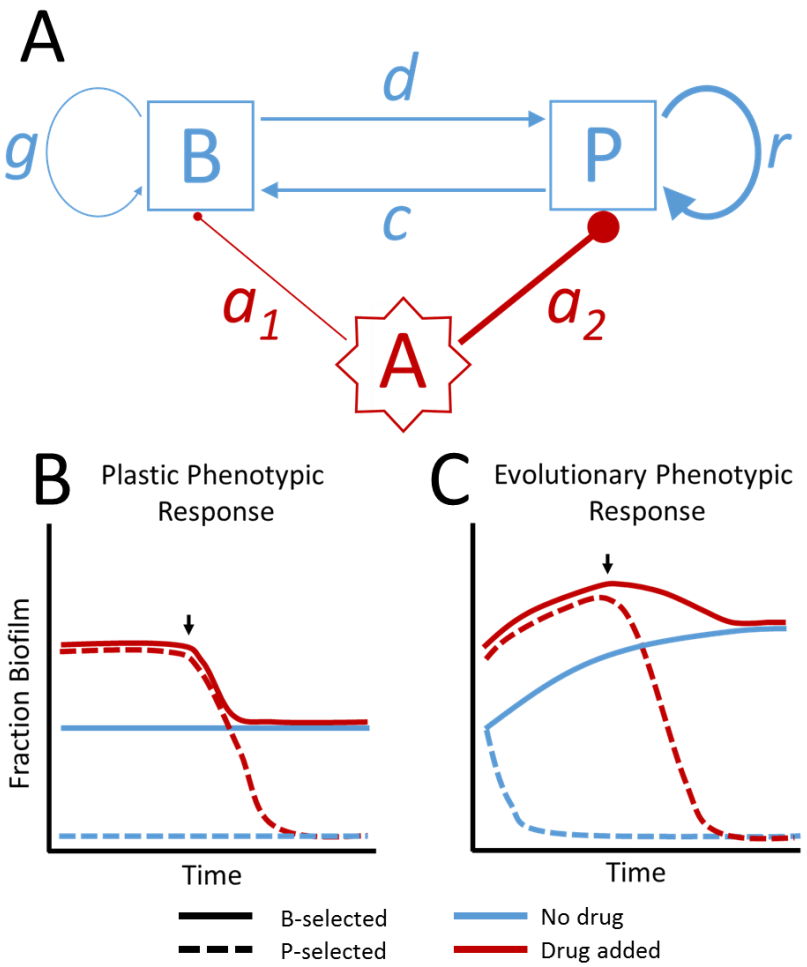

Figure 3.2: Schematic of biofilm/plankton dynamics under antibiotic assault and predictions for experimental evolution. **A**, Schematic of a bacterial population, comprised of surface-attached biofilm (*B*) and free-swimming planktonic cells (*P*) exposed to antibiotics, adapted from Chapter 2. Cells can allocate into one of two compartments, the biofilm *B* or the plankton *P*. The relative abundances of *B* and *P* are controlled directly by the rates of colonization *c* and dispersal *d*, and indirectly by the growth rates *r* and *g*, with $r >> g$. Treatment with antibiotic *A* inhibits growth in each fraction, to degree a_1 or a_2, respectively, and we postulate $a_2 > a_1$, i.e. the biofilm fraction provides some degree of resistance to the population. We assume that the antibiotic has no direct effect on the rates of colonization or dispersal. **B** and **C**, predictions for experimental outcomes for cases of purely plastic or mixed plastic and evolutionary responses. Blue lines, no drug control; red lines, drug added; solid lines, biofilm fraction passaged (B-selected); dashed lines, planktonic fraction passaged (P-selected). Arrows indicate point at which genetic resistance evolves.

We find preliminary evidence that biofilm resistance (as measured by relative biofilm investment) is indeed evolutionary labile, showing strong directional responses of both increasing and decreasing relative investment towards the biofilm, with the specific patterns dependent on the antibiotic and transmission environment. In particular, we find that biofilm investment is maximal under biofilm transmission and intermediate drug doses, but that biofilm is also favored transiently under high drug doses regardless of passaging regime. We suggest that in this latter case biofilm resistance is a stop-gap measure aiding survival, by providing a safe haven until a suitable genetic resistance mutant evolves. This stop-gap model implies that the degree and duration of increasing biofilm resistance will be dictated by the frequency at which genetic resistance mutants arise. By evolving populations under antibiotics with a loose hierarchy in accessibility of genetic resistance mutations, we observed patterns broadly consistent with this prediction. However, further study, in particular obtaining genetic sequence information of the evolved isolates, will be necessary to help validate the largely phenotypic results presented here.

3.3 Methods

3.3.1 Passaging

Populations of *Pseudomonas aeruginosa* PAO1 were grown statically in 200 uL of LB medium (with antibiotics, if appropriate; see below) in wells of 96 well plate with a single 3 mm sterile glass bead, at room temperature within a humidified chamber, and sealed with Aeraseal tape. After each growth period (~10 hours), the planktonic fraction was transferred to a new plate and the OD(600) measured. Biofilms (cells attached to the bead and walls of the well) were washed with sterile water via pipetting, then resuspended in 200 uL of fresh LB by sealing the plates with acetate tape and vortexing at 2000 rpm for 15 minutes. The resuspended biofilm cells were then transferred to a new plate and the OD(600) measured. Either biofilm or planktonic cells were transferred to a new plate with fresh media and antibiotics (see Figure 3.3). An inoculum density of 0.01 OD units was used for the first three

passages, but this was relaxed to 0.05 for subsequent passaged to make bottlenecks less stringent.

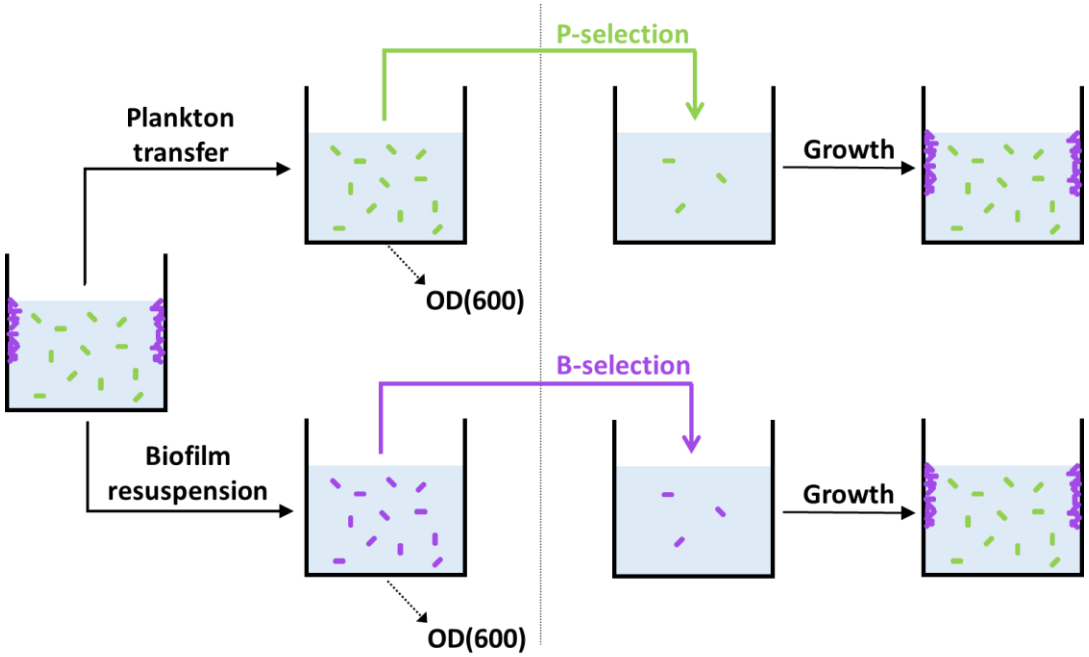

Figure 3.3: Passaging procedure for selection experiment. For each well, the biofilm (purple) and planktonic (green) fractions were separated and the OD(600) measured to estimate cell density in each fraction. After density estimation, *either* the planktonic *or* the biofilm fraction was passaged to the next round, depending on the regime to which a given well had been assigned (represented by dashed line – only one of the two fractions was passaged for any single well). Growth then allowed the populations to expand and differentiate, after which the process is repeated. Glass beads present in all wells are omitted for clarity.

3.3.2 Antibiotics

Working stocks of rifampicin (from 50 mg/mL in methanol), tobramycin (10 mg/mL in water) and meropenem (10 mg/mL in water) were filter-sterilized and pre-aliquoted to minimize freeze/thaw cycling that may affect activity during the passaging experiment. MICs for each were determined by growing the ancestral PAO1 overnight in LB containing various concentrations of each antibiotic (Figure S3.3). MICs were found to be 16 ug/mL for rifampicin, 2 ug/mL for tobramycin and 4 ug/mL for meropenem; these concentrations were used as the baselines for the passaging treatments (see below).

3.3.3 Treatments

A factorial combination of 3 antibiotics (rifampicin, tobramycin, and meropenem – chosen because they represent a hierarchy in the availability of resistance mutations, see main text), at 8 doses (0, 1/32, 1/16, 1/8, ¼, ½, 1, 2X MIC for each drug), and across two passaging regimes (biofilm or planktonic cells transferred) were used, each with four replicates, totaling 192 independently evolving lineages.

3.3.4 Data analysis

For each lineage, regression models (as quadratic, linear or intercept models, chosen on the basis of minimizing AIC (Akaike, 1981)) were fit to the blank-corrected optical density readings for each fraction (i.e. biofilm and planktonic OD) for every lineage as a function of passage number. Any negative values in the regression models were fixed at zero. The data for figures and downstream analyses were drawn from the predicted values of the fitted models to dampen effects of noise (primarily due to temporal fluctuations in the duration of growth periods, which ranged from 8.5 to 11.5 hours). The number of generations was estimated by summing $\log_2(\frac{OD_B+OD_P-OD_{inoculum}}{OD_{inoculum}})$ over the 20 passages. All statistical analyses were performed in R (R Core Team, 2015).

3.4 Results

3.4.1 No-drug control treatments

We first consider the non-antibiotic control lines to examine the base effects of the passaging regimes (Figure 3.4 R1, T1, M1). Under each regime, we see strong evidence for evolutionary responses in biofilm investment, as the fraction biofilm (i.e. the proportion of total cells allocated to the biofilm) does not remain static with successive passaging. In the planktonically-selected (P-selected, green) lines, we recover the expected result (based on previous theory in Chapter 2) of a rapid decline in the fraction of the population allocated to the biofilm to a low steady-state level.

The B-selected lines (purple) also behave generally as expected from theoretical predictions, showing a mild increase followed by a gradual decline in biofilm. An

increase in fraction biofilm when only biofilm cells are passaged is expected as cells adapt to the passaging environment, and our theory suggests the subsequent decline is due to the population relying on growth in the planktonic fraction for biofilm expansion rather than direct increases in colonization rates (Figure S3.1).

3.4.2 Role of plasticity

We can assess the extent of plastic tuning of the biofilm phenotype by examining how the degree of biofilm investment varies with increasing drug dose (Figure 3.5) after a single growth period. Under the 'damage sensing' hypothesis (Cornforth and Foster, 2013), one would expect the amount of biofilm to increase with antibiotic dose, up to some presumable limiting threshold. However, we did not find support for biofilm allocation being an increasing function of dose (Figure 3.5A); instead, we found allocation to be unresponsive with low doses, declining at intermediate doses, then rising again at the high doses, a pattern that can be roughly approximated by a cubic function in dose (Figure 3.5B). The specific antibiotics used did not have drastic effects on this overall trend, but tobramycin responded more robustly to increasing dose, while meropenem showed only minor changes. This pattern suggests low antibiotic concentrations inhibit biofilm colonization and/or promote dispersal from the biofilm, up until some threshold dose is reached, but above which the more intuitive outcome of increased biofilm formation in the face of an environmental threat is restored. This curious result requires further investigation, but is not of primary concern in this work.

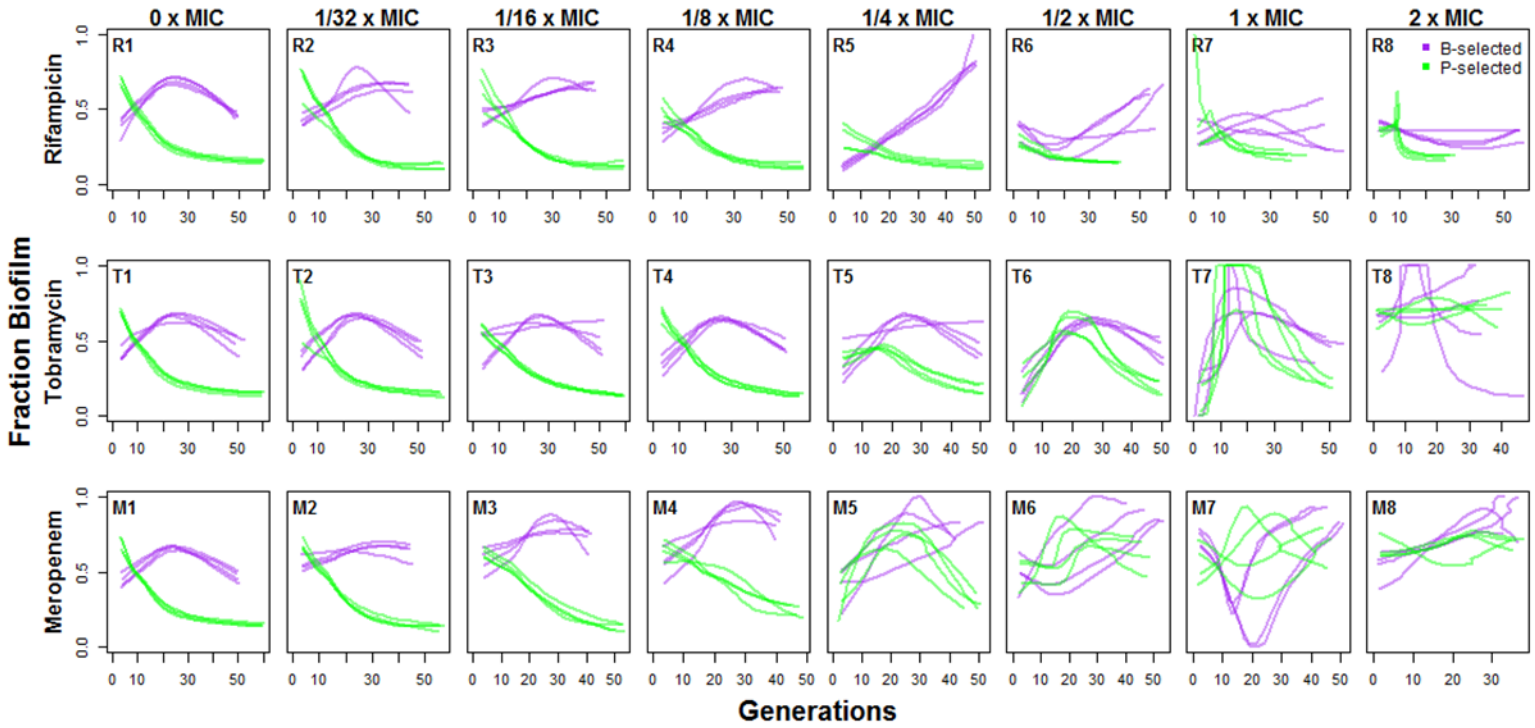

Figure 3.4: Evolutionary Trajectories of biofilm investment as a function of antibiotic and transmission regime. The fraction of biofilm cells relative to the total population is plotted against the estimated total generations over 20 passages. Each panel displays the trajectories for fraction biofilm as calculated from the predicted values of regression models fit to the OD measurements of each cellular fraction (see methods) for each of four independent replicate lineages, with color denoting the selection regime (purple, B-selected; green, P-selected), and rows corresponding to antibiotic, with dose increasing from left (no drug control) to right (2x MIC). Note the scale of the x-axis changes to better discern temporal patterns within trajectories with increasing dose.

A

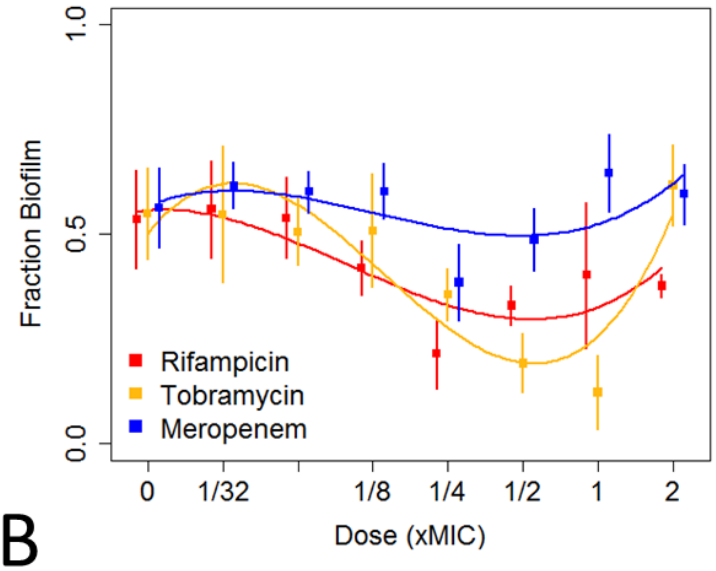

B

Residuals:	Min	1Q	Median	3Q	Max
	-0.33	-0.09	-0.01	0.10	0.68
Coefficients:					
	Estimate	**SE**	**t-statistic**	**p-value**	
Intercept	0.534	0.032	16.474	<2E-16	*
log.dose	0.069	0.030	2.298	0.023	*
log.dose^2	0.036	0.017	2.138	0.034	*
rif	-0.217	0.046	-4.744	4.26E-06	*
toby	-0.277	0.046	-6.035	8.85E-09	*
log.dose:rif	-0.013	0.043	-0.308	0.758	
log.dose:toby	0.096	0.043	2.255	0.025	*
log.dose^2:rif	0.007	0.024	0.280	0.780	
log.dose^2:toby	0.078	0.024	3.285	0.001	*
log.dose^3:mero	0.004	0.002	1.776	0.077	
log.dose^3:rif	0.004	0.002	2.041	0.043	*
log.dose^3:toby	0.013	0.002	6.109	6.05E-09	*

Residual standard error: 0.1498 on 180 degrees of freedom					
Multiple R-squared: 0.4262, Adjusted R-squared: 0.3911					
F-statistic: 12.15 on 11 and 180 DF, p-value: < 2.2e-16					

Figure 3.5: Plastic responses in biofilm formation are inconsistent with a pure damage-sensing response. **A**, Fraction biofilm is plotted for populations as a function of dose after a single growth period. Points indicate averages of eight replicates (as the transfer regime has not yet been imposed), error bars the 95% confidence intervals, and curves the predicted results of the model in B. Points are offset to reduce overlap. **B**, Regression of fraction biofilm on $\log_2$-transformed dose. The maximal model was fitted as fraction biofilm as a function of antibiotic and a cubic in $\log_2$(dose) with all two-way interactions, and simplified via removal of insignificant terms to maximize parsimony. Control treatments were modelled as the

next log-step down from the smallest antibiotic dose (i.e. $\log_2(1/32) = -5$, controls modelled as -6). Log transformation also means the intercept values reflect biofilm fraction at the 1xMIC dose.

We next ask whether and how plastic responses change during the course of evolution. Here the definitive experiments will involve the characterization of plastic responses to antibiotic challenge in intermediate and evolved clones. As a preliminary analysis, we focus on biofilm investment through evolutionary time (Figure 3.4). We predict that a purely plastic response to antibiotic challenge will be indicated by an initial period where biofilm fraction remains constant (i.e. is not influenced by the passaging regime), and this unresponsive period may be followed by a decline in fraction biofilm (due to a selective sweep by genetic resistance mutants) or continue for the duration of the experiment (in the absence of selective sweeps) (see Figure 3.2B).

Under the working definition for purely plastic responses presented above, we find that biofilm remains roughly constant more frequently at high doses of antibiotic (Figure 3.4 R8, T8, M8), but also sporadically at lower doses (for instance, Figure 3.4 R6, M2). Plastic responses occurring more frequently with high dose is consistent with the model in which plasticity facilitates adaptation under extreme challenge (West-Eberhard, 2003; Leggett *et al.*, 2014). However, the apparent evolutionary response under control conditions (discussed above) makes it impossible to assess the relative impacts of plasticity in biofilm formation at lower doses without further phenotypic investigation. In particular, it will be necessary to differentiate evolutionary responses to passaging and plastic responses to antibiotic treatment.

3.4.3 Evolution of biofilm resistance

Our model process indicates evolutionary adaptation in biofilm formation will manifest as sustained directional sweeps in fraction biofilm through time (Figure 3.2C), with changes in direction a potential result of evolution of genetic resistance

mutants under antibiotic challenge. We present evidence towards biofilm resistance evolution for each transfer regime in turn.

3.4.2.1 Planktonic selection under antibiotics

Under P-selection (Figure 3.4, green lines), when populations are exposed to antibiotics we observe clear evidence for the evolution of biofilm resistance as predicted in Figure 3.2C, with rapid directional changes in fraction biofilm through time. The direction of this change is dictated primarily by dose: with low doses (Figure 3.4 R1-4, T1-4, M1-2), the trajectories mirror those of the control lines with a rapid decline to minimal biofilm. With further increasing dose, however, we begin to see an increase in the fraction of the population allocated to the biofilm, in direct opposition to the effects of the base selection regime and indicating strong selective pressure for increased biofilm resistance. The presence and magnitude of an increase in fraction biofilm under P-selection is influenced by the specific antibiotic, generally being stronger under meropenem and tobramycin treatment, and weaker with rifampicin (Figure 3.6 ACE).

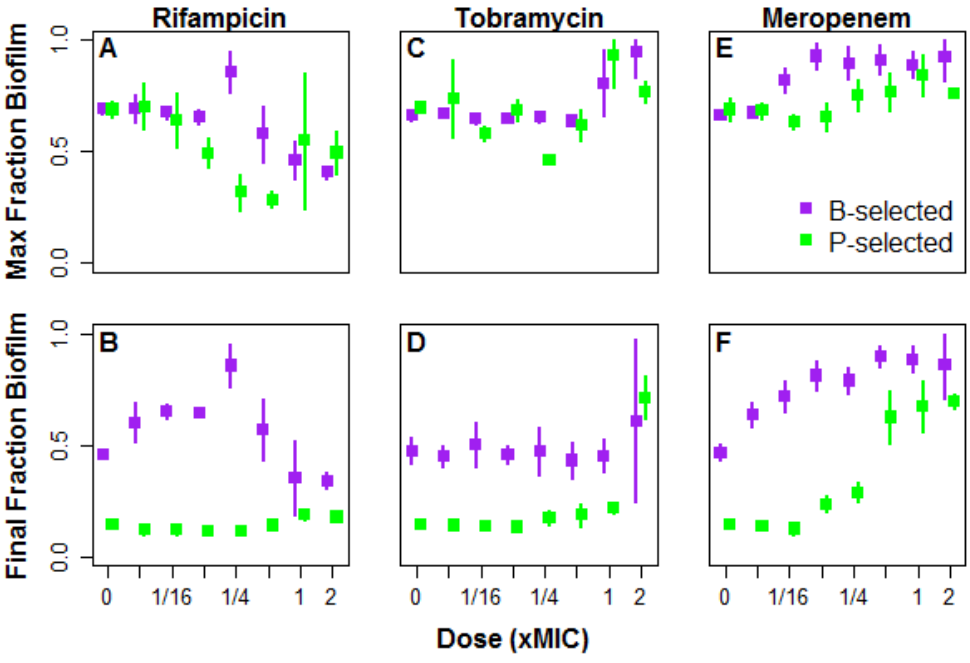

Figure 3.6: Both genetic and biofilm resistance evolution are responsive to antibiotic profile and transmission regime. The maximum in fraction biofilm

observed over the course of the experiment (A,C,E) and the fraction biofilm after 20 passages (B,D,F) are plotted as a function of antibiotic (A,B, rifampicin; C,D, tobramycin; E,F, meropenem), dose (x-axis) and transmission regime (green, P-selected; purple, B-selected). Points indicate averages of four replicate lineages with 95% CI error bars, and are offset to reduce overlap.

The increases also generally appear to be transient, with a decline in fraction biofilm following the initial induction period, leading to a hump shape in the evolutionary trajectories (Figure 3.4 R8, T5-7, M5-7; also compare the maximum fraction biofilm with the fraction biofilm at the end of the experiment in the top and bottom rows of Figure 3.6). Such abrupt transitions in the direction of the evolutionary response are consistent with the evolution of genetic resistance mutants changing the cost-benefit relationship of biofilm investment (Figure 3.2A). Under the model process outlined in Figure 3.2A, genetic resistance mutants would effectively nullify the resistance asymmetry between B and P cells under antibiotic treatment (i.e., rendering $a_1 = a_2 = 0$), and the direction of selection would therefore return to that as dictated solely by the transmission regime in the absence of drugs, in this case with a rapid decline in fraction biofilm (Figure 3.2C).

3.4.2.2 B-selection under antibiotics

When biofilm cells are passaged, we also observe changes in fraction biofilm consistent with evolution of increased biofilm resistance (Figure 3.4, purple lines). However, the pattern of the evolutionary trajectories shows a much stronger dependence on the specific antibiotic used, with tobramycin showing little response at all but the highest doses, while rifampicin and meropenem show more graded responses.

The temporal dynamics of biofilm allocation are again broadly consistent with the predictions in Figure 3.2C, with relative biofilm investment increasing with successive passaging, and more so with increasing doses of antibiotics (Figure 3.4, Figure 3.6 ACE, possibly excluding the case for high-doses of rifampicin, discussed further below). However, with antibiotic treatment it is less often the case that

increases in fraction biofilm are followed by a decline (as with the no-drug control lines); this is generally restricted to doses at or above 1x MIC. This is expected given the differences in selection regimes – under P-selection, genetic mutants are able to exploit the fraction favored for transmission, and therefore genetic resistance mutants will enjoy a massive fitness benefit; conversely, B-selection favors transmission of mutants with enhanced biofilm resistance, thereby greatly reducing the fitness benefits associated with genetic resistance. One curious exception to this trend occurs at higher doses of meropenem under B-selection (Figure 3.4 M7; also potentially much less dramatically with rifampicin in Figure 3.4 R8), where the opposite transition occurs, with fraction biofilm initially plummeting, followed by a rapid increase. This trend may reflect the action of meropenem reducing the efficacy of biofilm colonization, followed by an adaptation restoring colonization ability (unlikely, but see below), or may simply be an artifact of extremely low cell densities (Figure S3.2) – in either case, further investigation towards this anomaly is warranted.

3.4.3 Conditions favoring phenotypic and/or genetic resistance

We hypothesized that the conditions favoring biofilm resistance would be sensitive to environmental factors (B or P transmission routes, antibiotic dose) and also to the genetic details of resistance – in particular, the availability of resistance mutations and the fitness costs they impose.

The antibiotics used in this study (rifampicin, tobramycin and meropenem) were chosen as they represent a hierarchy in the availability of resistance mutations. Rifampicin is expected to have a comparative abundance of available resistance mutations, as numerous SNPs can provide resistance (Qi *et al.*, 2016). Tobramycin requires multiple mutations to accumulate to confer appreciable resistance (El'Garch *et al.*, 2007), making resistance to tobramycin less genetically available than rifampicin resistance. Finally, meropenem is expected to be the most difficult target for resistance to evolve, as multiple specific mutations are required to confer resistance (Pai *et al.*, 2001; Rodríguez-Martínez *et al.*, 2009). During the subsequent sequencing

and phenotypic characterization phase of this project, we will examine the evidence towards this hierarchy in our results.

As an initial survey, we address which apparent resistance mechanisms are favored by examining the experimental outcomes for each treatment in turn.

3.4.3.1 Rifampicin

We expected rifampicin to be relatively easier to evolve genetic resistance mechanisms, and our experimental results are largely consistent with this, especially under P-selection. Lines exposed to rifampicin showed the smallest relative investment towards the biofilm (Figure 3.6A). Only under rifampicin treatment did P-selected lines universally display patterns consistent with evolving genetic resistance mechanisms (Figure 3.6B). However, we also observed strong induction of biofilm resistance investment with rifampicin treatment (Figure 3.4 R2-6), and although biofilm investment is relatively low under B-selection with high doses of rifampicin (Figure 3.6A), the trajectories are not consistent with selective sweeps of genetic resistance mutants (Figure 3.4 R7-8, Figure 3.2C).

Notably, rifampicin treatment was unique in that B- and P-selection showed sharply divergent outcomes in total growth (Figure 3.7A), with the total number of generations achieved under B-selection far exceeding P-selection treatments with increasing dose (nearly double at 2x MIC). Indeed, under B-selection net growth increases by 2.2 generations with each increasing step in rifampicin dose (regression of generations on $\log_2$-transformed dose excluding control treatments; SE=0.22, $p=3.56*10^{-10}$). The combined results of low levels of biofilm investment and increased total growth suggest proliferation of more rapidly dividing genetic resistance mutants, but because the evolutionary trajectories in Figure 3.4 do not reflect this further work will be required to understand why larger doses of rifampicin accelerate growth under B-selection.

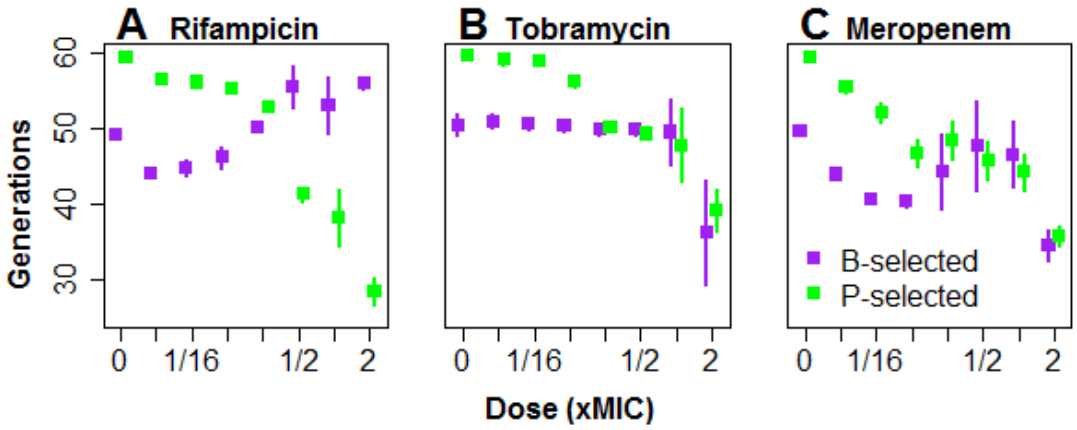

Figure 3.7: Growth advantage of P-selection diminishes with increasing antibiotic load and decreasing availability of resistance mutations. Total growth over the course of the experiment (estimated generations) is plotted as a function of dose (**A**, rifampicin, **B**, tobramycin, **C**, meropenem) and selection treatment (green, P-selected, purple, B-selected). Points display averages across four replicates in each treatment group with 95% CI error bars, and are offset to reduce overlap.

3.4.3.2 Tobramycin

Tobramycin was expected to be a middle-ground in terms of ease of resistance evolution. Consistent with this, we observed that tobramycin treatment induced greater allocation to the biofilm than rifampicin, but less than meropenem (Figure 3.6C). Additionally, under P-selection genetic resistance appears to readily evolve, but not to the highest dose (Figure 3.6D). Unexpectedly, the responses to tobramycin were largely unaffected by dose (Figure 3.6CD; also Figure 3.7B, primarily under B-selection); only at the highest concentrations (at least 1x MIC) was an appreciable effect observed (as an increase in the maximum fraction biofilm and a decline in final fraction biofilm). Further investigation of the genetic changes accrued across doses of tobramycin will help to better discern the mechanisms of resistance – specifically, in attempts to differentiate whether 1) biofilm provides sufficient resistance to tobramycin, leading to a constant level of biofilm across low to intermediate doses; 2) if genetic resistance mechanisms evolved in a dose-dependent manner, and the fraction biofilm remaining constant is largely coincidental or a simple byproduct of

the passaging regime; or 3) if a single resistance mechanism evolved that imposed a dose-dependent cost, for example upregulation of an efflux pump with an upper threshold in the concentration of antibiotic it could mitigate.

Interestingly, the evolutionary response to tobramycin also tentatively suggests that biofilm resistance may facilitate genetic resistance, in that the trends in final fraction biofilm between selection regimes appear to 'cross' between 1x and 2x MIC (Figure 3.6E). However, we note the high degree of variation between replicates at high doses makes it difficult to discern such general trends, and again genetic information may help to explain some of this variance; further passaging would also be of use to determine if it is indeed the case, as Figure 3.4 T8 suggests trajectories consistent with resistance evolution are much more common under B-selection. Overall, these results suggest a closer balance between the costs of biofilm and genetic resistance pathways to tobramycin treatment, with biofilm resistance favored more broadly across both dose and selection regime, but with genetic resistance still often selected for.

3.4.3.3 Meropenem

We hypothesized that meropenem would be the most difficult drug for genetic resistance to evolve, due to its proposed two-step mechanism (Pai *et al.*, 2001; Rodríguez-Martínez *et al.*, 2009). Our results were again consistent with this expectation, as meropenem treatment resulted in the greatest increase of biofilm, the least indication of genetic resistance, and the strongest response to increasing dose (Figure 3.6EF), and little evidence consistent with selective sweeps towards planktonic growth in the evolutionary trajectories (Figure 3.4 M2-8, with the possible exception of 1/4xMIC in Figure 3.4 M5); these observations will be corroborated with further phenotypic and sequence analysis. With the apparent rarity of resistance mutations, we find that biofilm resistance is then of primary importance to growth and survival under meropenem, as evidenced by the strong increase in biofilm formation even under P-selection (Figure 3.6E) and the convergence of total growth achieved under B- and P-selection at much lower doses (Figure 3.7C).

3.4.4 Concluding remarks

Considering these preliminary results of all treatment combinations, we propose the following working model for the evolution of biofilm resistance and its interaction with the evolution of genetic resistance mechanisms (Figure 3.8). We expect biofilm resistance to be favored essentially whenever an antibiotic challenge is encountered. Whether such a response proliferates, resulting in an increase in investment towards the biofilm, will depend on the relative costs and benefits associated with genetic resistance. If genetic resistance is relatively accessible (equivalently, for example, numerous mutation sites and low metabolic costs, or higher metabolic costs coupled with selection biased against biofilm resistance), it will evolve readily and proliferate within the population (Figure 3.8, blue line; similar to the case of rifampicin treatment and P-selection). If genetic resistance is relatively inaccessible (influenced jointly by the rarity and cost of resistance mutations), the relative strength of selection (mediated by drug dose as well as whether the selective regime facilitates or antagonizes biofilm resistance) will determine whether genetic resistance evolves. At low to intermediate selective pressures, the metabolic costs of genetic resistance prevent mutants from proliferating within the population, and biofilm resistance dominates (Figure 3.8, gold line; similar to the case of low dose rifampicin under B-selection). Under severe selection pressures, even mutants carrying extreme metabolic deficiencies will enjoy a reproductive benefit and proliferate, thereby reducing or eliminating the need for cellular allocation to biofilm resistance; here, biofilm resistance mutations will likely accumulate until a suitable genetic resistance mutant evolves (Figure 3.8, red line; similar to the case of high-dose tobramycin under P-selection, and potentially the case with meropenem treatment as well, where further passages my eventually yield genetic resistance mutants and a consequent drop in relative biofilm investment).

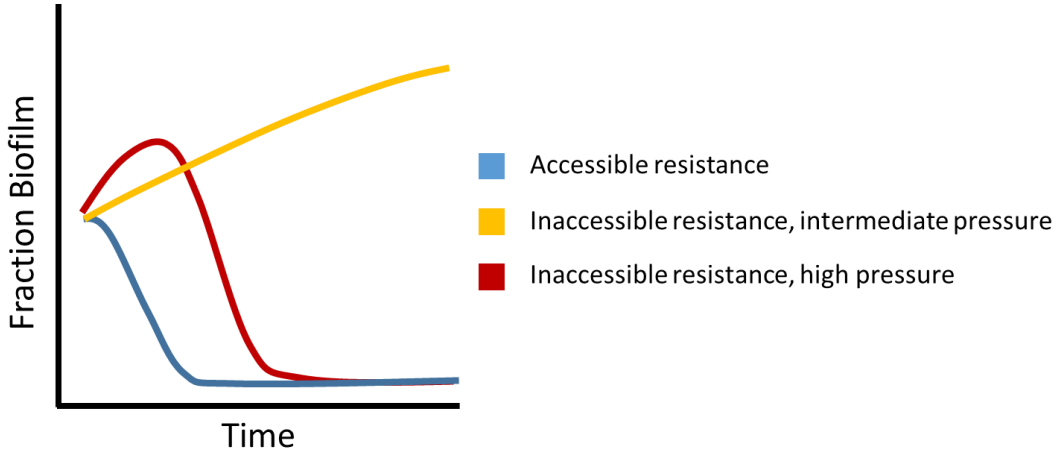

Figure 3.8: Biofilm resistance is maximized at intermediate selection pressure. Low cost resistance mutants quickly proliferate, reducing relative allocation to the biofilm within the population. Higher cost mutants will tend towards biofilm resistance, with genetic resistance subsuming the phenotypic response when the antibiotic pressure is sufficiently severe.

3.5 Discussion

By monitoring the allocation of cellular resources within populations of *P. aeruginosa* experimentally evolved under various passaging and antibiotic treatment regimes, we found preliminary evidence suggesting that biofilm resistance can evolve much that same way direct genetic resistance mechanisms evolve. Increasing biofilm resistance, as measured by allocation of cellular resources towards biofilm formation, showed dependence upon the specific costs of resistance in the environment: we found that it was favored under nearly all cases with B-selection, and at higher antibiotic dose with P-selection. Furthermore, and especially so at high doses, increasing biofilm formation was often transient, followed by a relatively steep decline in biofilm. This pattern is consistent with the evolution of genetic resistance mutants, which gain a fitness advantage due to their ability to better exploit the planktonic phase where more rapid cell division can occur. Indeed, patterns in the dynamics of biofilm formation through time suggested the biofilm resistance may facilitate genetic resistance evolution – however, further phenotypic and sequencing

analysis is necessary to confirm observations relating to the evolution and spread of genetic resistance.

Our data also suggest that induction of biofilm resistance is highly sensitive to the specific environmental conditions, with induction being more likely when biofilm cells provided reproductive value to the population at intermediate costs of antibiotic treatment, or at high cost of antibiotic treatment when planktonic cells were transmitted. These results are broadly consistent with a model in which biofilm resistance is favored when the costs of genetic resistance mutations are inflated relative to the growth benefits they provide, which can arise either when the drug dose and transmission regime are such that genetic resistance provides little net reproductive benefit to the population, or when genetic resistance mutations are rare, in which case biofilm resistance mechanisms will proliferate transiently until a suitable genetic resistance mutant evolves and subsequently sweeps through the population.

We observed that in response to antibiotic treatment, plastic phenotypic responses lead to declining biofilm formation with increasing dose, until an apparent threshold was reached, upon which it rebounded to levels on par with the no-drug control response. Given that previous theory (Cornforth and Foster, 2013) and observation (Oliveira *et al.*, 2015) have linked damage with increasing biofilm formation, we reason that our observations are due to higher overall concentrations of antibiotic being used. For instance, rifampicin, shared in both studies experimental studies, was found to reduce biofilm formation quite severely at doses over 2 ug/mL in (Oliveira *et al.*, 2015), which corresponds to the 1/8xMIC dose in this work. Our results then indicate that plastic responses to antibiotic treatment may rebound at higher doses, suggesting either multiple regulatory mechanisms may govern this response, or alternatively that growth is suppressed severely enough to essentially prevent any plastic response.

The apparent evolutionary tuning in the biofilm resistance response to antibiotics suggests this is an important part of the general resistance response to antibiotic

treatment. That biofilm formation provides general resistance to non-antibiotic threats such as phages and immune effectors is particularly troubling, as it suggests evolutionary responses to any of these factors may increase resistance to all of them. This points to biofilm formation as a leading candidate for the development of so-called 'antibiotic adjuvants' (Gill *et al.*, 2014), which disrupt various cellular processes or phenotypes and thereby increase efficacy of co-administered antibiotics.

We conclude by reiterating that these data report preliminary findings and are still awaiting validation via further sequencing and phenotypic analysis. In particular, screening apparent genetic resistance mutants for increased MIC along with sequencing analysis will be crucial to validate and understand the dynamics of genetic resistance evolution in the context of simultaneous biofilm resistance evolution. We will also seek to better understand the role of plasticity over evolutionary time by screening relative biofilm investment in evolved isolates under conditions different from those to which they have adapted (e.g. both higher and lower doses of antibiotics).

However, we note that further study will be necessary to validate our observations. In particular, sequencing data will be essential to shed light on the mechanisms by which biofilm resistance evolves in response to antibiotic treatment, as well as to corroborate our observations on the timing of the evolution of genetic resistance mutants. Phenotyping evolved isolates, in particular their allocation response in the absence of drug treatment, will also help to shed light on the nature of the plastic response in biofilm allocation.

3.6 Supplemental Data

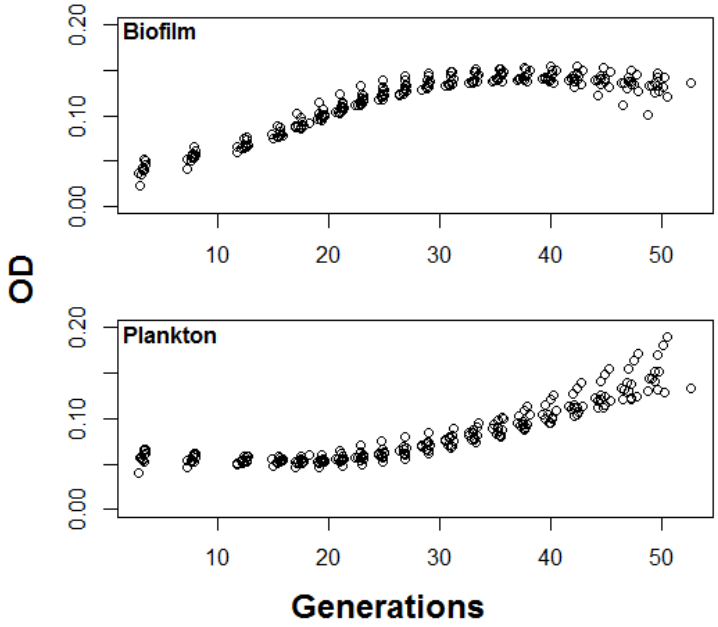

Figure S3.1: Accumulation of biofilm cells is driven by planktonic reproduction in the absence of antibiotic. The ODs of each cellular fraction are plotted as a function of estimated generations (i.e. evolutionary time) under B-selection and in the absence of antibiotic. In the first half of the experiment, biofilm increases while planktonic density remains roughly constant, and this pattern reverses in the second half of the experiment.

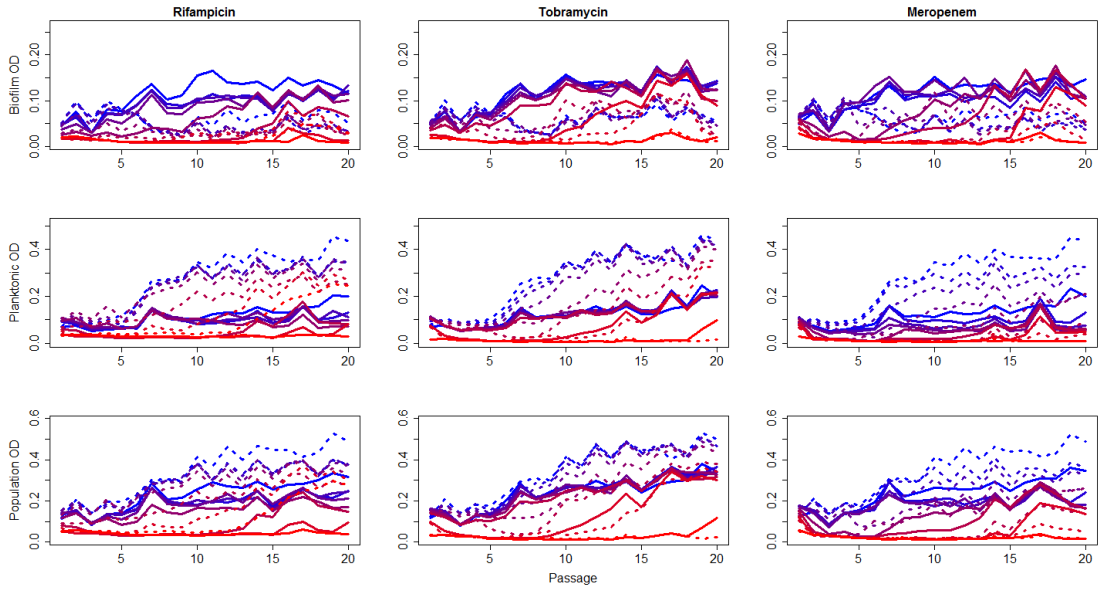

Figure S3.2: Population ODs through time (by passage, i.e. chronological time). OD at the conclusion of each growth cycle is plotted as a function of passage number for each treatment combination. The different populations are in each row, and columns denote antibiotics used. Dose is indicated by color scale (blue, 0xMIC, red, 2xMIC), and dashed lines indicate P-selection, while solid lines indicate B-selection.

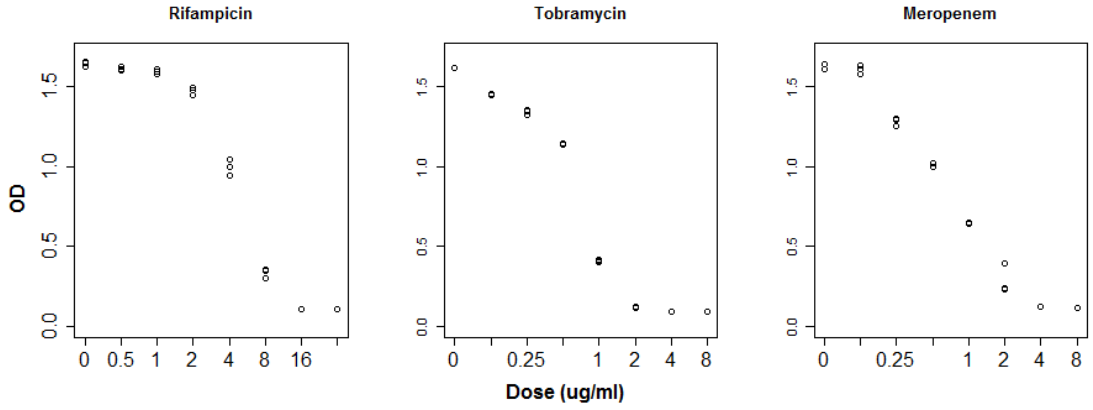

Figure S3.3: MIC determination of antibiotics used in this study. PAO1 was grown for 24 hours in LB containing antibiotic, and the OD measured to estimate cell density. MICs were determined as 16 ug/mL for rifampicin, 2 ug/mL for tobramycin and 4 ug/mL for meropenem; these concentrations were used as the baselines for the passaging experiments.

4 Persistence is age-independent in *E. coli*

Nicholas Lowery & Sam P. Brown

4.1 Abstract

Bacterial persistence, in which a small subpopulation of bacterial cells shows a greatly reduced degree of killing by antibiotic treatment without any means of genetic resistance, has become increasingly recognized as a contributing factor to recalcitrant bacterial infections. The low frequency of persister cells and apparent redundancy in genes associated with persistence has hampered attempts to understand the mechanisms governing their formation. While important progress in this regard has been made, virtually all models of persister formation rely to some extent on stochastic metabolic disruption as the key progenitor leading to the focal cell becoming a persister. Noting significant overlap between phenotypic markers of persistence and the markers of aging in bacteria, we hypothesized that persister formation may be deterministically influenced by the age of the individual cell, with older cells more likely to become persisters. However, using FACS to sort *E. coli* cells based on a fluorescent marker of cellular age, we found no relationship between age and persistence when cells were exposed to varying doses of ampicillin. Nevertheless, we note that in general demographic determinants are a largely unexplored set of factors that may potentially influence persister formation, and may yet prove fruitful in our understanding of the causes of persistence and other phenotypes, especially as the techniques available to probe populations at the single-cell level improve.

4.2 Introduction

4.2.1 Mechanisms of Persistence

Bacterial persistence refers to the phenomenon by which a small subpopulation of cells survive treatment with antibiotics for a prolonged period of time, and in the

absence of any mechanism of genetic resistance (Figure 4.1). Such cells are problematic, as they allow infectious bacteria to 'wait out' treatment regimes, then resume growth when the antibiotic has been removed, contributing to recurrent and recalcitrant infections, as well as increasing the mutational supply for the evolution of genetic resistance mechanisms (Lewis, 2010).

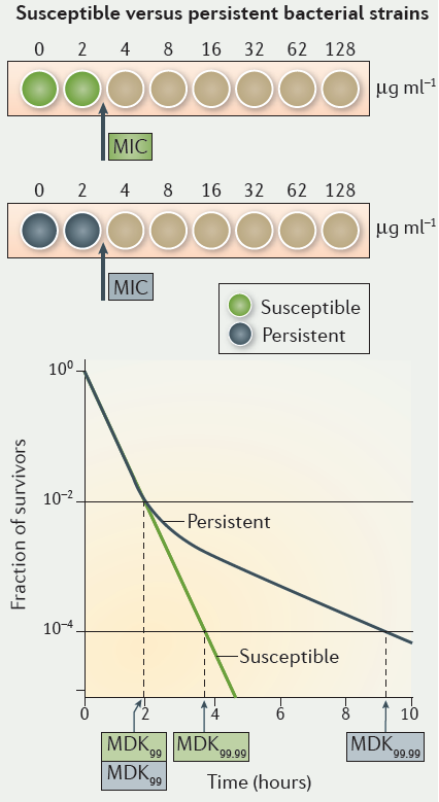

Figure 4.1: Biphasic death curves define persister cells. Figure adapted from (Brauner *et al.*, 2016). Persistent cells show no differences in antibiotic resistance as measured by MIC testing, but display a characteristic biphasic death curve in which a small fraction of the original population persists for a prolonged period under antibiotic treatment.

The mechanisms of persistence are beginning to be unraveled. In general, it is thought that persistence occurs when a cell enters a transient dormant or slow-growing state via stochastic metabolic dysregulation (Keren *et al.*, 2004b), which can occur via several pathways. Perhaps the best understood of these routes to

persistence is via induction of toxin-antitoxin (TA) modules. Bacteria carrying TA modules produce two antagonistic compounds, a toxin and an anti-toxin. In healthy cells, the toxin is neutralized by an antitoxin that is continually produced, protecting the cell from self-harm. However, a transient drop in the labile antitoxin production allows the more stable toxin to become active, thereby forcing the cell into a metabolically stunted or inactive state; genetic manipulations of this system can induce orders of magnitude differences in levels of persistence (Lewis, 2010; Wood *et al.*, 2013; Maisonneuve *et al.*, 2013a).

Bacterial stress responses have also been implicated in persistence. In *E. coli*, when the stress response genes RelA and SpoT are induced via multiple stress pathways, the alarmone guanosine tetraphosphate (ppGpp) is produced (Gerdes *et al.*, 2005), which goes on to induce further downstream stress regulators such as RpoS (among others), but has also been linked to the efficacy of cellular endotoxins and persistence in a number of systems (Aizenman *et al.*, 1996; Korch *et al.*, 2003; Amato and Brynildsen, 2014; Maisonneuve *et al.*, 2013a). However, because stress responses often act to temporarily slow or stop cellular division, the pathways and causal effects governing the formation of persister cells retain a high degree of redundancy, and the specific mechanisms and definitions differentiating stress from persistence are still being unraveled.

4.2.2 A Role for Aging?

While persistence was first noted shortly after the discovery of antibiotics (Bigger, 1944), aging in bacteria was observed relatively recently. Ackermann (2003) first observed a decline in the reproductive rate of asymmetrically dividing *Caulobacter crescentus* cells, where the stalked mother cells showed a gradual decline in the rate of reproductive events with each successive generation. Shortly thereafter, Stewart et al. (2005) observed a similar effect in symmetrically dividing *E. coli* cells. In *E. coli* and all (roughly) symmetrically dividing organisms, the age of an individual is commonly conceptualized as the age of subcellular components, and can vary depending on whether a given component is created *de novo* or inherited from the

parent during the division cycle. In Stewart et al., the authors focused on the age of the cell poles, with each daughter cell inheriting an 'old pole' and synthesizing a 'new pole' from the fission site. As a colony grows, a distribution of pole ages naturally emerges, and Stewart et al. (2005) found that cells with older poles divided more slowly. Further work showed that this aging effect correlated with the presence of insoluble protein aggregates which were primarily inherited along with the 'old pole' (Lindner *et al.*, 2008). In other experimental systems, aging *E. coli* cells were also more likely to induce stress responses such as SOS and filamentation (Wang *et al.*, 2010).

The significant overlap between phenotypes associated with persistence and aging (reduction in growth rate, induction of stress responses, increased protein aggregation (Leszczynska *et al.*, 2013)) in bacteria led us to hypothesize that aging processes may have causal effects on the formation of persister cells, a result that has also been postulated from a theoretical standpoint (Klapper *et al.*, 2007). This would offer an alternative and deterministic explanation for the current understanding of stochastic formation of persister cells, in that persister cells could simply be the oldest subpopulation of cells, or more likely that the phenotypic switch governing persister formation is weighted by the age of the cell. In any case, any indication of non-random induction of the persister phenotype would be informative to further studies of the persister mechanism and towards methodologies to combat the clinical problems persisters present.

We therefore sought to experimentally test whether aging, as defined by an intracellular aggregate marker (Lindner 2008), influenced levels of persistence in *E. coli*. We found, however, that there was no difference in the frequency of persister cells in populations enriched in either old or young cells, in support of current models of stochastic induction of the persister phenotype.

4.3 Methods

To discriminate among age classes within a population, we utilized the MGAY strain of *E. coli* (Lindner *et al.*, 2008), kindly provided by Ariel Lindner. MGAY contains a YFP tag conjugated to IbpA, a protein which binds to and stabilizes protein

aggregates. Because these aggregates accumulate and are preferentially inherited by the 'old pole' cells, the magnitude of the YFP signal correspondingly increases as cells age. This fluorescent tag was used to segregate populations of old and young cells via FACS.

For each of two independent replicate MGAY populations (grown to mid-exponential phase in 5mL LB broth), 500,000 candidate 'old' cells (brightest ~10% of the YFP distribution) and 500,000 candidate 'young' cells (dullest ~10%) were sorted into fresh LB medium in a 24-well plate. These thresholds were chosen as they allowed for sufficiently large populations to be sorted in less time than a typical division cycle in *E. coli* (roughly 20 minutes), as any cell division will immediately begin to break down the stratification in age. Each of the sorted populations was divided into nine replicate 200 uL aliquots in a 96 well plate. A sample from each population was plated on LB agar to determine pre-treatment CFU, then LB containing ampicillin was added to a final concentration of 1, 10 or 100 ug/mL in each of 3 replicates, yielding 36 final populations (2 initial populations x 2 age treatments x 3 ampicillin doses x 3 replicates). After one hour incubation at 37 °C with shaking, another sample was plated on LB agar to determine persister frequency. All results are reported as fractional survival compared to the pre-treatment measures.

4.4 Results

We found no difference in persister frequencies in age-segregated subpopulations of *E. coli* (Figure 4.2). No significant differences were detected between old and young cells overall or in a dose-dependent manner (Table 4.1), and similar results were obtained in a replicate experiment in which cells were exposed to a higher dose of ampicillin as well (Figure S4.1).

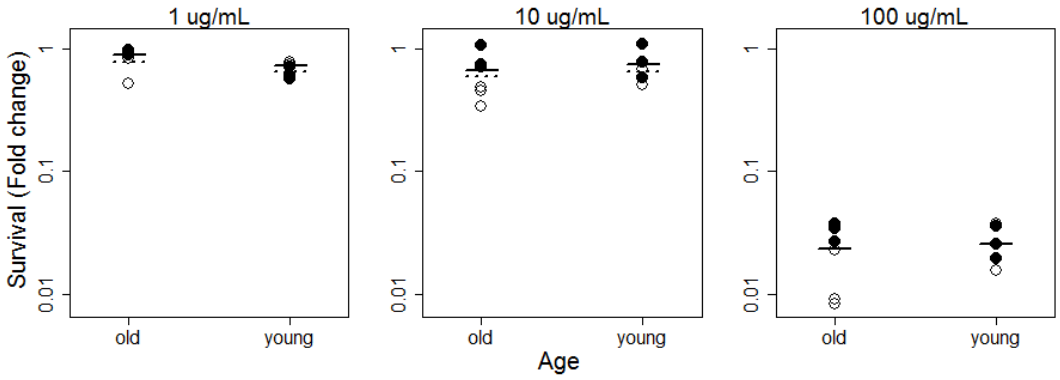

Figure 4.2: Persistence is age-independent. No significant differences were detected between old and young cells after antibiotic treatment with regards to the fraction of surviving populations when plated on LB agar. Antibiotic dose is indicated in the title of each panel, and the two replicate populations are indicated by filled vs. empty circles. Points are individual replicates and lines indicate predicted values from model fit.

Table 4.1: GLMM of survival as a function of age and antibiotic treatment. A generalized linear mixed model (GLMM) was fit to the fold change in survival across age class, dose, and their interaction (to test for dose-dependent effects) as fixed effects, and the replicate populations as a random effect. A gamma error structure with the inverse link function was used to account for variance increasing with the estimate of the mean under a given condition; note the reported estimates must be back-transformed (inverted) to return the scale of the original data, as was done for Figure 4.2. The intercept indicates the estimate for old cells exposed to 1 ug/ul ampicillin, and the remaining estimates indicate deviations from the intercept. Significant effects are highlighted in bold.

Fixed effects:	*Estimate*	*SE*	*p-value*
(Intercept)	**1.21**	**0.21**	**1.28E-08**
young	0.25	0.24	0.308
dose10	0.38	0.26	0.139
dose100	**41.76**	**5.66**	**1.62E-13**
young:dose10	-0.40	0.37	0.28
young:dose100	-4.05	7.66	0.597

For age structure to have no effect on levels of persistence is surprising, as aging in *E. coli* leads directly to phenotypes associated with increased levels of persistence. It may be the case that physiological effects due strictly to age are confounded with

other factors influencing persistence, for instance nutrient depletion and the accumulation of toxic byproducts from cellular division and metabolism, or accumulation of spontaneous mutants that occur with every division cycle and may affect persister frequency. However, we attempted to minimize effects of environmental degradation in this experiment by keeping growth times short and cell densities relatively low (see Methods). We also found that simple simulation models indicate that the evolution of mutant lineages predisposed to persistence would have a negligible effect on overall persister frequency at these time scales (Supplemental Data, Figure S4.2).

4.5 Discussion

The results of our experiment suggest that persistence is independent of age in *E. coli*, using protein aggregation as a marker for cellular age. However, we limited this experiment to a single time point, and one of the hallmarks of the persister phenotype is a biphasic survival curve under antibiotic exposure (Keren *et al.*, 2004a; Brauner *et al.*, 2016). We attempted to account for this by exposing age-stratified populations to varying doses of antibiotic, thereby manipulating the slope of the killing curve, but it may be the case that monitoring survival through time rather than dose may reveal more subtle effects of aging on tolerance that were not observed here.

It may also be the case that our age stratification of the brightest ~10% of the original population was insufficiently stringent to detect age-dependent effects, but further purifying cells based on FACS methods may be difficult to achieve. Narrowing the age spectrum (for instance to the oldest 1%) while maintaining sorting accuracy would come at the cost of either increased sorting time or decreased population sizes. Increasing the sort time will also increase the time that cells have to start growing before pre-treatment samples can be taken and antibiotics added, thereby disrupting the imposed age stratification. On the other hand, decreasing the population size will increase the effects of noise in persister frequency; this could in turn be mitigated by increasing the number of replicates, but the problem of increased time before treatment again becomes the issue. Our protocol was chosen in attempts to optimize

across these trade-offs in speed and accuracy, but it may be of interest to return to these experiments if improved FACS technology (or indeed alternative methods of cell sorting) become available.

The MGAY strain of *E. coli* relies on protein aggregation as a correlate of age (Lindner 2008), and our results indicate protein aggregation does not play a causal role in the formation of persister cells. However, others have found a correlation between protein aggregation and persistence (Leszczynska *et al.*, 2013) at stationary phase, suggesting that persistence may be induced by protein aggregates that do not associate with IbpA (the labelled protein of the MGAY strain), or alternatively that persistence is induced at a step upstream in the aggregation pathway, and other factors (such as growth phase, a major difference between this study and that of Leszczynska et al.) may determine whether aggregation does or does not correlate with persistence.

Overall, this result agrees with the current hypothesis of stochastic metabolic dysregulation as the underlying mechanism of persister formation, as we failed to find any evidence for an effect of age on persister frequency. However, this result does not preclude the effects of other demographic determinants of persistence, and whether or not persister formation is truly stochastic remains an open question. The classic methodology for testing for lineage vs. stochastic effects would be a fluctuation test (Luria and Delbruck, 1943), but our models (Supplemental text, Figure S2) suggest such experiments would not be informative due to the inherently slow or non-existent growth rate of the phenotype of interest. Nevertheless, tests for other demographic factors (e.g. cell size, other types of inclusion bodies, etc.) may yet provide new insights into the genetic and metabolic aspects contributing to levels of persistence in bacteria, especially as methods for analysis of microbial populations at the single cell level improve.

4.6 Supplemental Data

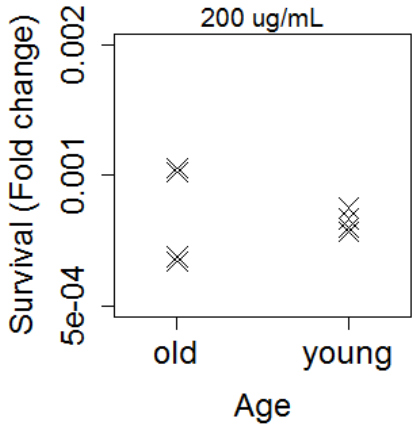

Figure S4.1: Persistence is age independent. Replicate experiments at a higher dose (200 ug/mL ampicillin) showed no effect of age on frequency of persistence (Welch 2-sample t-test, t = 0.45, df = 3.23, p = 0.68). In these experiments, the same protocol as in the methods was followed, except 100,000 cells were sorted into each candidate age fraction from four independent replicate MGAY populations.

4.6.1 Supplemental Text: Modelling predisposition to persistence

Could de novo evolution of a mutant lineage with increased levels of persistence have an effect on the overall persister frequency of the population in our experiment? If such a mutant were to have an appreciable effect on persister frequency, A) populations harboring mutant lines must have higher frequencies of persistence, and B) within populations harboring mutants, the frequency of persistence will correlate negatively with the time until the mutant appears, i.e. mutants appearing early on will generate more persister cells by the end of the experiment.

To test our assumption that such a lineage would not have any effect on our experiments, we performed a simple individual-based simulation of a growing population of cells (Figure S4.2A). Cells can have one of two genotypes: wild type dividing cells (G1), mutant dividing cells (G2). At each time step, all growing cells (G1 and G2) divide, with the genotypes of the mother retained by the daughters. After division, each cell can then mutate and switch its genotypes, or switch its phenotype to a persister cell (P) which then remains dormant for the duration of the simulation. G1 cells can become persisters at rate k_1, or mutate to G2 cells at rate m;

G2 cells can become persister cells at rate k_2, and we assume no reversion of mutants or persisters. The results of the simulations are displayed in Figure S4.2.

We found that populations in which no enhanced-persistence mutants arose actual had a small but significantly higher fraction of persisters (Figure S4.2B, Welch 2-sample t-test, 95% CI for difference in means = (5.65×10^{-7} – 6.08×10^{-6}), p = 0.019), and in Figure S4.2C, we see that no correlation exists between the time it takes for mutants to evolve within the population and the fraction of persisters in the final population (95% CI for Pearson correlation coefficient = (-0.32, 0.17)). We therefore conclude that our experimental assumption that de novo evolution will have a negligible effect under these conditions is valid.

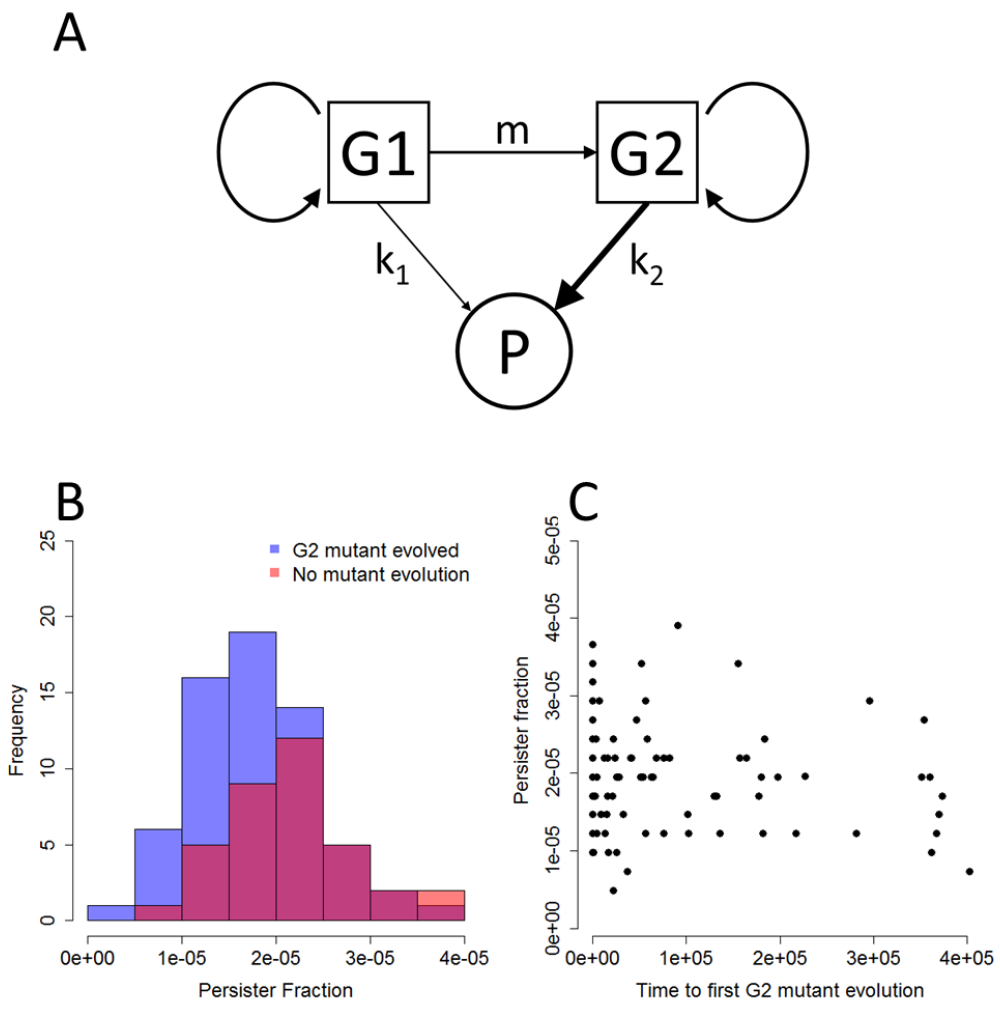

Figure S4.2: Individual based simulations of persister population dynamics. 100 replicate simulations of the evolution of a mutant lineage with enhanced frequency

of persistence. **A**, Model schematic. **B**, Distribution of persister fractions across replicates, with blue bars indicating simulations where a G2 mutant evolved at some point, and red bars indicating cases in which no G2 mutants arose. **C**, Time to G2 mutant evolution as a predictor of persister fraction in the final population. Simulations were inoculated with 100 G1 cells, and allowed to grow for 12 generations, with $k1 = 10^{-5}$, $k2 = 10^{-3}$ and $m = 10^{-6}$. The mutation rate was chosen to ensure mutants would evolve in a reasonable fraction of replicates, as the goal of these simulations is to determine whether such a mutant would be detectable in the analogous wet-lab experiment.

5 A global survey of phenotypic diversity in the opportunistic pathogen *Pseudomonas aeruginosa*

Nicholas Lowery & Sam P. Brown

5.1 Abstract

It is well established that different strains of the opportunistic pathogen *P. aeruginosa* can display impressive variation in clinically relevant phenotypes such as virulence factor production and antimicrobial resistance. However, the extent to which this variation is constrained by environmental origin and tradeoffs among traits remains largely unexplored, especially so when considering strains isolated from outside the cystic fibrosis (CF) lung environment. In this work, we seek to address this gap by surveying a broad suite of phenotypes related to growth, antibiotic resistance, biofilm formation and virulence factor production across a diverse library of 230 clinical and environmental isolates of *P. aeruginosa*, and ask to what extent higher-level organizing principles influence patterns of phenotypic expression? We observed an impressive diversity across all phenotypes measured, with little evidence of dependency on environmental origin or tradeoffs among traits. Strains sampled from the lung of CF patients illustrated the greatest phenotypic bias, with CF strains typically slower growing, forming biofilms containing more extracellular DNA, and preferentially expressing the siderophore pyochelin. However, environmental source only explains a small portion (much less than 25%) of total phenotypic variation. Ongoing genomic sequencing analysis will provide greater insights into the sources of phenotypic diversity across *P. aeruginosa*, including the ability to partition the role of phylogeny in shaping phenotypic diversity.

5.2 Introduction

Pseudomonas aeruginosa is an important nosocomial pathogen, imposing a growing health burden due to its environmental ubiquity, intrinsic resistance to antibiotic

treatment, and ability to form highly recalcitrant biofilms. The domesticated lab strain, PAO1, is a popular model organism for studies of bacterial social behaviors (Diggle *et al.*, 2007b, 2007a; Wilder *et al.*, 2011; West *et al.*, 2006), biofilm formation (Popat *et al.*, 2012; Wei and Ma, 2013; Rice *et al.*, 2009; Wang *et al.*, 2014; Barraud *et al.*, 2009), and pathogenicity (Köhler *et al.*, 2009; Rice *et al.*, 2009; Jimenez *et al.*, 2012; Rumbaugh *et al.*, 2009). *P. aeruginosa* also shows capacity for rich behavioral plasticity (Kümmerli *et al.*, 2009b; Sauer *et al.*, 2004; Huynh *et al.*, 2012; Oliveira *et al.*, 2015), and studies of both natural and laboratory isolates have indicated considerable phenotypic variation, for example with regards to antibiotic resistance (Darch *et al.*, 2015) and biofilm composition (Chew *et al.*, 2014; Mann and Wozniak, 2012).

The debate over the validity of lab strains representing natural isolates is an old one. It has generally been resolved by characterizing the lab strain for the phenotype of interest, then comparing the presence or absence of the trait in a sample of natural isolates of the same species. However, this approach can run into issues where the lab strain does not express a relevant phenotype – for example, the lab strain PA14 has lost several genes in the *psl* operon, an important matrix component (Mann and Wozniak, 2012). This can force reliance on different strains for different phenotypes of interest, which may hinder comparative analyses and synthesis of experimental results due to genetic confounds among multiple 'reference' strains. Furthermore, even when a reference strain possesses the requisite genes to express a given trait, plastic regulation may mask its expression, and comprehensive testing to generate reaction norms across environments is often prohibitive.

Establishing organizing principals of phenotypic variation within a species is therefore necessary to effectively transfer knowledge gained in the lab to applications in the clinic and elsewhere. This can be achieved by understanding the life history of the organism, and mapping observed patterns in phenotypes of interest to the evolutionary and ecological pressures that select for them. Understanding the rules of how traits respond to varying selective pressures allows us to move from asking "what is the extent of observed variation?" to "what are the causes of observed

variation?" By establishing how genetic and environmental factors influence evolution of a given phenotype, and in what direction, we gain greater predictive power. The extent of plastic regulation in the trait is also an important component, as this can serve to buffer or accelerate adaptive evolution depending on the severity of the environmental perturbations experienced by a lineage (West-Eberhard, 2003).

Here we aim to increase our understanding of the nature, causes and constraints on phenotypic diversity in *P. aeruginosa*. We assess the extent of phenotypic variation in a broad suite of traits across a library of over 200 natural and clinical isolates of *P. aeruginosa*, and use the environmental origin of the isolates as a proxy to map phenotypes on to evolutionary history (in lieu of forthcoming genomic sequencing and phylogenetic information). We find that *P. aeruginosa* varies widely in all of the phenotypes investigated here, and despite the limitations of our proxy for evolutionary history, uncover candidate evolutionary signatures in characteristics of growth, antibiotics resistance, biofilm formation and virulence factor secretion.

5.3 Methods

5.3.1 Strains

The library of strains used here was kindly provided by Dr. Gabriel Perron (Bard College), see the Appendix for information on individual strains.

5.3.2 Media

Unless otherwise noted, all experiments were conducted in a rich defined medium (hereafter 'growth medium') consisting of M9 salts supplemented with 10 mM Glucose, 1% Cas-amino acids, 1mM $MgSO_4$, 100uM $CaCl_2$ and 1X Hutner's trace elements (Hutner *et al.*, 1950).

5.3.3 Growth curves

Mid-exponential phase starter cultures were used to inoculate each strain at an OD(600) of 0.05 into 150 uL growth medium in a single well of a 96 well plate, with tobramycin (2 ug/mL) or carbenicillin (32 ug/mL) as appropriate. Plates were

incubated at 37 °C with shaking in a Varioskan plate reader, and the OD(600) measured hourly to track cell density.

5.3.4 Biofilm allocation and composition

Mid-exponential phase starter cultures were used to inoculate each strain at an OD(600) of 0.05 into 150 uL growth medium in a single well of a 96 well plate, which was incubated statically in a humidified 37 °C incubator for 6 hours. This time point was chosen to minimize the effects of plastic regulation on biofilm formation, and better reflects the 'hard-wired' biofilm formation tendency of the strain. After growth, the OD(600) of the planktonic phase was measured, and the bulk fluid removed via pipetting. The biofilms were then washed by pipetting up and down with sterile water, then resuspended in 150 uL sterile 0.85% NaCl by adding 5-10 sterile 1mm glass beads, sealing the plates with acetate tape and votexing for 15 minutes at 2000 rpm. The resuspended biofilm was then transferred to a new plate and the OD measured.

The composition of the biofilm was assessed via two methods. First, an aliquot of 50 uL was taken for carbohydrate determination, as in (Masuko *et al.*, 2005). Briefly, in a 96-well plate 150 uL concentrated sulfuric acid is added to the 50 uL aliquot, followed by 30 uL 5% phenol in water. The plate is then incubated at 90 °C by floating on a water bath for 5 minutes, then cooled to room temperature and the A(490) measured. This absorbance is reported normalized to the OD(600) of the biofilm suspension measured above. Note that this method measures total carbohydrates in the biofilm (including intracellular carbohydrates), so there may be some confounds due to variation between the intrinsic carbon content between strains, which is unknown. However, these effects should be minimal as the cells were exposed to ideal growth conditions and restricted to relatively low cell densities, limiting the impact of starvation and other stress responses that directly impact carbon sequestration in the cell (Timmermans and Van Melderen, 2010).

The remaining biofilm suspension was then subjected to live/dead staining via manufacturer's specifications (Invitrogen). Generally, live cells are measured via

green fluorescent dye Syto-9 (S9; ex/em 485/530 nm), while dead cells and extracellular DNA are measured via fluorescence of red-fluorescent propidium iodide (PI; ex/em 485/630 nm); both dyes intercolate with DNA. Intact membranes block diffusion of PI into the cell, therefore live cells are primarily stained green, while PI outcompetes S9 when the two interact, meaning dead cells (with damaged membranes) and extracellular DNA stain red. The fluorescence of each dye is then measured, and reported as normalized to the OD(600) of the resuspended biofilm.

5.3.5 Virulence factor production

Secretion of virulence factors is highly dependent on the growth phase of the culture. Due to asynchrony in the growth kinetics across isolates, we harvested supernatants for virulence factor secretion in groups based on when they were expected to enter late exponential phase from earlier growth curves (previous pilot data from our lab indicates this to be the peak point of secretion). Cultures were grown in 150 uL of growth medium with shaking at 37 °C until the appropriate time, at which the OD(600) of the culture was measured. The culture was then transferred to a 1.5 mL tube and cells were pelleted by centrifugation at 14,000 rpm for 1 minute. The supernatant was then collected and passed through a 0.22 um filter to obtain the cell-free supernatant, and downstream analyses were performed immediately following collection.

Pyochelin and pyoverdin production were measured via fluorescence of the supernatant aliquot as described in (Dumas *et al.*, 2013). Elastase production was quantified using the elastin-Congo red (ECR) assay (Ohman *et al.*, 1980). Briefly, 100 uL of supernatant was added to 900 uL ECR buffer (100 mM Tris, 1 mM $CaCl_2$, pH 7.5) containing 20 mg ECR (Sigma), which was incubated with shaking for 20 hours at 37 °C. Remaining insoluble ECR was pelleted via centrifugation for 1 minute at 14,000 rpm, and 200 uL of supernatant was transferred to a 96 well plate and the absorbance at 495 nm measured. Measurements for pyochelin, pyoverdin and elastase production are all reported as normalized to the OD(600) of the culture at time of harvest.

Pigment production was measured by taking a full absorbance spectrum (300-1000 nm, bucketed by color: 300 < UV ≤ 380 nm, 380 < violet ≤ 450 nm, 450 < blue ≤ 495 nm, 495 < green ≤ 570 nm, 570 < yellow ≤ 590 nm, 590 < orange ≤ 620 nm, 620 < red ≤ 750 nm, 750 < IR < 1000 nm) of 150 uL cultures in growth medium after 48 hours incubation with shaking at 37 °C. Absorbance readings were corrected by subtraction the absorbance values of a well containing sterile medium, then normalized in density by dividing the curves by the absorbance at 600 nm (the standard OD estimating cell density).

5.3.6 Statistics

All statistical analyses were performed in R (R Core Team, 2015). Principal component analyses (PCAs) were visualized using the factoExtra package (Kassambara and Mundt, 2016).

5.4 Results

The strain library contains detailed meta-data on the source environment for each strain (see Appendix). We grouped isolates into three broad categories: samples from the lungs of cystic fibrosis patients ("CF"), samples associated with a host organism (including human, animals and plants; "host"), or non-host associated samples (e.g. soil, water, built environments; "env"), summarized in Table 5.1.

Table 5.1: Demographic breakdown of strain library.

EVIRONMENTAL SOURCE	NUMBER OF ISOLATES	% OF TOTAL
CYSTIC FIBROSIS (CF)	56	24
HOST-ASSOCIATED (HOST)	106	46
ENVIRONMENTAL (ENV)	68	30
TOTAL	230	100

5.4.1 Growth and Antibiotic Resistance

We grew each strain in a defined rich medium (see methods) for 48 hours, with no antibiotic or with the addition of carbenicillin or tobramycin. Principal components analysis (PCA) showed good agreement between the parameters estimated for each growth curve (max growth rate, carrying capacity, and area under the curve (AUC), Figure S5.1), and AUC was chosen as the metric to describe growth under each condition (Figure 5.1).

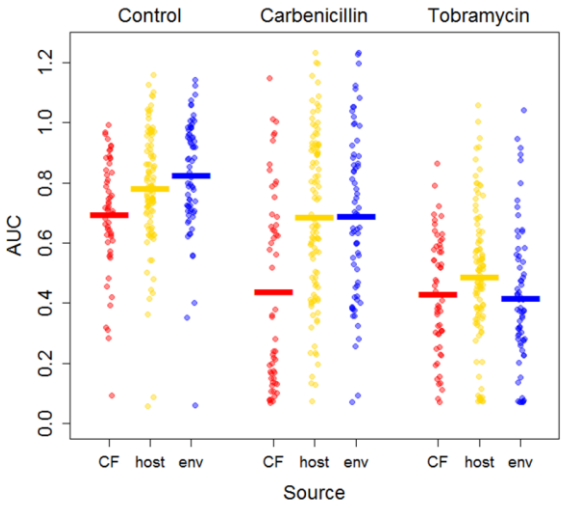

Random effects:

Formula: ~1 | strain

	(Intercept)	Residual
StdDev:	0.144	0.186

Fixed effects: AUC ~ treatment * source

	Value	*Std.Error*	*DF*	*t-value*	*p-value*
(Intercept)	0.696	0.031	454	22.11	0.000
Carb	-0.256	0.035	454	-7.28	0.000
Toby	-0.266	0.035	454	-7.56	0.000
Env	0.129	0.043	227	3.04	0.003
Host	0.087	0.039	227	2.23	0.027
carb:env	0.121	0.048	454	2.56	0.011
toby:env	-0.142	0.048	454	-2.99	0.003
carb:host	0.161	0.044	454	3.70	0.000
toby:host	-0.028	0.044	454	-0.64	0.521

Standardized Within-Group Residuals:

Min	Q1	Med	Q3	Max
-3.71	-0.58	0.02	0.58	2.69

Figure 5.1: Growth differs significantly based on environmental origin. Left, AUC plotted as a function of treatment (control, carbenicillin, tobramycin) and environmental source (CF=cystic fibrosis, red; host=host-associated, yellow; env=environmental, blue). Each point depicts an individual strain, and lines indicate within-source averages. Right, results table of linear mixed model of AUC as a function of treatment and environmental source with interactions, and individual strain fitted as a random effect. Intercept refers to CF isolates under control conditions, and estimates indicate deviations from the intercept.

We found that isolates originating from CF lungs grew significantly slower than samples from environmental or host-associated sources, had greater relative resistance to tobramycin than other environmental sources, and curiously were more sensitive to carbenicillin (Figure 5.1). We also note a large amount of variation

between isolates within each treatment block, indicating other important factors besides environment of origin dictate growth ability under a given condition.

5.4.2 Biofilm Formation

Biofilm formation is a key phenotype of *P. aeruginosa*, allowing populations to persist in harsh environments (see Chapters 2 and 3). However, biofilm formation has also been associated with reduced virulence in other species (Otto, 2004; Mikonranta *et al.*, 2012). We therefore sought to measure the relative propensities of each strain to form biofilm by measuring the relative allocation of cellular resources into the planktonic and biofilm fractions (Figure 5.2; note this is the same data presented in Chapter 2 Figure 2.4, but structured here by environmental source).

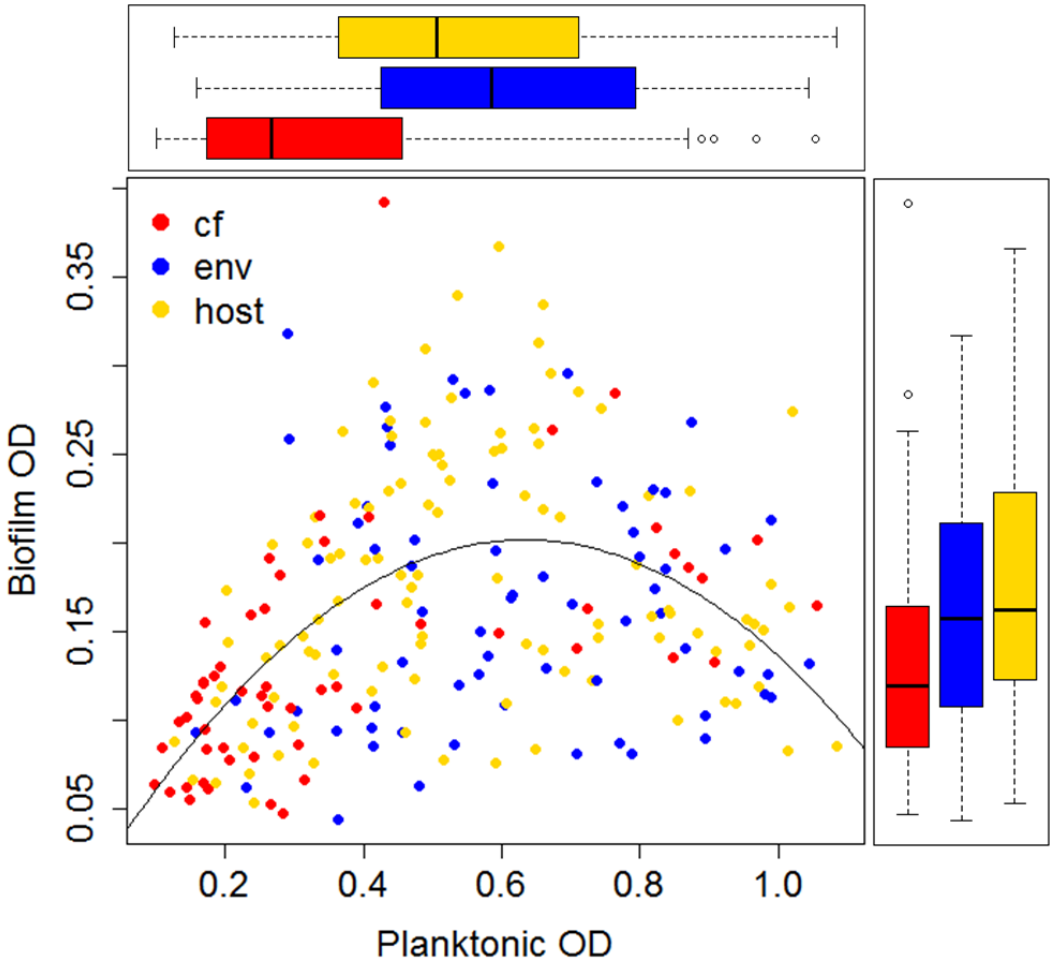

Figure 5.2: Biofilm allocation follows a humped pattern across the strain library. OD of the resuspended biofilm is plotted as a function of the planktonic OD after 6 hours of growth. The curve represents regression of biofilm OD on planktonic OD with a quadratic term in planktonic OD (see main text), and marginal boxplots display breakdown of biofilm and planktonic ODs by environmental source (see Table 5.2).

We previously developed theory (Chapter 2) that predicted a peak in biofilm density at intermediate planktonic density when comparing strains that varied in growth rate and biofilm colonization rates, which we recover in this strain library (regression of biofilm OD on planktonic OD gives $B = 0.63*P - 0.49*P^2$, with respective standard errors (p-values) of 0.074 ($3.1*10^{-15}$) and 0.064 ($3.8*10^{-13}$) in the linear and quadratic predictors). The rationale for this hump shape is that strains may take advantage of increased cellular division in the planktonic phase to indirectly drive expansion in

the biofilm (as opposed to directly increasing the colonization rate, which would lead to a strict negative relationship between the biofilm and planktonic population densities).

Table 5.2: CF isolates show reduced growth but greater relative investment to the biofilm. Tukey's Honest Significant Differences calculated from anovas of planktonic and biofilm ODs and fraction biofilm across environmental sources.

Planktonic OD				
Difference	**Estimate**	**95% CI**		**p-value**
env-CF	0.231	0.128	0.335	0.0000
host-CF	0.175	0.080	0.269	0.0001
host-env	-0.057	-0.146	0.033	0.2942
Biofilm OD				
Difference	**Estimate**	**95% CI**		**p-value**
env-CF	0.029	0.000	0.059	0.0482
host-CF	0.043	0.016	0.070	0.0006
host-env	0.013	-0.012	0.039	0.4193
Fraction Biofilm				
Difference	**Estimate**	**95% CI**		**p-value**
env-CF	-0.073	-0.113	-0.032	0.0001
host-CF	-0.036	-0.074	0.001	0.0592
host-env	0.036	0.001	0.071	0.0424

If Figure 5.1 we observed that CF isolates generally grew more slowly and to lower carrying capacities than other strains. Figure 5.2 reflects this finding, as CF isolates showed a marked reduction in planktonic density (average difference of roughly -0.2 OD units, Table 5.2) and a minor decrease in biofilm density. However, some CF strains still showed robust planktonic investment; these differences may reflect divergent strategies within the lung (e.g. hypervirulence vs. survival), or may simply be reflective on time spent in the CF lung with selection acting solely to reduce planktonic investment. On average, though, we find that CF isolates generally have slightly higher levels of relative investment to biofilm (Figure 5.3D, Table 5.2), suggesting that biofilm formation is selected for as a survival / slow growth adaptation in the CF environment. However, we also note that these differences do

not explain the majority of variation in growth among isolates, and are of minor impact towards gross phenotypic patterning across the library.

We further broke down biofilm phenotypes by measuring relative content of live cells, dead cells /extracellular DNA, and polysaccharides within the biofilm, and compared that to the relative investment of each strain towards the biofilm fraction (Figure 5.3). Per-capita live cells correlated positively with strains that invested more in biofilm (Figure 5.3A, Table S5.1), while polysaccharide content correlated negatively (Figure 5.3C, Table S5.1). These data suggest that strains favoring higher levels of biofilm investment are generally composed of more live cells and less matrix, a somewhat counterintuitive result when the matrix is viewed as the main component offering protection to the cellular inhabitants of the biofilm. However, this does point towards a slow-growing but viable state as an important factor for the survival of biofilms following environmental challenge, as suggested previously (Høiby *et al.*, 2010b).

Interestingly, the relationship between fraction biofilm and eDNA / dead cell content interacted significantly with environmental source (Figure 5.3B, Table S5.1), with higher levels of eDNA in CF isolates showing higher biofilm investment, and the opposite trend in host-associated and environmental strains. This discrepancy may reflect the need for further increases in protection within the CF lung environment, potentially helping to compensate for less polysaccharides per capita, and points to apoptosis as an important mechanism of biofilm formation within that niche (Allesen-Holm *et al.*, 2006; Mulcahy *et al.*, 2008)

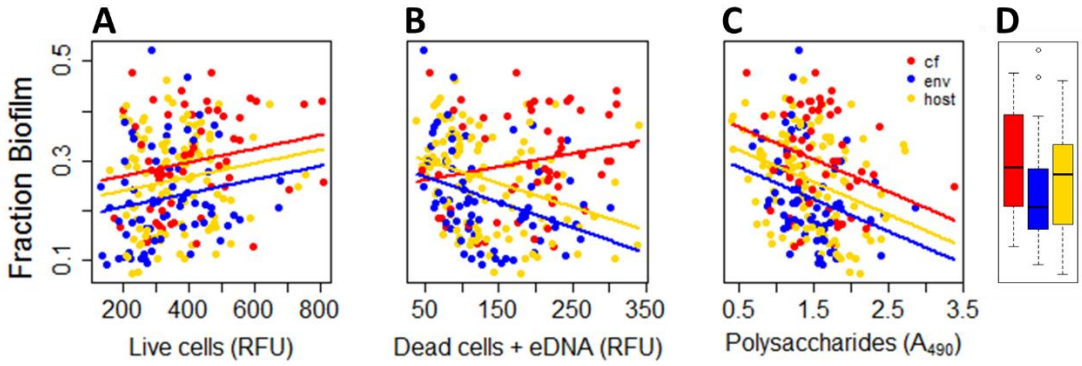

Figure 5.3: Greater biofilm investment correlates with more live cells and less matrix. Fraction biofilm (ratio of resuspended biofilm OD to sum of biofilm and planktonic OD) is plotted against **A**, live cell content, **B**, dead cell and eDNA content, **C**, polysaccharide content, and **D**, environmental source. Each measurement for biofilm components is normalized to the OD of the resuspended biofilm. Lines indicate regressions of fraction biofilm onto each component (see Table S5.1).

5.4.3 Secreted Virulence Factors

We measured the virulence capacity of each strain by assessing production of secreted virulence factors (VFs) elastase, pyoverdin and pyochelin. Because these factors act as public goods, social 'cheats' (non-producers) can gain fitness advantages by not paying the cost of producing the molecules and simply using those secreted by neighboring 'cooperative' cells. We can make a preliminary assessment of cheating strains by examining the distributions of VF secretion across the isolate library (Figure 5.4), where strains that produce little public goods relative to the population average are candidate cheating strains.

The distribution of elastase production is consistently bimodal across all environmental sources, suggesting that elastase non-producing 'cheat' lineages are commonly found across environments. This pattern is consistent with the wide-spread observation of quorum-sensing 'cheat' strains (particularly *lasR* mutants that are defective in signal response (Wilder *et al.*, 2011; Allen *et al.*, 2016)), which are defective in the production of an array of QS-controlled secreted factors including elastase. Further work, in particular testing for enrichment of candidate cheats in co-

culture with known producers, will be necessary to validate cheater phenotypes in any of the candidate cheat isolates.

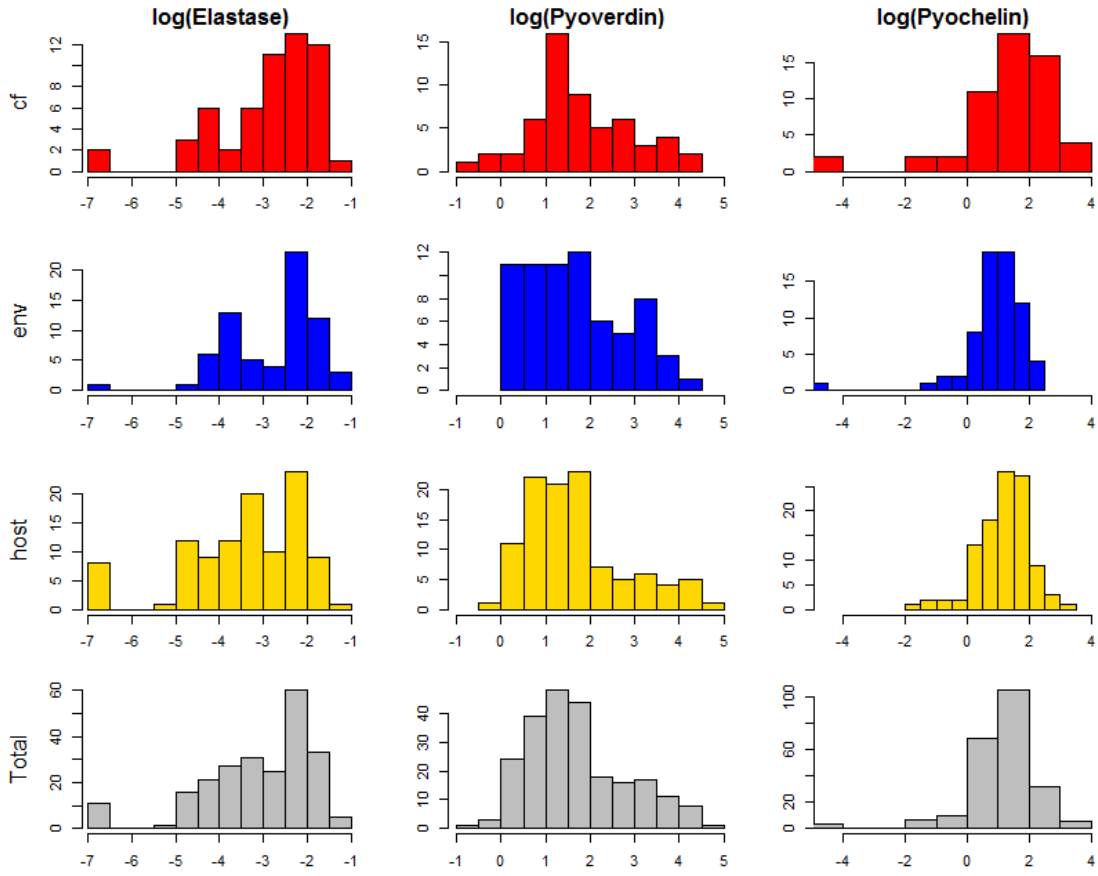

Figure 5.4: Distributions of VF secretion levels suggest presence of elastase cheating strains. Histograms show log-transformed measurements of elastase, pyoverdin and pyochelin secretions (normalized to culture density at time of harvest) broken down by environmental source and across the entire library. Log transformations were performed to better differentiate strains producing low levels of secreted products.

Noting the high degree of variability in VF secretion across the library (Figure 5.4), we asked whether patterns in VF secretion might reduce the dimensionality of our virulence metrics (Figure 5.5). Aside from the siderophores pyocyanin and pyochelin, we found little evidence of correlation between any of the factors we

measured, nor meaningful differences between strains from different environmental sources.

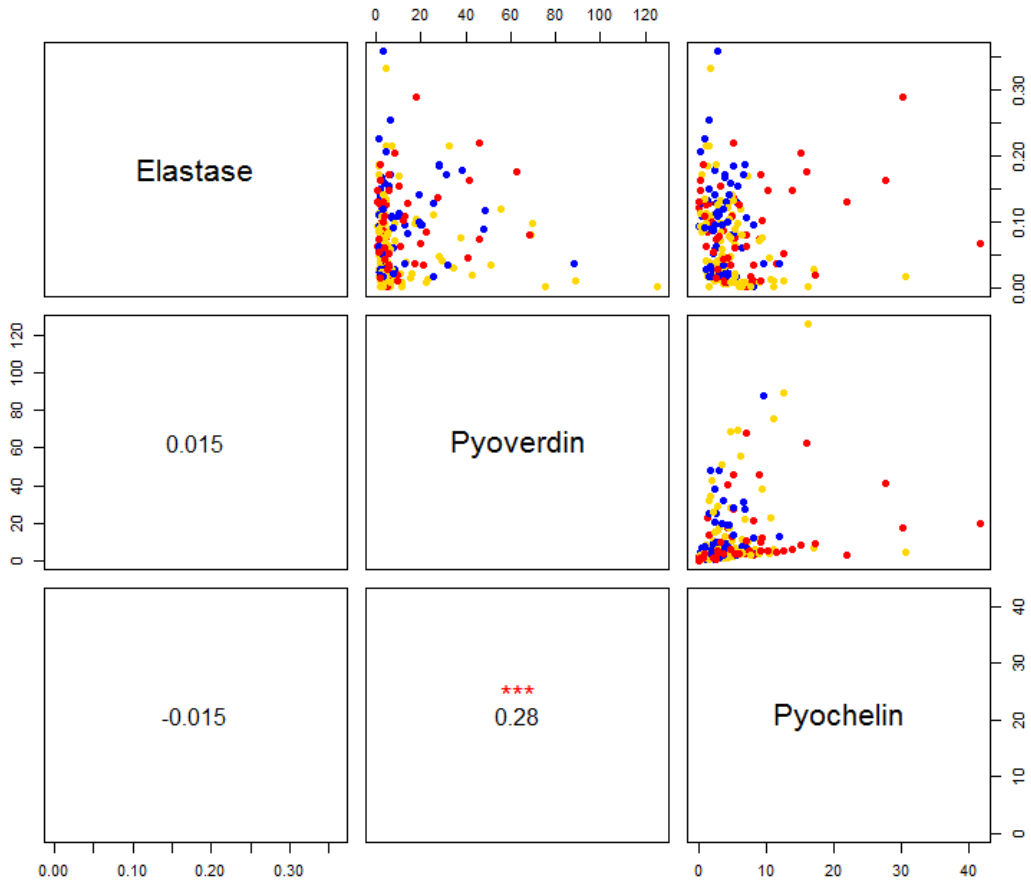

Figure 5.5: Secreted virulence factors show little correlation with each other. Each associated virulence metric is plotted against the others in the upper panels, with the Pearson correlation coefficient and significance indicators in the lower panels.

The "V"-shaped pattern observed in production of the two iron-scavenging siderophores pyoverdin and pyochelin is intriguing, as it suggests two distinct groupings that preferentially secrete one of the two molecules. PCA indicated that the first principle component primarily described overall siderophore production, while the second dictated which siderophore was preferred (Figure 5.6). We found that CF isolates predominantly favored pyochelin, while environmental and host-

associated isolated favored pyoverdin (Figure 5.6), based on the relative orientation of the confidence ellipses. However, it should be noted that some isolates in each background of origin do not fall under this pattern, and it would be of interest to discern the causes behind such divergence.

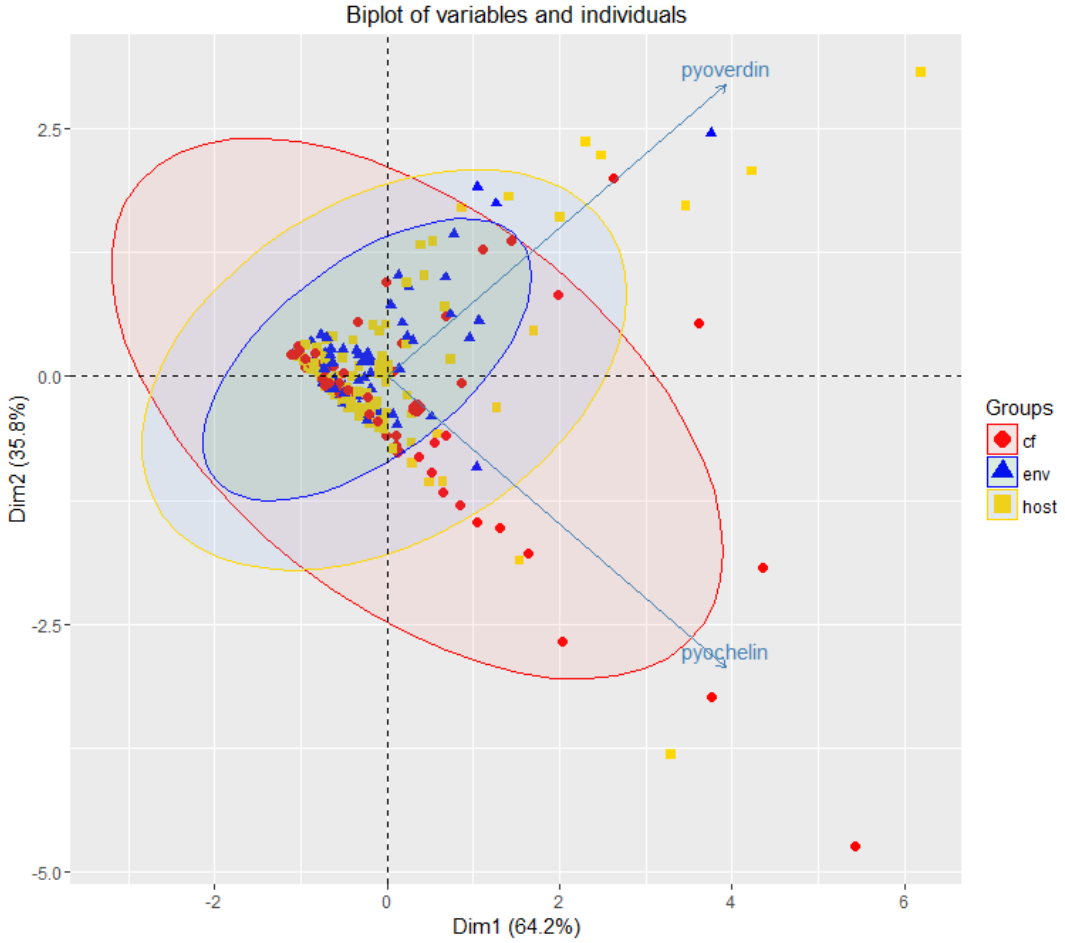

Figure 5.6: Preferential siderophore production depends on environmental origin. Biplot of principal components analysis describing siderophore production shows PC1 (x-axis, 64.2% of variation) primarily describes the total amount of siderophore expressed, while PC2 (y-axis, 35.8% of variation) describes which siderophore is expressed, with positive values tending towards pyoverdin expression and negative values towards pyochelin expression. Ellipses indicate 95% confidence levels for each isolate group.

Finally, it was noted over the course of the experiments that the strain library produced impressively diverse pigmented molecules (Figure 5.7A), and in *P. aeruginosa* such secreted products often function as virulence factors (the green color associated with pyoverdin production is perhaps the most familiar example). We measured absorbance across the visible spectrum for a subset of the strain library at stationary phase, and compared absorbance at different wavelengths with our previous measures of secreted virulence factors via PCA (Figure 5.7BC).

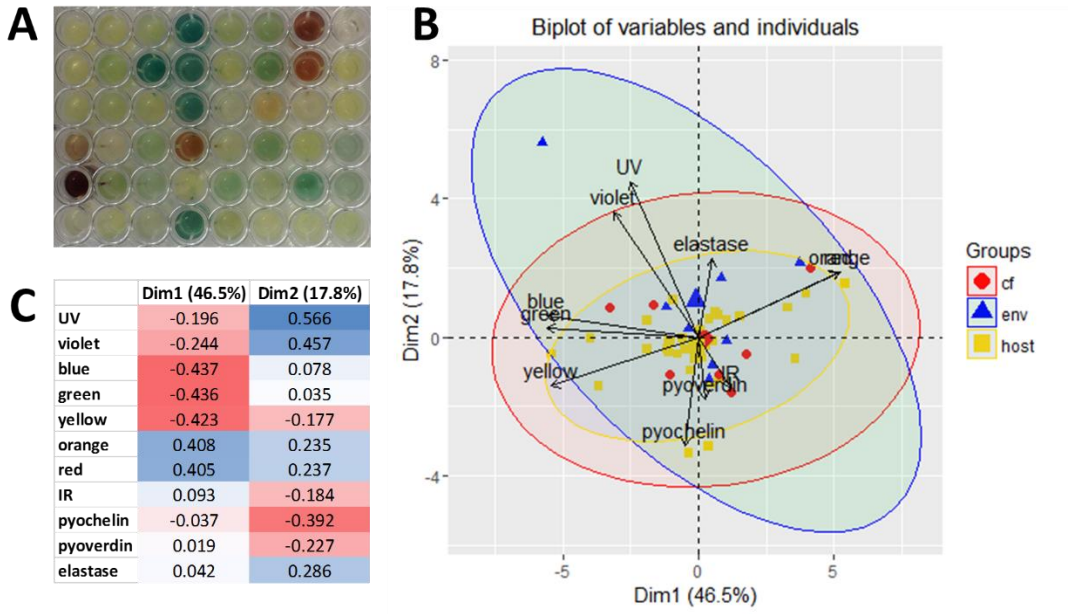

C

	Dim1 (46.5%)	Dim2 (17.8%)
UV	-0.196	0.566
violet	-0.244	0.457
blue	-0.437	0.078
green	-0.436	0.035
yellow	-0.423	-0.177
orange	0.408	0.235
red	0.405	0.237
IR	0.093	-0.184
pyochelin	-0.037	-0.392
pyoverdin	0.019	-0.227
elastase	0.042	0.286

Figure 5.7: PA isolates display extensive pigment variation. **A**, pigment production from a sample of 47 strains from the isolate library after 48 hours growth. "Blank" well containing sterile medium is in the top right corner. **B**, PCA of absorbance across UV/visible spectrum and previously described secreted virulence factors. Ellipses correspond to 95% confidence levels for each environmental origin (color scale). **C**, Table displaying loadings of variables on first two principle components, corresponding to arrows in B. Red indicates negative correlation, blue indicates positive correlation.

Few guiding principles are apparent in the production of pigment molecules in our strain library. The first principal component (Figure 5.7B, x-axis) explains the highest proportion of variance (46.5%) and primarily differentiates blue-green strains

(absorbing primarily red wavelengths, negative correlation with PC1) and red-brown strains (absorbing primarily blue-green wavelengths, positive values of PC1). The second component indicates that specific virulence factors correlate weakly with pigment production, but no obvious relationships between coloration and molecules produced are apparent; testing an expanded catalogue of secreted products with known absorbance properties could help to identify putative matches, or alternatively by molecularly characterizing secreted products and looking for patterns across groups of strains of the same color. We also found no evidence for significant differences between pigment production and environmental origin, based on the overlap of the confidence ellipses in Figure 5.7B, but this may in part be due to the reduced sample size, and bias within the sample towards host-derived strains.

5.4.4 Correlations between phenotypic classes

To investigate gross patterns in phenotypic covariation, we performed a PCA on the phenotypes of interest from each category discussed above (Figure 5.8). We found a high degree of overlap persisted in differentiating strains by environmental source, but the first principal component (explaining 25.5% of the total variation) did weakly differentiate CF isolates from the others, mostly via characteristics previously discussed (e.g., higher proportional content of dead cells and eDNA in biofilms, preferential secretion of pyochelin, higher relative investment to biofilm fraction).

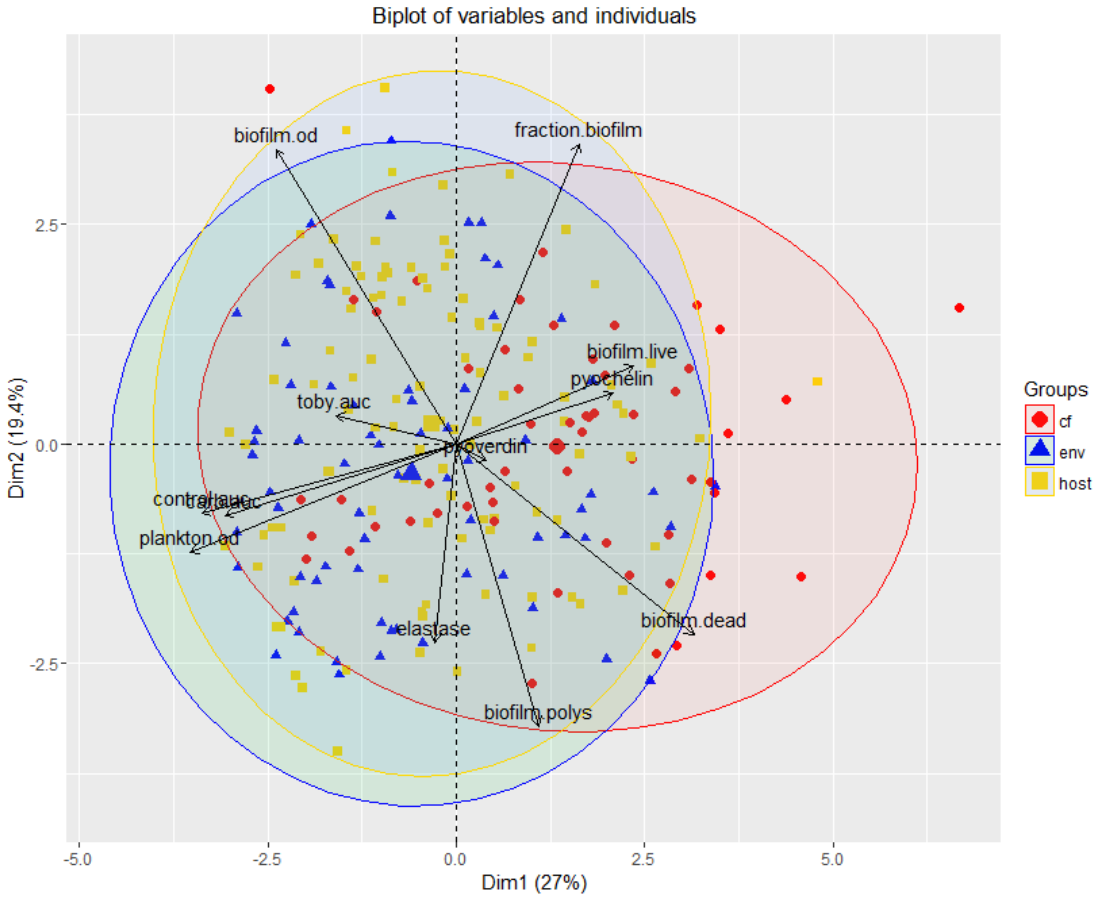

Figure 5.8: PCA reveals largely independent variation in most of the phenotypes considered. Biplot of first two components (27% and 19.4% of total variation, respectively) from PCA of 13 phenotypic parameters (labelled arrows) across all strains in the isolate library (points). Ellipses indicate 95% confidence levels for each group of environmental sources (color scale).

Outside of differences due to environmental source, Figure 5.8 suggests a weak clustering between biofilm phenotypes (correlated positively with PC1) and growth-associated phenotypes (correlated negatively with PC1), which is expected from the trade-offs between biofilm and planktonic cells. However, PC1 only explains 25% of the total variation in the measured phenotypes, and the suggested trade-off is weak within those bounds. In terms of overall patterning, we therefore conclude 1) a high degree of variation is observed in all of the traits measured across the library, 2) most of these dimensions are largely independent of one another, and 3) most traits are only weakly influenced by the environmental source of the isolate.

5.5 Discussion

In this work, we screened numerous phenotypes relating to virulence across a diverse library of clinical and environmental isolates of the opportunistic pathogen *P. aeruginosa*. Gross patterns in the data suggest few organizing principles relating phenotypes in growth, biofilm formation and virulence factor secretion. Each trait showed a high degree of variability that was only weakly explained by environmental origin of the isolate. Within this, however, we observed greater divergence in phenotypic signatures associated with isolates originating from the CF lung as compared to environmental or host-associated isolates; specifically, we found CF isolates to be slower growing, more sensitive to carbenicillin, resistant to tobramycin, to have increased eDNA content in the biofilm matrix, and to preferentially secrete pyochelin. The extensive variation in all measured phenotypes suggests that behavioral plasticity has had little buffering effect on adaptive evolution within the library isolates. This is not to say that we expect the isolates to have lost the capacity for plastic responses; rather, the phenotypic variation observed in this work under identical experimental conditions suggest considerable divergence in baseline expression levels and/or regulatory networks modulating all measured traits.

The CF lung is potentially unique as an evolutionary niche for *P. aeruginosa*, in that lineages may persist in an infection context for decades; it is therefore unsurprising that CF isolates would show the greatest divergence compared to the other environmental sources. Many of the traits we observed are adaptive in the CF lung: slow growth and eDNA in the biofilm matrix are both associated with general recalcitrance (Mulcahy *et al.*, 2008; Høiby *et al.*, 2010b), and tobramycin resistance will promote survival under treatment with this common CF therapeutic. That CF isolates are relatively more sensitive to carbenicillin is unexpected, given that beta lactams including carbenicillin are routinely co-administered with aminoglycosides during CF treatment (Flume *et al.*, 2009; Pleasants, 1994) - this suggests that CF isolates may lose or downregulate resistance mechanisms specific to beta-lactams in the CF lung

(potentially relying on resistance provided by other community members (Darch *et al.*, 2015), or tolerance attributed to slower growth (Tuomanen *et al.*, 1986; Yang *et al.*, 2008)), and more detailed study of the antibiotic resistance profiles across the library would be of interest.

The bias of environmental origin on preferential siderophore secretion may reflect the relative abundance or iron in various environments. The ability to switch between pyoverdin and pyocyanin has been suggested as a cost-saving mechanism in response to changes in relative iron availability in the environment (Dumas *et al.*, 2013), with the higher affinity but costlier pyoverdin being reserved for iron-limited conditions. Iron is relatively abundant in the CF lung (Ghio *et al.*, 2013), so CF isolates favoring pyochelin is consistent with the cost interpretation given in (Dumas *et al.*, 2013); however, this opens the question of why strains from other sources continue to secrete the more expensive pyoverdin when iron is less limited, as iron was relatively abundant in the media used in this experiment (roughly 18 uM). It may be the case that these strains start producing pyoverdin late in the growth cycle as the iron concentration declines; alternatively, the ability to switch and/or the threshold at which switching occurs is evolutionarily labile in *P. aeruginosa*. Further testing of growth and siderophore production under iron limitation would help to differentiate these outcomes.

Importantly, we note that the environmental source of an isolate is not an ideal proxy for its evolutionary history, for two related reasons. First, *P. aeruginosa* can disperse with relative ease between the sources considered here (e.g., an established CF isolate being coughed up and isolated from an environmental source), so it is a strong assumption that isolates taken from a given environment are in fact well adapted to that environment. Second, comparing strains based on environment cannot control for phylogenetic correlations, i.e. we cannot account for the null expectation of genetically similar strains also being phenotypically similar. To this end, work is currently underway to sequence the genomes of all strains in our library, which will allow us to construct a phylogeny from which a more accurate model of evolutionary

history can be inferred, as well as attempt to associate genetic markers to observed phenotypic variants.

Our finding that most of the measured phenotypes display little correlation with one another mirrors those of a recent investigation of morphologically identical *P. aeruginosa* isolates taken from a single CF patient (Darch *et al.*, 2015). Darch *et al*. also found little evidence for linkage between specific genetic mutations and measured phenotypes, instead finding phenotypes to be associated with regions of high recombination. This will be an interesting benchmark for future work upon the completion of the sequencing mentioned above, allowing us to compare and contrast patterns of phenotypic and genetic diversity across scales (e.g., within-morphotype vs. within-disease site vs. within-species).

5.6 Supplemental Data

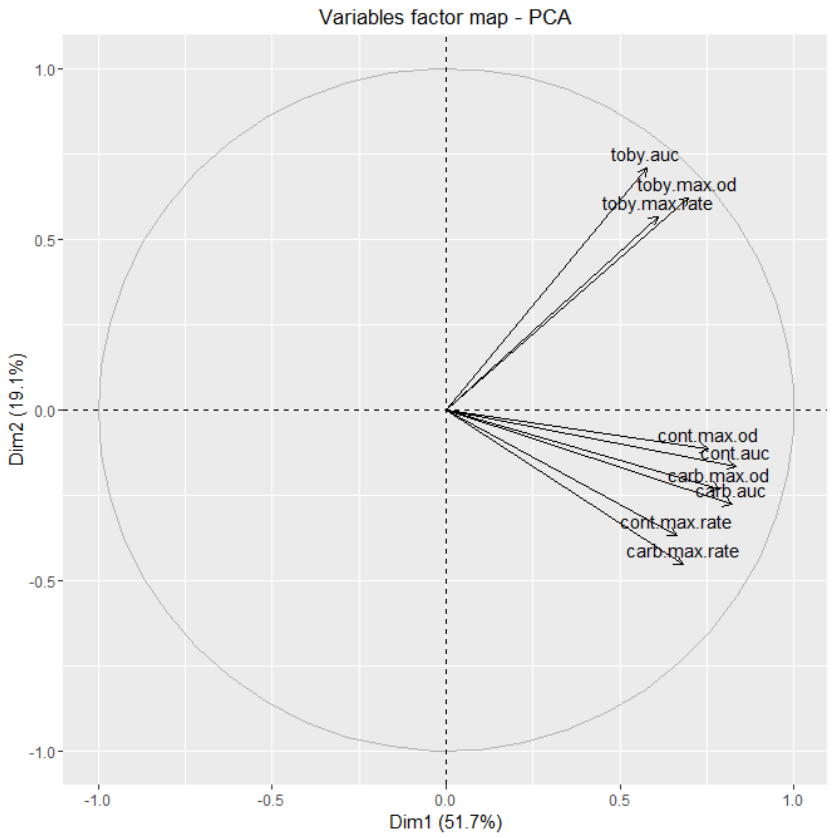

Figure S5.1: PCA of growth parameters. High correlation was observed between max growth rate (max.rate), carrying capacity (max.od) and area under the curve (auc). "Cont" = no drug control, "carb" = 32 ug/mL carbenicillin, "toby" = 2 ug/mL tobramycin.

Table S5.1: Regression of fraction biofilm onto biofilm components. Each model was originally fit with an interaction term between biofilm component and environmental source; this was only retained in the regression for dead cells + eDNA (see formula for specified model call in each heading).

Fraction biofilm ~ live cells + source					
Residuals:					
Min	1Q	Median	3Q	Max	
-0.195	-0.081	-0.005	0.070	0.304	
Coefficients:					
	Estimate	SE	t value	p-value	
(Intercept)	0.240	0.024	9.85	< 2E-16	***
live	1.38E-04	5.09E-05	2.72	0.0071	**
env	-0.062	0.018	-3.53	0.0005	***
host	-0.029	0.016	-1.85	0.0658	.
Fraction biofilm ~ dead cells:source + source					
Residuals:					
Min	1Q	Median	3Q	Max	
-0.181	-0.075	-0.007	0.068	0.254	
Coefficients:					
	Estimate	Std. Error	t value	Pr(>|t|)	
(Intercept)	0.2468	0.0334	7.40	2.74E-12	***
env	0.0464	0.0425	1.09	0.2759	
host	0.0776	0.0389	2.00	0.0469	*
dead:cf	0.0003	0.0002	1.62	0.1063	
dead:env	-0.0005	0.0002	-2.88	0.0043	**
dead:host	-0.0005	0.0001	-3.58	0.0004	***
Fraction biofilm ~ polysaccharides + source					
Residuals:					
Min	1Q	Median	3Q	Max	
-0.192	-0.074	-0.001	0.070	0.288	
Coefficients:					
	Estimate	Std. Error	t value	Pr(>|t|)	
(Intercept)	0.399	0.024	16.83	< 2E-16	***
polys	-0.065	0.013	-5.01	1.11E-06	***
env	-0.080	0.017	-4.82	2.58E-06	***
host	-0.046	0.015	-3.01	0.0029	**

6 Discussion

6.1 Summary

As the antimicrobial resistance crisis worsens, it becomes increasingly important to understand why treatment of susceptible populations fail, and how these failures may influence the evolution of genetic resistance mechanisms. In many cases, treatment failure can result from the presence of heterogeneous phenotypes within the population that display reduced susceptibility to antibiotics, and while significant work has gone towards describing these phenotypes, their evolutionary and ecological dynamics remain poorly understood.

In this work, we presented four experiments seeking to help fill this gap. We found that biofilm investment, a widespread source of phenotypic resistance to antibiotics, is evolutionarily labile, and responsive to both transmission biases and antibiotic treatment (Chapters 2 and 3). The canonical formulation of the biofilm 'life cycle' poses the biofilm as analogous to the soma and motile planktonic cells serve as dispersal propagules (O'Toole *et al.*, 2000; Hall-Stoodley *et al.*, 2004). Our modelling and experimental results in Chapter 2 suggest that this conceptualization can be flipped on its head, with a mixed planktonic cells functioning as the growing soma, and biofilm cells as dispersal agents. We also observed that biofilm can function as a cost-effective hedge against unpredictability within the environment, further expanding the range of conditions under which a mixed population is expected to persist.

Our preliminary results in Chapter 3 show that relative investment towards biofilm formation is responsive to antibiotic treatments. We observed patterns in the evolutionary trajectories that suggested biofilm-mediated phenotypic resistance may interact with conventional genetic resistance mechanisms, and in particular may form a bridge to genetic resistance; however, these observations are based on purely phenotypic data, and future sequencing analysis is required to properly test our predictions.

For persister cells, the genetic and physiological mechanisms of their formation are poorly understood, yet essential to understand the proximate and ultimate causes of their existence. To this end, we hypothesized that cellular age may serve as a demographic determinant of the persister state, but found no evidence in support of this hypothesis. However, we maintain that screening persister cells for other biochemical features at the single-cell level will be fruitful towards understanding how and why cells enter the persister state.

Screening a diverse library of 230 natural isolates of *P. aeruginosa*, we observed a high degree of variation in multiple traits related to growth, antibiotic tolerance, biofilm formation, and secretion of virulence factors. We observed that a handful of these phenotypes showed signatures depending on the environmental source of the isolate, such as slower growth and preferential secretion of the siderophore pyochelin in isolates originating from the lungs of patients with cystic fibrosis. Together, our results indicate few organizing principles governing the extensive phenotypic variation in *P. aeruginosa*, suggesting many traits related to growth, survival and virulence can evolve relatively independently of one another. However, the use of environmental source as a proxy for evolutionary history is problematic, and ongoing genomic sequencing will seek to address these limitations by replacing environmental source with phylogenetic relationships.

6.2 Biofilms and Life Cycles

A key theme in this thesis is the importance of understanding interactions among multiple phenotypic states, rather than focusing on the specific nature of each component phenotype separately. Our results suggest that interactions – particularly transition rates - are evolutionary labile, and changes in these interactions can have important ecological and clinical consequences.

Considering the interaction between biofilm and planktonic cells within a population, the historical paradigm suggests that biofilms function as the growing 'soma', and motile planktonic cells served as dispersal agents (O'Toole *et al.*, 2000; Hall-Stoodley *et al.*, 2004; Hammerschmidt *et al.*, 2014; Poltak and Cooper, 2010). We find the

opposite cycle to be favored under a broad range of environmental conditions, with biofilm as dispersal agent and a mixed population as the growing soma. This conceptualization is consistent with the common observation that outside the laboratory microbes are most commonly found in biofilms regardless of environment (Costerton *et al.*, 1987) – under our division of labor interpretation, this would imply that we commonly observe biofilms both during dispersal events and in preparation for dispersal, with planktonic cells utilized as a growth accelerant when conditions allow. Biofilms provide several key benefits as dispersal, namely increased durability (Marks *et al.*, 2014; Kramer *et al.*, 2006), competitive advantages upon colonization (Kragh *et al.*, 2016; Melaugh *et al.*, 2016), resisting Allee effects (Smith *et al.*, 2014), and maintenance of cooperation (Kümmerli *et al.*, 2009a). One exception to this rule could be when active motility is required for dispersal, for instance where patches are connected via static fluid channels and in the absence of suitable transmission vectors, though this could potentially be accomplished by biofilm cells as well via swarming motility (Kuchma *et al.*, 2010; Anyan *et al.*, 2014; Wang *et al.*, 2014; Pollitt *et al.*, 2015).

Our results indicate biofilm investment is labile on both regulatory and evolutionary timescales, and the assumption that dispersal is primarily and robustly via biofilm (or planktonic) cells is strong. Previous work has identified planktonic cells as the key dispersal route (O'Toole *et al.*, 2000; Hammerschmidt *et al.*, 2014; Poltak and Cooper, 2010), and by flagging biofilm dispersal as a viable transmission route it is not our intention to suggest that these routes are exclusive. Indeed, our model in Chapter 2 suggests mixed strategies are favored under a broad range of growth and transmission conditions. This flexibility reflects a key difference between microbial and metazoan life histories, namely that microbial cells are not easily defined within a higher-order organizing unit or 'body' (Queller and Strassmann, 2009). In this sense, microbial life histories may not respond in the same way to analogous pressures as the better studied cases of metazoan life histories, and it will be interesting to uncover the extent of these differences as the field of microbial ecology and evolution continues to grow.

In Chapter 3, we experimentally imposed distinct life cycles (strictly biofilm or strictly planktonic transmission) upon bacterial populations exposed to antibiotics, and found that biofilm investment was responsive in evolutionary time to antibiotic treatment. The observed patterns also suggested phenotypic resistance mediated by biofilms may interact with genetic resistance mechanisms (pending further work discussed below), which may have broader implications for antibiotic control strategies. Our imposed life cycles represent something of a worst case scenario from a clinical perspective towards antibiotic resistance, with lower antibiotic doses promoting prolonged survival under antibiotic exposure, and strong selection towards a phenotype that was clearly associated with a distinct mechanism of resistance (biofilm and phenotypic resistance, plankton and genetic resistance). We hypothesize that infection contexts (both within a host and within the hospital environment) will largely select for increasing biofilm investment, due to the combined biofilm benefits of antibiotic resistance, resistance to immune effectors and chemical insult, and physical recalcitrance attributed to the extracellular matrix (Høiby *et al.*, 2010b; Wei and Ma, 2013; Fux *et al.*, 2005); our B-selection treatment is therefore likely a closer proxy to a 'real world' within-hospital transmission model. However, our experiment does not account for differences in the factors promoting selection towards increasing biofilm (e.g. antibiotic exposure alternating with desiccation and disinfectant treatment), and it would be interesting to test whether variation in selective forces changed the nature of the evolutionary response both in biofilm formation and genetic resistance mechanisms.

6.3 Phenotypic heterogeneity and cellular condition

The model described in Chapter 2 assumes that cells can switch stochastically between biofilm and planktonic phenotypes at defined rates c and d. In Chapter 3, we introduce the possibility of environmental conditioning (i.e. plasticity) on the biofilm switching response, where cells may switch more frequently towards the biofilm in more damaging environments. Under the 'damage hypothesis' model (Cornforth and Foster, 2013; Oliveira *et al.*, 2015), biofilm investment is expected to

increase with greater accrual of damage. Our results suggest that there may be thresholds in this response, as we observed declining biofilm investment with increasing antibiotic dose, but a rebound in biofilm formation at the highest doses.

The damage hypothesis and biofilm formation are just one example of a broader link between environmental condition and internal state, which can often manifest as cellular damage. In Chapter 4, we expand upon this link by hypothesizing that the persister phenotype also shows dependence upon cellular damage, specifically via accumulation of insoluble protein aggregates associated with cellular aging in *E. coli*. Our experiments suggest that persistence in *E. coli* is independent of the age structure of the population, but we concede that experimental limitations may have prevented testing this hypothesis definitively; given that the persister cells occur at such a low frequency, it may be the case that only the oldest 1% or even less of the population may display measurable differences in persister frequency.

6.4 Phenotypic heterogeneity across broader environmental scales

While the theory presented in Chapter 2 is quite general, the experimental studies in Chapters 3 and 4 respectively rely on two well-studied and highly domesticated lab-strains of bacteria, *P. aeruginosa* PAO1 and a tagged variant of *E. coli* MG1655. The use of laboratory-adapted reference strains offers many advantages, for instance in developing general protocols for experimental procedures, and facilitating comparisons of results generated in different studies. However, reference strains also impose limitations, most notably in what can be inferred from a reference strain to the species it represents. For instance, this can even manifest as differences in phenotypes between reference strains for the same species – *P. aeruginosa* serves as a popular model organism for biofilm formation, but PAO1 relies primarily on *psl* as the main polysaccharide component of the biofilm matrix, while the slightly more virulent reference strain PA14 produces more *pel* polysaccharide (Mann and Wozniak, 2012), and neither readily produces alginate to the extent of many mucoid isolates commonly found in the CF lung (Ciofu *et al.*, 2010).

In Chapter 5, we examined the broader phenotypic diversity displayed by *P. aeruginosa* to explore just how representative PAO1 is towards a bacterial species known for behavioral diversity, and to ask whether such extraordinary phenotypic plasticity serves to buffer evolutionary change by allowing a single genotype to produce diverse phenotypes in response to widely varying environmental challenges (West-Eberhard, 2003). In contrast with the 'plasticity-buffers-evolution' hypothesis, we observed considerable phenotypic variation across natural isolates within fixed experimental assay conditions, also indicating PAO1 is indeed a poor representative of the phenotypic diversity of which the species is capable. Furthermore, our experimental results in Chapter 3 also suggest adaptive evolutionary responses overwhelm the effects of phenotypic plasticity in *P. aeruginosa*. Together, Chapters 3 and 5 point to an impressive evolvability and diversity of phenotypes across *P. aeruginosa*. However, we note that these will require additional genomic sequencing analyses for a more comprehensive interpretation.

6.5 Future work

Completion of sequencing projects in Chapters 3 and 5 is an obvious first step in directions for future work. In Chapter 3, this will allow for more precise determination of the dynamics of genetic resistance evolution, in particular towards answering our hypothesis that biofilm resistance facilitates the evolution of genetic resistance mutants. Additional phenotyping to gauge the evolution of plasticity in the biofilm resistance response is also a key interest, as the evolutionary dynamics of plastic resistance responses to antibiotics are generally unknown, in addition to being generally informative about the role of plasticity in the generation and maintenance of diversity in *P. aeruginosa*, as discussed above.

Genomic sequencing of the isolate library used in Chapter 5 will allow greater insights into the genomic and evolutionary determinants of the observed and dramatic phenotypic variation. It will also facilitate comparisons of the genetic signatures of related phenotypes (biofilm, in particular) evolved 'naturally' in the CF lung and other environmental contexts from the isolate library, and experimentally

in Chapter 3. Furthermore, a robust sequence-based phylogeny will allow us to explore the extent to which variation is shaped by evolutionary history, and also allow us to test comparative predictions with appropriate controls for common phylogenetic descent (Hadfield, 2010). For example, we are interested in exploring the distribution of cheating strains in a phylogenetic context. Specifically, we can ask whether cheating strains repeatedly evolve de novo as 'dead ends' (i.e., similarly to cancer), or whether 'professional' cheating strains exists, which co-evolve along with cooperating lineages and function more as an obligate parasite (or potentially as mutualists; for instance in (Hammerschmidt *et al.*, 2014), where the authors suggest that cheating strains may actually facilitate division of labor and thereby serve a beneficial function to the overall population).

It would be of interest to see if the frequency of persisters in a population is evolutionarily labile in a similar manner to biofilm formation, as they are functionally equivalent to the biofilm cells in the model presented in Chapter 2. However, given the difficulty of studying persister cells in the lab, this may be difficult to achieve without better understanding the causes of their formation. Persisters have been thought to function as a bet hedge against antibiotic treatment (ref? not consistent with metabolic noise hypothesis… not sure if actually adaptive), similarly to the minimal levels of biofilm investment maintained by populations in Chapter 2; it would be interesting to evolve cells in a randomly varying environment (e.g. in antibiotic concentration) and monitor whether persister fraction adaptively evolves.

In conclusion, the results presented in this thesis indicate consideration of heterogeneous phenotypes will be an important factor in the design of comprehensive antibiotic control strategies. Our findings suggest biofilms are a prime target, given their virtual ubiquity, intrinsic phenotypic resistance, and adaptive responsiveness to antibiotic treatment. One promising avenue to address this is the co-administration of 'antibiotic adjuvants' (Gill *et al.*, 2014) which disrupt biofilm function and therefore render populations more sensitive to antibiotic clearance, e.g. by degrading key components of the biofilm matrix (Alipour *et al.*,

2009). Other possible routes would be to reduce the frequency of biofilm transmission within e.g. a hospital environment, thereby potentially imposing trade-offs between transmission and survival. However, a better understanding of microbial life histories in general will be of crucial importance to designing control strategies that are effective and robust across (rapid) evolutionary time.

Bibliography

Van Acker H, Van Dijck P, Coenye T. (2014). Molecular mechanisms of antimicrobial tolerance and resistance in bacterial and fungal biofilms. *Trends Microbiol* **22**: 326–33.

Ackermann M, Stearns SC, Jenal U. (2003). Senescence in a bacterium with asymmetric division. *Science* **300**: 1920.

Aguilar C, Vlamakis H, Guzman A, Losick R, Kolter R. (2010). KinD is a checkpoint protein linking spore formation to extracellular matrix production in Bacillus subtilis biofilms. *MBio* **1**: e00035–10.

Aizenman E, Engelberg-Kulka H, Glaser G. (1996). An Escherichia coli chromosomal ' addiction module ' regulated by 3 ', 5 " -bispyrophosphate : A model for programmed bacterial cell death. *Proc Natl Acad Sci* **93**: 6059–63.

Akaike H. (1981). Likelihood of a model and information criteria. *J Econom* **16**: 3–14.

Alipour M, Suntres ZE, Omri A. (2009). Importance of DNase and alginate lyase for enhancing free and liposome encapsulated aminoglycoside activity against Pseudomonas aeruginosa. *J Antimicrob Chemother* **64**: 317–25.

Alizon S, Hurford A, Mideo N, Van Baalen M. (2009). Virulence evolution and the trade-off hypothesis: history, current state of affairs and the future. *J Evol Biol* **22**: 245–59.

Allen RC, McNally L, Popat R, Brown SP. (2016). Quorum sensing protects bacterial cooperation from exploitation by cheats. *ISMEJ (in Rev*.

Allesen-Holm M, Barken KB, Yang L, Klausen M, Webb JS, Kjelleberg S, *et al.* (2006). A characterization of DNA release in Pseudomonas aeruginosa cultures and biofilms. *Mol Microbiol* **59**: 1114–1128.

Amato SM, Brynildsen MP. (2014). Nutrient transitions are a source of persisters in Escherichia coli biofilms. *PLoS One* **9**: 1–9.

Andersen SB, Marvig RL, Molin S, Johansen HK, Griffin AS. (2015). Long-term social dynamics drive loss of function in pathogenic bacteria. *PNAS* **112**: 10756–10761.

Anderson RM, May RM. (1982). Coevolution of hosts and parasites. *Parasitology* **85**: 411–426.

Anderson RM, May RM. (1990). Immunisation and herd immunity. *Lancet* **335**: 641–645.

Anyan ME, Amiri A, Harvey CW, Tierra G, Morales-Soto N, Driscoll CM, *et al.* (2014). Type IV pili interactions promote intercellular association and moderate swarming of Pseudomonas aeruginosa. *Proc Natl Acad Sci* **111**: 201414661.

Ashish A, Paterson S, Mowat E, Fothergill JL, Walshaw MJ, Winstanley C. (2013). Extensive diversification is a common feature of Pseudomonas aeruginosa populations during respiratory infections in cystic fibrosis. *J Cyst Fibros* **12**: 790–793.

Balasubramanian D, Schneper L, Kumari H, Mathee K. (2013). A dynamic and intricate regulatory network determines Pseudomonas aeruginosa virulence. *Nucleic Acids Res* **41**: 1–20.

Barraud N, Hassett DJ, Hwang S-H, Rice S a, Kjelleberg S, Webb JS. (2006). Involvement of nitric oxide in biofilm dispersal of Pseudomonas aeruginosa. *J Bacteriol* **188**: 7344–53.

Barraud N, Schleheck D, Klebensberger J, Webb JS, Hassett DJ, Rice S a, *et al.* (2009). Nitric oxide signaling in Pseudomonas aeruginosa biofilms mediates phosphodiesterase activity, decreased cyclic di-GMP levels, and enhanced dispersal. *J Bacteriol* **191**: 7333–42.

Belas R. (2014). Biofilms, flagella, and mechanosensing of surfaces by bacteria. *Trends Microbiol* **22**: 517–527.

Bigger JW. (1944). Treatment of staphylococcal infections with penicillin. *Lancet* 497–500.

Blair JM a., Webber M a., Baylay AJ, Ogbolu DO, Piddock LJ V. (2014). Molecular mechanisms of antibiotic resistance. *Nat Rev Microbiol* **13**: 42–51.

Boles BR, Singh PK. (2008). Endogenous oxidative stress produces diversity and adaptability in biofilm communities. *Proc Natl Acad Sci U S A* **105**: 12503–8.

Boles BR, Thoendel M, Singh PK. (2004). Self-generated diversity produces 'insurance effects' in biofilm communities. *Proc Natl Acad Sci U S A* **101**: 16630–5.

Bragonzi A, Farulla I, Paroni M, Twomey KB, Pirone L, Lorè NI, *et al.* (2012). Modelling co-infection of the cystic fibrosis lung by Pseudomonas aeruginosa and Burkholderia cenocepacia reveals influences on biofilm formation and host response. *PLoS One* **7**: e52330.

Branda SS, González-Pastor JE, Ben-Yehuda S, Losick R, Kolter R. (2001). Fruiting body formation by Bacillus subtilis. *Proc Natl Acad Sci U S A* **98**: 11621–6.

Brauner A, Fridman O, Gefen O, Balaban NQ. (2016). Distinguishing between resistance, tolerance and persistence to antibiotic treatment. *Nat Rev Microbiol* **14**: 320–30.

Brown SP, Cornforth DM, Mideo N. (2012). Evolution of virulence in opportunistic pathogens: generalism, plasticity, and control. *Trends Microbiol* **20**: 336–42.

Buffie CG, Bucci V, Stein RR, McKenney PT, Ling L, Gobourne A, *et al.* (2015). Precision microbiome reconstitution restores bile acid mediated resistance to Clostridium difficile. *Nature* **517**: 205–8.

Buffie CG, Pamer EG. (2013). Microbiota-mediated colonization resistance against intestinal pathogens. *Nat Rev Immunol* **13**: 790–801.

Buivydas A, Pasanen T, Sencilo A, Daugelavi R, Vaara M, Bamford DH. (2013). Clinical isolates of Pseudomonas aeruginosa from superficial skin infections have different physiological patterns Andrius. *FEMS Microbiol Lett* **343**: 183–189.

Cano RJ, Borucki MK. (1995). Revival and identification of bacterial spores in 25- to 40-million-year-old Dominican amber. *Science* **268**: 1060–1064.

CDC. (2011). Haiti Cholera Outbreak. http://www.cdc.gov/haiticholera/haiti_cholera.htm (Accessed December 6, 2015).

Chew SC, Kundukad B, Seviour T. (2014). Dynamic Remodeling of Microbial Biofilms by Functionally Distinct. e-pub ahead of print, doi: 10.1128/mBio.01536-14.Editor.

Ciofu O, Mandsberg LF, Bjarnsholt T, Wassermann T, Høiby N. (2010). Genetic adaptation of Pseudomonas aeruginosa during chronic lung infection of patients with cystic fibrosis: strong and weak mutators with heterogeneous genetic backgrounds emerge in mucA and/or lasR mutants. *Microbiology* **156**: 1108–19.

Clark ST, Caballero JD, Cheang M, Coburn B, Wang PW, Donaldson SL, *et al.* (2015). Phenotypic diversity within a Pseudomonas aeruginosa population infecting an adult with cystic fibrosis. *Sci Rep* **5**: 10932.

Cohen NR, Lobritz MA, Collins JJ. (2013). Microbial Persistence and the Road to Drug Resistance. *Cell Host Microbe* **13**: 632–642.

Cornforth DM, Foster KR. (2013). Competition sensing: the social side of bacterial stress responses. *Nat Rev Microbiol* **11**: 285–293.

Cornforth DM, Popat R, McNally L, Gurney J, Scott-Phillips TC, Ivens A, *et al.* (2014). Combinatorial quorum sensing allows bacteria to resolve their social and physical environment. *Proc Natl Acad Sci U S A* **111**: 4280–4284.

Cornforth DM, Sumpter DJT, Brown SP, Brännström Å. (2012). Synergy and group size in microbial cooperation. *Am Nat* **180**: 296–305.

Corona F, Martinez J. (2013). Phenotypic Resistance to Antibiotics. *Antibiotics* **2**: 237–255.

Costerton JW, Cheng KJ, Geesey GG, Ladd TI, Nickel JC, Dasgupta M, *et al.* (1987). Bacterial biofilms in nature and disease. *Ann Rev Microbiol* **41**: 435–464.

Damkiær S, Yang L, Molin S, Jelsbak L. (2013). Evolutionary remodeling of global regulatory networks during long-term bacterial adaptation to human hosts. *Proc*

Natl Acad Sci **110**: 7766–71.

Darch SE, McNally A, Harrison F, Corander J, Barr HL, Paszkiewicz K, *et al.* (2015). Recombination is a key driver of genomic and phenotypic diversity in a Pseudomonas aeruginosa population during cystic fibrosis infection. *Sci Rep* **5**: 7649.

Davies JC. (2002). Pseudomonas aeruginosa in cystic fibrosis: pathogenesis and persistence. *Paediatr Respir Rev* **3**: 128–134.

Dennis DT, Staples JE. (2009). Plague. In: Evans A, Brachman P (eds). *Bacterial Infections of Humans: Epidemiology and Control*. Springer, pp 597–611.

Diggle SP, Crusz SA, Cámara M. (2007a). Quorum sensing. *Curr Biol* **17**: 907–910.

Diggle SP, Griffin AS, Campbell GS, West SA. (2007b). Cooperation and conflict in quorum-sensing bacterial populations. *Nature* **450**. e-pub ahead of print, doi: 10.1038/nature06279.

Diggle SP, Matthijs S, Wright VJ, Fletcher MP, Chhabra SR, Lamont IL, *et al.* (2007c). The Pseudomonas aeruginosa 4-Quinolone Signal Molecules HHQ and PQS Play Multifunctional Roles in Quorum Sensing and Iron Entrapment. *Chem Biol* **14**: 87–96.

Dow JM, Crossman L, Findlay K, He Y-Q, Feng J-X, Tang J-L. (2003). Biofilm dispersal in Xanthomonas campestris is controlled by cell-cell signaling and is required for full virulence to plants. *Proc Natl Acad Sci U S A* **100**: 10995–11000.

Drescher K, Shen Y, Bassler BL, Stone H a. (2013). Biofilm streamers cause catastrophic disruption of flow with consequences for environmental and medical systems. *Proc Natl Acad Sci U S A* **110**: 4345–50.

Driscoll JA, Brody SL, Kollef MH. (2007). The epidemiology, pathogenesis and treatment of Pseudomonas aeruginosa infections. *Drugs* **67**: 351–368.

Dumas Z, Ross-gillespie A, Kümmerli R, B PRS. (2013). Switching between apparently redundant iron-uptake mechanisms benefits bacteria in changeable environments. *Proc R Soc B Biol Sci* **280**: 20131055.

El'Garch F, Jeannot K, Hocquet D, Llanes-Barakat C, Plésiat P. (2007). Cumulative

effects of several nonenzymatic mechanisms on the resistance of Pseudomonas aeruginosa to aminoglycosides. *Antimicrob Agents Chemother* **51**: 1016–1021.

Elena SF, Lenski RE. (2003). Evolution experiments with microorganisms: the dynamics and genetic bases of adaptation. *Nat Rev Genet* **4**: 457–69.

Fauvart M, de Groote VN, Michiels J. (2011). Role of persister cells in chronic infections: Clinical relevance and perspectives on anti-persister therapies. *J Med Microbiol* **60**: 699–709.

Flemming H, Wingender J. (2010). The biofilm matrix. *Nat Rev Microbiol* **8**: 623–33.

Flint HJ, Scott KP, Louis P, Duncan SH. (2012). The role of the gut microbiota in nutrition and health. *Nat Rev Gastroenterol Hepatol* **9**: 577–589.

Flume PA, Mogayzel PJ, Robinson KA, Goss CH, Rosenblatt RL, Kuhn RJ, *et al.* (2009). Cystic fibrosis pulmonary guidelines: Treatment of pulmonary exacerbations. *Am J Respir Crit Care Med* **180**: 802–808.

Fonseca AP, Correia P, Sousa JC, Tenreiro R. (2007). Association patterns of Pseudomonas aeruginosa clinical isolates as revealed by virulence traits , antibiotic resistance , serotype and genotype. *FEMS Immunol Med Microbiol* **51**: 505–516.

Francolini I, Donelli G. (2010). Prevention and control of biofilm-based medical-device-related infections. *FEMS Immunol Med Microbiol* **59**: 227–238.

Frank S a. (1996). Models of parasite virulence. *Q Rev Biol* **71**: 37–78.

Fridman O, Goldberg A, Ronin I, Shoresh N, Balaban NQ. (2014). Optimization of lag time underlies antibiotic tolerance in evolved bacterial populations. *Nature* **99**: 418–421.

Fux CA, Costerton JW, Stewart PS, Stoodley P. (2005). Survival strategies of infectious biofilms. *Trends Microbiol* **13**: 34–40.

Gaspar MC, Couet W, Olivier J-C, Pais a a CC, Sousa JJS. (2013). Pseudomonas aeruginosa infection in cystic fibrosis lung disease and new perspectives of treatment: a review. *Eur J Clin Microbiol Infect Dis* **32**: 1231–52.

Gerdes K, Christensen SK, Løbner-Olesen A. (2005). Prokaryotic toxin-antitoxin stress response loci. *Nat Rev Microbiol* **3**: 371 – 382.

van Gestel J, Vlamakis H, Kolter R. (2015). Division of Labor in Biofilms : the Ecology of Cell Differentiation. *Microbiol Spectr* **3**: MB–0002–2014.

Ghio AJ, Roggli VL, Soukup JM, Richards JH, Randell SH, Muhlebach MS. (2013). Iron accumulates in the lavage and explanted lungs of cystic fibrosis patients. *J Cyst Fibros* **12**: 390–398.

Gill EE, Franco OL, Hancock REW. (2014). Antibiotic Adjuvants: Diverse Strategies for Controlling Drug Resistant Pathogens. *Chem Biol Drug Des*. e-pub ahead of print, doi: 10.1111/cbdd.12478.

Goerke C, Gressinger M, Endler K, Breitkopf C, Wardecki K, Stern M, *et al.* (2007). High phenotypic diversity in infecting but not in colonizing Staphylococcus aureus populations. *Environ Microbiol* **9**: 3134–3142.

Green JL, Bohannan BJM, Whitaker RJ. (2008). Microbial biogeography: from taxonomy to traits. *Science (80-)* **320**: 1039–1043.

Greulich P, Waclaw B, Allen R. (2012). Mutational Pathway Determines Whether Drug Gradients Accelerate Evolution of Drug-Resistant Cells. *Phys Rev Lett* **109**: 1–5.

Gudelj I, Weitz JS, Ferenci T, Claire Horner-Devine M, Marx CJ, Meyer JR, *et al.* (2010). An integrative approach to understanding microbial diversity: From intracellular mechanisms to community structure. *Ecol Lett* **13**: 1073–1084.

Gupta K, Marques CNH, Petrova OE, Sauer K. (2013). Antimicrobial Tolerance of Pseudomonas aeruginosa Biofilms Is Activated during an Early Developmental Stage and Requires the Two-Component Hybrid SagS. *J Bacteriol* **195**: 4975–87.

Haaber J, Cohn MT, Frees D, Andersen TJ, Ingmer H. (2012). Planktonic aggregates of Staphylococcus aureus protect against common antibiotics. *PLoS One* **7**: e41075.

Hadfield JD. (2010). MCMC Methods for Multi-Response Generalized Linear Mixed Models: The MCMCglmm R Package. Journal of Statistical Software, 33(2), 1-22.

URL http://www.jstatsoft.org/v33/i02/. **33**. http://www.jstatsoft.org/v33/i02/.

Hall-Stoodley L, Costerton JW, Stoodley P. (2004). Bacterial biofilms: from the natural environment to infectious diseases. *Nat Rev Microbiol* **2**: 95–108.

Hammerschmidt K, Rose CJ, Kerr B, Rainey PB. (2014). Life cycles, fitness decoupling and the evolution of multicellularity. *Nature* **515**: 75–79.

Hansen S, Lewis K, Vulić M. (2008). Role of global regulators and nucleotide metabolism in antibiotic tolerance in Escherichia coli. *Antimicrob Agents Chemother* **52**: 2718–2726.

Harmsen M, Yang L, Pamp SJ, Tolker-Nielsen T. (2010). An update on Pseudomonas aeruginosa biofilm formation, tolerance, and dispersal. *FEMS Immunol Med Microbiol* **59**: 253–68.

Heineman RH, Brown SP. (2012). Experimental evolution of a bacteriophage virus reveals the trajectory of adaptation across a fecundity/longevity trade-off. *PLoS One* **7**: e46322.

Hilker R, Munder A, Klockgether J, Losada PM, Chouvarine P, Cramer N, *et al.* (2015). Interclonal gradient of virulence in the Pseudomonas aeruginosa pangenome from disease and environment. *Environ Microbiol* **17**: 29–46.

Hochberg ME, Rankin DJ, Taborsky M. (2008). The coevolution of cooperation and dispersal in social groups and its implications for the emergence of multicellularity. *BMC Evol Biol* **8**: 238.

Høiby N, Bjarnsholt T, Givskov M, Molin S, Ciofu O. (2010a). Antibiotic resistance of bacterial biofilms. *Int J Antimicrob Agents* **35**: 322–32.

Høiby N, Bjarnsholt T, Givskov M, Molin S, Ciofu O. (2010b). Antibiotic resistance of bacterial biofilms. *Int J Antimicrob Agents* **35**: 322–32.

Huse HK, Kwon T, Zlosnik JEA, Speert DP, Marcotte EM, Whiteley M. (2010). Parallel Evolution in Pseudomonas aeruginosa over 39,000 Generations In Vivo. *MBio* **1**: e00199–10.

Hutner SH, Provasoli L, Schnatz A, Haskins CP. (1950). Some Approaches to the Study of the Role of Metals in the Metabolism of Microorganisms Author (s): S . H . Hutner , L . Provasoli , Albert Schatz and C . P . Haskins Reviewed work (s): Published by : American Philosophical Society Stable URL : http://. *Proc Am Philos Soc* **94**: 152–170.

Huynh TT, McDougald D, Klebensberger J, Al Qarni B, Barraud N, Rice S a, *et al.* (2012). Glucose starvation-induced dispersal of Pseudomonas aeruginosa biofilms is cAMP and energy dependent. *PLoS One* **7**: e42874.

Irie Y, Roberts AEL, Kragh KN, Gordon V, Hutchison JB, Allen RJ, *et al.* (2016). The Pseudomonas aeruginosa PSL polysaccharide is a social but non-cheatable trait in biofilms. *BioRxiv*. e-pub ahead of print, doi: http://dx.doi.org/10.1101/049783.

Jain R, Rivera MC, Moore JE, Lake JA. (2003). Horizontal gene transfer accelerates genome innovation and evolution. *Mol Biol Evol* **20**: 1598–1602.

Jeukens J, Boyle B, Kukavica-ibrulj I, Ouellet MM, Aaron SD, Charette SJ, *et al.* (2014). Comparative Genomics of Isolates of a Pseudomonas aeruginosa Epidemic Strain Associated with Chronic Lung Infections of Cystic Fibrosis Patients. *PLoS One* **9**: e87611.

Jimenez PN, Koch G, Thompson J a, Xavier KB, Cool RH, Quax WJ. (2012). The multiple signaling systems regulating virulence in Pseudomonas aeruginosa. *Microbiol Mol Biol Rev* **76**: 46–65.

Jorth P, Staudinger BJ, Wu X, Bruce JE, Timothy L, Singh PK, *et al.* (2015). Regional Isolation Drives Bacterial Diversification within Cystic Fibrosis Lungs. *Cell Host Microbe* **18**: 307–319.

Kaplan JB. (2010). Biofilm dispersal: mechanisms, clinical implications, and potential therapeutic uses. *J Dent Res* **89**: 205–18.

Karatan E, Watnick P. (2009). Signals, regulatory networks, and materials that build and break bacterial biofilms. *Microbiol Mol Biol Rev* **73**: 310–47.

Kassambara A, Mundt F. (2016). factoextra: Extract and Visualize the Results of Multivariate Data Analyses. https://cran.r-project.org/package=factoextra.

Kassen R, Llewellyn M, Rainey PB. (2004). Ecological constraints on diversification in a model adaptive radiation. *Nature* **431**: 984–989.

Keren I, Kaldalu N, Spoering A, Wang Y, Lewis K. (2004a). Persister cells and tolerance to antimicrobials. *FEMS Microbiol Lett* **230**: 13–18.

Keren I, Shah D, Spoering A, Kaldalu N, Lewis K. (2004b). Specialized Persister Cells and the Mechanism of Multidrug Tolerance in Escherichia coli. *J Bacteriol* **186**: 8172–8180.

de Kievit TR. (2009). Quorum sensing in Pseudomonas aeruginosa biofilms. *Environ Microbiol* **11**: 279–88.

Klapper I, Gilbert P, Ayati BP, Dockery J, Stewart PS. (2007). Senescence can explain microbial persistence. 3623–3630.

Köhler T, Buckling A, van Delden C. (2009). Cooperation and virulence of clinical Pseudomonas aeruginosa populations. *Proc Natl Acad Sci U S A* **106**: 6339–44.

Korch SB, Henderson TA, Hill TM. (2003). Characterization of the hipA7 allele of Escherichia coli and evidence that high persistence is governed by (p)ppGpp synthesis. *Mol Microbiol* **50**: 1199–1213.

Kragh KN, Hutchison JB, Melaugh G, Rodesney C, Roberts AEL, Irie Y, *et al.* (2016). Role of Multicellular Aggregates in Biofilm Formation. *MBio* **7**: e00237–16.

Kramer A, Schwebke I, Kampf G. (2006). How long do nosocomial pathogens persist on inanimate surfaces? A systematic review. *BMC Infect Dis* **6**: 130.

Kruse H, Srum H. (1994). Transfer of multiple drug resistance plasmids Transfer of Multiple Drug Resistance Plasmids between Bacteria of Diverse Origins in Natural Microenvironments. **60**.

Kuchma SL, Ballok a. E, Merritt JH, Hammond JH, Lu W, Rabinowitz JD, *et al.* (2010). Cyclic-di-GMP-mediated repression of swarming motility by Pseudomonas

aeruginosa: The pilY1 gene and its impact on surface-associated behaviors. *J Bacteriol* **192**: 2950–2964.

Kümmerli R, Gardner A, West SA, Griffin AS. (2009a). Limited dispersal, budding dispersal, and cooperation: An experimental study. *Evolution (N Y)* **63**: 939–949.

Kümmerli R, Jiricny N, Clarke LS, West S a, Griffin a S. (2009b). Phenotypic plasticity of a cooperative behaviour in bacteria. *J Evol Biol* **22**: 589–98.

Lardon L a, Merkey B V, Martins S, Dötsch A, Picioreanu C, Kreft J-U, *et al.* (2011). iDynoMiCS: next-generation individual-based modelling of biofilms. *Environ Microbiol* **13**: 2416–34.

Leggett HC, Brown SP, Reece SE. (2014). War and peace: social interactions in infections. *Philos Trans R Soc Lond B Biol Sci* **369**: 20130365.

Leszczynska D, Matuszewska E, Kuczynska-wisnik D, Furmanek-blaszk B. (2013). The Formation of Persister Cells in Stationary-Phase Cultures of Escherichia Coli Is Associated with the Aggregation of Endogenous Proteins. **8**. e-pub ahead of print, doi: 10.1371/journal.pone.0054737.

Lewis K. (2010). Persister Cells. e-pub ahead of print, doi: 10.1146/annurev.micro.112408.134306.

Lieberman TD, Flett KB, Yelin I, Martin TR, McAdam AJ, Priebe GP, *et al.* (2014). Genetic variation of a bacterial pathogen within individuals with cystic fibrosis provides a record of selective pressures. *Nat Genet* **46**: 82–7.

Lindner AB, Madden R, Demarez A, Stewart EJ, Taddei F. (2008). Asymmetric segregation of protein aggregates is associated with cellular aging and rejuvenation. *Proc Natl Acad Sci U S A* **105**: 3076–81.

Lori C, Ozaki S, Steiner S, Böhm R, Abel S, Dubey BN, *et al.* (2015). Cyclic di-GMP acts as a cell cycle oscillator to drive chromosome replication. *Nature* **523**: 236–239.

Luria SE, Delbruck M. (1943). Mutations of bacteria from virus sensitivity to virus resistance. *Genetics* **28**: 491–511.

Lutz RA, Kennish MJ. (1993). Ecology of deep-sea hydrothermal vent communities: A review. *Rev Geophys* **31**: 211–242.

Maisonneuve E, Castro-Camargo M, Gerdes K. (2013a). (p)ppGpp Controls Bacterial Persistence by Stochastic Induction of Toxin-Antitoxin Activity. *Cell* **154**: 1140–1150.

Maisonneuve E, Castro-Camargo M, Gerdes K. (2013b). (p)ppGpp Controls Bacterial Persistence by Stochastic Induction of Toxin-Antitoxin Activity. *Cell* **154**: 1140–50.

Mann EE, Wozniak DJ. (2012). Pseudomonas biofilm matrix composition and niche biology. *FEMS Microbiol Rev* **36**: 893–916.

Marks LR, Reddinger RM, Hakansson AP. (2014). Biofilm formation enhances fomite survival of Streptococcus pneumoniae and Streptococcus pyogenes. *Infect Immun* **82**: 1141–6.

Markussen T, Marvig RL, Gomez-Lozano M, Aanaes K, Burleigh AE, Høiby N, *et al.* (2014). Environmental Heterogeneity Drives Within-Host Diversification and Evolution of Pseudomonas aeruginosa. *MBio* **5**: e01592.

Masuko T, Minami A, Iwasaki N, Majima T, Nishimura S-I, Lee YC. (2005). Carbohydrate analysis by a phenol-sulfuric acid method in microplate format. *Anal Biochem* **339**: 69–72.

Matz C, Webb JS, Schupp PJ, Phang SY, Penesyan A, Egan S, *et al.* (2008). Marine biofilm bacteria evade eukaryotic predation by targeted chemical defense. *PLoS One* **3**: e2744.

McDougald D, Rice S a., Barraud N, Steinberg PD, Kjelleberg S. (2011). Should we stay or should we go: mechanisms and ecological consequences for biofilm dispersal. *Nat Rev Microbiol* **10**: 39–50.

Melaugh G, Hutchison J, Kragh KN, Irie Y, Roberts A, Bjarnsholt T, *et al.* (2016). Shaping the growth behaviour of biofilms initiated from bacterial aggregates. *PLoS One* **11**: 1–18.

Van Melderen L, De Bast MS. (2009). Bacterial toxin-Antitoxin systems: More than selfish entities? *PLoS Genet* **5**. e-pub ahead of print, doi: 10.1371/journal.pgen.1000437.

Mikonranta L, Friman V-P, Laakso J. (2012). Life history trade-offs and relaxed selection can decrease bacterial virulence in environmental reservoirs. *PLoS One* **7**: e43801.

Monds RD, O'Toole G a. (2009). The developmental model of microbial biofilms: ten years of a paradigm up for review. *Trends Microbiol* **17**: 73–87.

Mowat E, Paterson S, Fothergill JL, Wright EA, Ledson MJ, Walshaw MJ, *et al.* (2011). Pseudomonas aeruginosa Population Diversity and Turnover in Cystic Fibrosis Chronic Infections. *Am J Respir Crit Care Med* **183**: 1674–9.

Mulcahy H, Charron-Mazenod L, Lewenza S. (2008). Extracellular DNA chelates cations and induces antibiotic resistance in Pseudomonas aeruginosa biofilms. *PLoS Pathog* **4**. e-pub ahead of print, doi: 10.1371/journal.ppat.1000213.

Nadell CD, Xavier JB, Foster KR. (2009). The sociobiology of biofilms. *FEMS Microbiol Rev* **33**: 206–24.

Nguyen D, Joshi-Datar A, Lepine F, Bauerle E, Olakanmi O, Beer K, *et al.* (2011). Active Starvation Responses Mediate Antibiotic Tolerance in Biofilms and Nutrient-Limited Bacteria. *Science (80-)* **334**: 982–6.

O'Toole GA, Kaplan HB, Kolter R. (2000). Biofilm formation as microbial development. *Annu Rev Microbiol* **54**: 49–79.

O'Toole GA, Kolter R. (1998). Flagellar and twitching motility are necessary for Pseudomonas aeruginosa biofilm development. *Mol Microbiol* **30**: 295–304.

Ohman DE, Cryz SJ, Iglewski BH. (1980). Isolation and characterization of a Pseudomonas aeruginosa PAO mutant that produces altered elastase. *J Bacteriol* **142**: 836–842.

Oliveira NM, Martinez-Garcia E, Xavier J, Durham WM, Kolter R, Kim W, *et al.*

(2015). Biofilm formation as a response to ecological competition. *PLoS Biol* **13**: 1–23.

Otto M. (2004). Quorum-sensing control in Staphylococci - A target for antimicrobial drug therapy? *FEMS Microbiol Lett* **241**: 135–141.

De Paepe M, Taddei F. (2006). Viruses' life history: towards a mechanistic basis of a trade-off between survival and reproduction among phages. *PLoS Biol* **4**: e193.

Pai H, Kim J, Kim J, Lee JH, Lee JIH. (2001). Carbapenem Resistance Mechanisms in Pseudomonas aeruginosa Clinical Isolates Carbapenem Resistance Mechanisms in Pseudomonas aeruginosa Clinical Isolates. *Antimicrob Agents Chemother* **45**: 480.

Patriquin GM, Banin E, Gilmour C, Tuchman R, Greenberg EP, Poole K. (2008). Influence of quorum sensing and iron on twitching motility and biofilm formation in Pseudomonas aeruginosa. *J Bacteriol* **190**: 662–71.

Pflughoeft KJ, Versalovic J. (2012). Human microbiome in health and disease. *Annu Rev Pathol* **7**: 99–122.

Pleasants R a. (1994). Allergic Reactions to Parenteral Beta-lactam Antibiotics in Patients With Cystic Fibrosis. *CHEST J* **106**: 1124.

Pollitt EJG, Crusz SA, Diggle SP. (2015). Staphylococcus aureus forms spreading dendrites that have characteristics of active motility. *Sci Rep* **5**: 17698.

Poltak SR, Cooper VS. (2010). Ecological succession in long-term experimentally evolved biofilms produces synergistic communities. *ISME J* **5**: 369–78.

Popat R, Crusz S a, Messina M, Williams P, West S a, Diggle SP. (2012). Quorum-sensing and cheating in bacterial biofilms. *Proc R Soc B Biol Sci*. e-pub ahead of print, doi: 10.1098/rspb.2012.1976.

Qi Q, Toll-Riera M, Heilbron K, Preston GM, MacLean RC. (2016). The genomic basis of adaptation to the fitness cost of rifampicin resistance in Pseudomonas aeruginosa. *Proc R Soc B Biol Sci* **283**: 20152452.

Queller DC, Strassmann JE. (2009). Beyond society: the evolution of organismality. *Philos Trans R Soc Lond B Biol Sci* **364**: 3143–55.

R Core Team. (2015). R: A language and environment for statistical computing. https://www.r-project.org/.

Rainey PB, Travisano M. (1998). Adaptive radiation in a heterogeneous environment. *Nature* **394**: 69–72.

Rice S a, Tan CH, Mikkelsen PJ, Kung V, Woo J, Tay M, *et al.* (2009). The biofilm life cycle and virulence of Pseudomonas aeruginosa are dependent on a filamentous prophage. *ISME J* **3**: 271–82.

Rodríguez-Martínez JM, Poirel L, Nordmann P. (2009). Molecular epidemiology and mechanisms of carbapenem resistance in Pseudomonas aeruginosa. *Antimicrob Agents Chemother* **53**: 4783–4788.

Rossolini GM, Arena F, Pecile P, Pollini S. (2014). Update on the antibiotic resistance crisis. *Curr Opin Pharmacol* **18**: 56–60.

Rumbaugh KP, Diggle SP, Watters CM, Ross-Gillespie A, Griffin AS, West S a. (2009). Quorum sensing and the social evolution of bacterial virulence. *Curr Biol* **19**: 341–5.

Sauer K, Camper AK, Ehrlich GD, William J, Davies DG, Costerton JW. (2002). Pseudomonas aeruginosa Displays Multiple Phenotypes during Development as a Biofilm. *J Bacteriol* **184**: 1140–1154.

Sauer K, Cullen MC, Rickard AH, Zeef LAH, Gilbert P, Davies DG. (2004). Characterization of Nutrient-Induced Dispersion in Pseudomonas aeruginosa PAO1 Biofilm. *J Bacteriol* **186**: 7312–7326.

Schleheck D, Barraud N, Klebensberger J, Webb JS, McDougald D, Rice S a, *et al.* (2009). Pseudomonas aeruginosa PAO1 preferentially grows as aggregates in liquid batch cultures and disperses upon starvation. *PLoS One* **4**: e5513.

Schuster M, Sexton DJ, Diggle SP, Greenberg EP. (2013). Acyl-Homoserine Lactone Quorum Sensing: From Evolution to Application. *Annu Rev Microbiol* 43–63.

Sender R, Fuchs S, Milo R. (2016). Revised estimates for the number of human and

bacteria cells in the body. *bioRxiv2* 1–21.

Singh R, Ray P, Das A, Sharma M. (2009). Role of persisters and small-colony variants in antibiotic resistance of planktonic and biofilm-associated Staphylococcus aureus: an in vitro study. *J Med Microbiol* **58**: 1067–73.

Skidmore ML, Foght JM, Sharp MJ. (2000). Microbial Life beneath a High Arctic Glacier. *Appl Environ Microbiol* **66**: 3214–3220.

Smith R, Tan C, Srimani JK, Pai A, Riccione K a, Song H, *et al.* (2014). Programmed Allee effect in bacteria causes a tradeoff between population spread and survival. *Proc Natl Acad Sci U S A* **111**. e-pub ahead of print, doi: 10.1073/pnas.1315954111.

Soetaert K, Petzoldt T, Setzer RW. (2010). Solving Differential Equations in R: Package deSolve. *J Stat Softw* **33**: 1–25.

Sperandio V, Hovde CJ (eds). (2015). Enterohemorrhagic Escherichia coli and Other Shiga Toxin-Producing E. coli. ASM Press.

Starkey M, Hickman JH, Ma L, Zhang N, De Long S, Hinz A, *et al.* (2009). Pseudomonas aeruginosa rugose small-colony variants have adaptations that likely promote persistence in the cystic fibrosis lung. *J Bacteriol* **191**: 3492–503.

Stearns. (1992). The Evolution of Life Histories.

Stewart EJ, Madden R, Paul G, Taddei F. (2005). Aging and death in an organism that reproduces by morphologically symmetric division. *PLoS Biol* **3**: e45.

Stewart PS. (2003). Diffusion in Biofilms. *J Bacteriol* **185**: 1485–1491.

Stewart PS, Franklin MJ. (2008). Physiological heterogeneity in biofilms. *Nat Rev Microbiol* **6**: 199–210.

Stover CK, Pham XQ, Erwin AL, Mizoguchi SD, Warrener P, Hickey MJ, *et al.* (2000). Complete genome sequence of Pseudomonas aeruginosa PAO1 , an opportunistic pathogen. **406**: 959–964.

Strateva T, Yordanov D. (2009). Pseudomonas aeruginosa - a phenomenon of bacterial resistance. *J Med Microbiol* **58**: 1133–48.

Taylor TB, Buckling A. (2010). Competition and dispersal in Pseudomonas aeruginosa. *Am Nat* **176**: 83–9.

Timmermans J, Van Melderen L. (2010). Post-transcriptional global regulation by CsrA in bacteria. *Cell Mol Life Sci* **67**: 2897–2908.

Tuomanen E, Cozens R, Tosch W, Zak O, Tomasz A. (1986). The Rate of Killing of Escherichia coli by P-Lactam Antibiotics Is Strictly Proportional to the Rate of Bacterial Growth. *J Gen Microbiol* **132**: 1297–1304.

Ueda A, Wood TK. (2009). Connecting quorum sensing, c-di-GMP, pel polysaccharide, and biofilm formation in Pseudomonas aeruginosa through tyrosine phosphatase TpbA (PA3885). *PLoS Pathog* **5**: e1000483.

Valle J, Solano C, García B, Toledo-Arana A, Lasa I. (2013). Biofilm switch and immune response determinants at early stages of infection. *Trends Microbiol* **21**: 364–71.

Vega NM, Gore J. (2014). Collective antibiotic resistance: Mechanisms and implications. *Curr Opin Microbiol* **21**: 28–34.

Vreeland RH, Rosenzweig WD, Powers DW. (2000). Isolation of a 250 million-year-old halotolerant bacterium from a primary salt crystal. *Nature* **407**: 897–900.

Wang P, Robert L, Pelletier J, Dang WL, Taddei F, Wright A, *et al.* (2010). Robust growth of escherichia coli. *Curr Biol* **20**: 1099–1103.

Wang S, Yu S, Zhang Z, Wei Q, Yan L, Ai G, *et al.* (2014). Coordination of swarming motility, biosurfactant synthesis, and biofilm matrix exopolysaccharides production in Pseudomonas aeruginosa. *Appl Environ Microbiol*. e-pub ahead of print, doi: 10.1128/AEM.01237-14.

Wei Q, Ma LZ. (2013). Biofilm matrix and its regulation in Pseudomonas aeruginosa. *Int J Mol Sci* **14**: 20983–1005.

Werner E, Roe F, Bugnicourt A, Michael J, Heydorn A, Molin S, *et al.* (2004). Stratified Growth in Pseudomonas aeruginosa Biofilms Stratified Growth in

Pseudomonas aeruginosa Biofilms. **70**: 6188–6196.

Wessel AK, Arshad TA, Fitzpatrick M, Connell JL, Bonnecaze RT, Shear JB, *et al.* (2014). Oxygen Limitation within a Bacterial Aggregate. *MBio* **5**: e00992.

West S a, Griffin AS, Gardner A, Diggle SP. (2006). Social evolution theory for microorganisms. *Nat Rev Microbiol* **4**: 597–607.

West-Eberhard MJ. (2003). Developmental plasticity and evolution. Oxford University Press: Oxford.

Wilder CN, Diggle SP, Schuster M. (2011). Cooperation and cheating in Pseudomonas aeruginosa: the roles of the las, rhl and pqs quorum-sensing systems. *ISME J* **5**: 1332–43.

Williams D, Evans B, Haldenby S, Walshaw MJ, Brockhurst MA, Winstanley C, *et al.* (2015). Divergent, Coexisting Pseudomonas aeruginosa Lineages in Chronic Cystic Fibrosis Lung Infections. *Am J Respir Crit Care Med* **191**: 775–785.

Winstanley C, Brien SO, Brockhurst MA. (2016). Pseudomonas aeruginosa Evolutionary Adaptation and Diversification in Cystic Fibrosis Chronic Lung Infections. *Trends Microbiol* **24**: 327–337.

Wiuff C, Zappala RM, Regoes RR, Garner KN, Levin BR. (2005). Phenotypic Tolerance : Antibiotic Enrichment of Noninherited Resistance in Bacterial Populations Phenotypic Tolerance : Antibiotic Enrichment of Noninherited Resistance in Bacterial Populations. *Antimicrob Agents Chemother* **49**: 1483.

Wolfram. (2015). Mathematica. Version 10. Wolfram Research Inc.: Champaign, Illinois.

Wong A, Rodrigue N, Kassen R. (2012). Genomics of Adaptation during Experimental Evolution of the Opportunistic Pathogen Pseudomonas aeruginosa. *PLoS Genet* **8**: e1002928.

Wood TK, Knabel SJ, Kwan BW. (2013). Bacterial persister cell formation and dormancy. *Appl Environ Microbiol* **79**: 7116–21.

Workentine ML, Sibley CD, Glezerson B, Purighalla S, Norgaard-gron JC, Parkins MD, *et al.* (2013). Phenotypic Heterogeneity of Pseudomonas aeruginosa Populations in a Cystic Fibrosis Patient. *PLoS One* **8**: e60225.

Wright EA, Fothergill JL, Paterson S, Brockhurst MA, Winstanley C. (2013). Sub-inhibitory concentrations of some antibiotics can drive diversification of Pseudomonas aeruginosa populations in artificial sputum medium. *BMC Microbiol* **13**: 170.

Wright EA, Di Lorenzo V, Trappetti C, Liciardi M, Orru G, Viti C, *et al.* (2015). Divergence of a strain of Pseudomonas aeruginosa during an outbreak of ovine mastitis. *Vet Microbiol* **175**: 105–113.

Xavier JB, Foster KR. (2007). Cooperation and conflict in microbial biofilms. *Proc Natl Acad Sci U S A* **104**: 876–81.

Yang L, Haagensen J a J, Jelsbak L, Johansen HK, Sternberg C, Høiby N, *et al.* (2008). In situ growth rates and biofilm development of Pseudomonas aeruginosa populations in chronic lung infections. *J Bacteriol* **190**: 2767–76.

Zhang Y, Yew WW, Barer MR. (2012). Targeting persisters for tuberculosis control. *Antimicrob Agents Chemother* **56**: 2223–2230.

Appendix

Table of natural and clinical isolates of P. aeruginosa used in Chapters 2 and 5.

ID	Location	Country	Date	Source
1	Paris	France	1882-1918	Surgical bandage
2	Paris	France	1882-1918	Wound
3	Paris	France	1882-1918	Wound
5	Paris	France	1882-1918	Wound
7	Paris	France	1882-1918	Wound
9	Paris	France	1882-1918	Leg ulcer
11	Paris	France	1882-1918	Wound
13	Paris	France	1882-1918	Wound
14	Paris	France	1882-1918	Rabbit
15	Bucarest	Romania	1965-1978	Faeces
23	Loltun	Mexico	2004	Cenote water
24	North Sea	Belgium	2007	Sea water (coastal)
26	Vancouver	Canada	2002	CF-patient
27	Ghent	Belgium	2003	Shallow pond water
28	Geel	Belgium	2004	Clinical non CF
29	Cambridge	UK	pre 1936	Plant
30	Hanover	Germany	1994	CF-patient
32	Tbilisi	Georgian Republic	1975	Pleural fluid
33	Tbilisi	Georgian Republic	Unknown	Wound
34	Ghent	Belgium	1999	Sputum
35	Ghent	Belgium	1992	Wound
37	Ghent	Belgium	1998	Urine
38	Brussels	Belgium	1993	Clinical non CF
39	Leuven	Belgium	2004	Clinical non CF
40	Leuven	Belgium	2004	Clinical non CF
41	De Haan	Belgium	1993	CF-patient
42	De Haan	Belgium	1993	CF-patient
45	Vancouver	Canada	2002	CF-patient
47	Melbourne	Australia	1955	Wound
48	Brussels	Belgium	1985	Urine
49	Buenos Aires	Argentina	pre 1984	Wound
50	Boston	USA	1971	Blood
51	Cali	Colombia	2003	Blood
52	Cali	Colombia	2003	Hospital environment
55	Unknown	India	Unknown	Dog
66	Unknown	UK	2004	Dog
69	Unknown	UK	2004	Dog
71	Unknown	UK	2004	Dog

73	Unknown	UK	2004	Dog
75	Unknown	UK	2004	Dog
76	Detroit	USA	1921	Unknown
78	London	UK	1924	Ear
79	London	UK	1923	Wound
80	London	UK	1937	Urine
81	Elstree	UK	1944	Urine
82	Elstree	UK	1944	Urine
84	California	USA	1949	Unknown
86	London	UK	1950	Urine
89	Unknown	The Philippines	1925	Tobacco plant
90	Colindale	UK	1962	Faeces
92	London	UK	1969	Human
93	Surrey	UK	1967	Sputum
94	Kentucky	USA	1982	Unknown
100	Mediterranean Sea	Tunisia	2000	Sea water (coastal)
101	Istanbul	Turkey	1997	Burn
109	Jekyll Island	USA	2004	Turtle egg (interior)
111	Jekyll Island	USA	2005	Turtle egg (interior)
113	Jekyll Island	USA	2005	Turtle egg (exterior)
115	Jekyll Island	USA	2005	Turtle egg (exterior)
116	Jekyll Island	USA	2006	Turtle egg (exterior)
119	Suruga Bay (N2, 200m)	Japan	2004	Sea water (coastal)
120	Suruga Bay (N2, 200m)	Japan	2004	Sea water (coastal)
121	Pacific Ocean (N7, 200m)	Japan	2004	Sea water (open ocean)
122	Pacific Ocean (N7, 0m)	Japan	2004	Sea water (open ocean)
123	Pacific Ocean (S2, 0m)	Japan	2004	Sea water (open ocean)
124	Pacific Ocean (S2, 0m)	Japan	2004	Sea water (open ocean)
125	Sagami Bay	Japan	2003	Sea water (coastal)
126	Pacific Ocean (S2, 0m)	Japan	2004	Sea water (coastal)
127	Sagami Bay (S1, 0m)	Japan	2004	Sea water (coastal)
128	Otshuchi Bay	Japan	2004	Dolphin
129	Pacific Ocean (S2, 0m)	Japan	2003	Sea water (coastal)
130	Pacific Ocean (S2, 0m)	Japan	2003	Sea water (open ocean)
131	Pacific Ocean (S2, 0m)	Japan	2003	Sea water (open ocean)
132	Pacific Ocean (S2, 0m)	Japan	2003	Sea water (open ocean)
133	Pacific Ocean (S2, 0m)	Japan	2003	Sea water (open ocean)
134	Pacific Ocean (S4, 0m)	Japan	2003	Sea water (open ocean)
135	Arakawa river	Japan	2003	River water
136	Arakawa river	Japan	2003	River water
137	Zenpukujii pond	Japan	2003	Pond water
138	Lake Tamako	Japan	2003	Lake water
139	Lake Tamako	Japan	2003	Lake water
140	Porto Alto	Portugal	2003	Horse vagina

141	Almada	Portugal	2004	Cat nose
142	Lisbon	Portugal	2005	Dog subcutaneous abcess
143	Santarém	Portugal	2006	Goat brain
144	Glória do Ribatejo	Portugal	2007	Parrot nose
146	Lisbon	Portugal	2005	Dog ear
147	Santarém	Portugal	2007	Cow milk
148	Lisbon	Portugal	2005	Dog skin
149	Lisbon	Portugal	2003	Seal organs
150	Lisbon	Portugal	2003	Dog mucosa
151	Lisbon	Portugal	2003	Dog eye
152	Lisbon	Portugal	2007	Dog eye
153	Lisbon	Portugal	2005	Dog ear
154	Lisbon	Portugal	2006	Dog pleural fluid
155	Lisbon	Portugal	2005	Parrot eye
156	Estoril	Portugal	2007	Horse uterus
157	Amadora	Portugal	2007	Turtle shell
158	Lisbon	Portugal	2006	Dog eye
159	Famões	Portugal	2003	Cat vagina
160	Glória do Ribatejo	Portugal	2007	Parrot nose
162	Lisbon	Portugal	2006	Dog eye
165	Alcobaça	Portugal	2005	Dog ear
167	Lisbon	Portugal	2006	Kangaroo blood
168	Lisbon	Portugal	2007	Dog eye
169	Santarém	Portugal	2004	Cow milk
170	Santo António	Portugal	2005	Dog ear
171	Porto Alto	Portugal	2004	Horse uterus
172	Lisbon	Portugal	2007	Dog uterus
174	Algarve	Portugal	2004	Dolphin skin Lesion
175	Algarve	Portugal	2004	Dolphin respiratory tract
176	Ghent	Belgium	2003	CF-patient
177	Antwerp	Belgium	2003	CF-patient
178	Antwerp	Belgium	2003	CF-patient
180	Leuven	Belgium	2003	CF-patient
183	Brussels	Belgium	2003	CF-patient
185	Brussels	Belgium	2003	CF-patient
186	Leuven	Belgium	2003	CF-patient
187	Brussels	Belgium	2003	CF-patient
189	Brussels	Belgium	2003	CF-patient
191	Ghent	Belgium	2003	CF-patient
192	Ghent	Belgium	2003	CF-patient
193	Brussels	Belgium	2003	CF-patient
195	Birmingham	UK	2003	CF-patient
196	Liverpool	UK	2003	CF-patient
197	Manchester	UK	2003	CF-patient
198	Australia	Australia	1999	CF-patient

200	Hobart	Australia	2003	Lung carcinoma
203	Hobart	Australia	2003	Sputum
209	Hobart	Australia	2005	Hospital environment
210	Hobart	Australia	2005	Swimming pool water
211	Derwent river tributary	Australia	2005	River water
213	Hobart	Australia	2004	Urine
217	Hobart	Australia	2003	CF-patient
218	Hobart	Australia	2003	CF-patient
226	Panama City	Panama	2006	Wound
229	Woluwe river	Belgium	2002	River water
230	Woluwe river	Belgium	2002	River water
231	Woluwe river	Belgium	2002	River water
232	Woluwe river	Belgium	2001	River water
233	Woluwe river	Belgium	2001	River water
234	Woluwe river	Belgium	2002	River water
235	Woluwe river	Belgium	2002	River water
236	Woluwe river	Belgium	2002	River water
237	Woluwe river	Belgium	2002	River water
248	Brussels	Belgium	1997	Hospital environment
252	Brussels	Belgium	1997	Hospital environment
253	Brussels	Belgium	1997	Plant rhizosphere
254	Brussels	Belgium	1997	Tap water room BWC
255	Brussels	Belgium	1998	Hospital environment
257	Brussels	Belgium	1998	Burn
259	Brussels	Belgium	1998	Sputum
260	Brussels	Belgium	1998	Burn
261	Brussels	Belgium	1998	Burn
262	Brussels	Belgium	1998	Burn
263	Brussels	Belgium	1998	Wound
264	Brussels	Belgium	1998	Burn
266	Brussels	Belgium	1998	Tap water operating theatre
267	Brussels	Belgium	1998	Throat
268	Brussels	Belgium	1998	Wound
269	Brussels	Belgium	1999	Nose
270	Brussels	Belgium	1999	Throat
271	Lisbon	Portugal	1997	CF-patient
272	Lisbon	Portugal	1997	CF-patient
275	Lisbon	Portugal	1998	Burn
276	London	UK	1996	Burn
277	London	UK	1996	Burn
280	London	UK	1996	Wound
292	Ann Arbor	USA	1997	Burn
293	Ann Arbor	USA	1997	Pressure sore
294	Ann Arbor	USA	1997	Burn
298	Aachen	Germany	1997	Burn

300	San Antonio	USA	1988	Wound
304	San Antonio	USA	1991	Urine
305	San Antonio	USA	1993	Urine
307	San Antonio	USA	1993	Sputum
308	San Antonio	USA	1993	Burn
310	San Antonio	USA	1996	Sputum
311	Boston	USA	1992	Burn
312	Boston	USA	1992	Burn
313	Boston	USA	1997	Burn
314	Boston	USA	1997	Blood
315	Karachi	Pakistan	1998	River water
316	Karachi	Pakistan	1998	River water
317	Brussels	Belgium	1999	Sputum
320	Hannover	Germany	1985	CF-patient
322	Hannover	Germany	1989	Hospital environment
324	Hannover	Germany	1988	CF-patient
325	Cotonu	Benin	2008	River water
327	Bucarest	Romania	1960-64	Water
329	Canas	Puerto Rico	1938	Shallow well water
330	Unknown	Puerto Rico	1961	Chinese evergreen
331	Lwiro	Congo	2001	Blood
333	Tacloban City	The Philippines	1993	Wound
334	Mülheim	Germany	1986	Drinking water
335	Ruhr river	Germany	1992	River water
336	Mülheim	Germany	1992	Swimming pool water
337	Tunis	Tunisia	1998	Ear
338	Tunis	Tunisia	1998	Sputum
340	King City, Ontario	Canada	2004	soil
341	Unknown	Canada	2004	soil
342	King City, Ontario	Canada	7/4/2010	soil
343	King City, Ontario	Canada	7/4/2010	soil
344	King City, Ontario	Canada	7/4/2010	soil
345	Toronto	Canada	8/4/2010	soil/water
346	Maysville, KY	USA	8/4/2010	soil
347	Maysville, KY	USA	8/4/2010	soil
348	Maysville, KY	USA	8/4/2010	soil/water
349	no data	South Africa	2006	golf course pond
350	Toronto	Canada	November 2005	CF-patient
351	Ottawa	Canada	November 2005	CF-patient
352	Toronto	Canada	November 2005	CF-patient
353	Ottawa	Canada	February 2006	CF-patient
354	Kitchener	Canada	November 2005	CF-patient
355	Hamilton	Canada	May 2008	CF-patient
356	Kitchener	Canada	January 2006	CF-patient

357	Hamilton	Canada	September 2006	CF-patient
358	Sudbury	Canada	January 2006	CF-patient
359	Toronto	Canada	January 2006	CF-patient
360	Hamilton	Canada	January 2006	CF-patient
361	Toronto	Canada	January 2006	CF-patient
362	Toronto	Canada	May 2006	CF-patient
363	Hamilton	Canada	March 2006	CF-patient
364	Toronto	Canada	April 2006	CF-patient
365	Hamilton	Canada	March 2006	CF-patient
366	Hamilton	Canada	April 2006	CF-patient
367	London	Canada	May 2006	CF-patient
368	London	Canada	June 2006	CF-patient
369	London	Canada	January 2008	CF-patient
370	Ottawa	Canada	September 2006	CF-patient
371	Toronto	Canada	January 2008	CF-patient
372	Sudbury	Canada	September 2006	CF-patient
373	Toronto	Canada	October 2006	CF-patient
374	Unknown	Korea	Unknown	Unknown